A modified Supercell Composite Parameter for supercell thunderstorms over the Gauteng Province, South Africa

BY

KEVIN JULIAN RAE

Submitted in partial fulfilment

of the requirements for the degree

MASTER OF SCIENCE

in the

Faculty of Natural & Agricultural Sciences

UNIVERSITY OF PRETORIA

PRETORIA

05 November 2014

DECLARATION

I, Kevin Julian Rae (ID: 6306045135089, U.P. student number: 85655547), declare that the dissertation, which I hereby submit for the degree Master of Science: Meteorology at the University of Pretoria, is my own work and has not previously been submitted by me for a degree at this or any other tertiary institution.

…….

(signed)

Date: 05 November 2014

"Information is not knowledge, knowledge is not wisdom, and wisdom is not foresight. Each grows out of the other and we need them all."

Sir Arthur C. Clarke. CBE. (1917 - 2008)

"People tend to find books when they are ready for them."

Neil Gaiman (1960 -)

ABSTRACT

South Africa is a country prone to frequent outbreaks of thunderstorms which are often of a severe nature. Supercell thunderstorms are a particular class of thunderstorm which are typically long-lived and are associated with severe thunderstorm phenomena in as many as 9 out of 10 instances. In particular, the southern African moist Highveld climatological region is known to experience one of the highest rates of occurrences of thunderstorms and lightning within southern Africa and indeed the world. The domain for this Highveld-based study chiefly encompassed the industrialised metropolis of the Gauteng province. The population and infrastructure of this province are vulnerable to a variety of adverse effects relating to severe thunderstorms, comprising one or more of strong damaging winds, large hail, urban flooding or even tornadoes of varying intensity. In this study a sample of 15 supercell (SUP) proximity soundings of upper air data for Irene, Gauteng was compared against a large, independant sample of 510 Irene proximity soundings for austral summers during the period 2007 to 2011, representing non-supercell (NON-SUP) thunderstorm days. Hypothesis testing as well as box and whisker representations of the SUP versus NON-SUP samples were applied to various thunderstorm parameters to determine which SUP parameters exhibit the greatest statistical departure from their NON-SUP counterparts. Selected quartiles of SUP parameters so identified were further utilised to formulate a Modified Supercell Composite Parameter (MSCP) tuned to Gauteng supercells. MSCP as well as formulations of the Supercell Composite Parameter (SCP) were subsequently applied to five case-study events where some of the events were associated with observed supercells and some not.

The results strongly indicated that, in a short-term forecast context, MSCP has useful discriminatory ability to provide quantitative predictive guidance as to the relative likelihood of the development of supercell thunderstorms in the Gauteng area. Prior to this research, neither the SCP nor the MSCP were in operational use in South

Africa. To the best of the author's knowledge this work is the first of its kind in southern Africa, especially with consideration to the unique high-altitude Highveld domain of the Gauteng province. In the light of the research results presented herein, it is proposed that MSCP be jointly implemented on point-based (upper air sounding analysis) platforms as well as that of gridpoint-based (deterministic NWP) platforms for short-term predictions of supercell-type thunderstorm conditions in Gauteng province.

PREFACE

The southern African Highveld is a region that is highly vulnerable to frequent occurrences of thunderstorms, particularly in the summer months. Many of these thunderstorms are severe and can be accompanied by large hail, strong surface winds and even tornadoes. Infrastructural damage in the wake of such storms is typically exacerbated by inadequate strength and/or poor quality of built structures. The generally destructive nature of severe storms however is indiscriminate in that in extreme cases such storms can prove fatal, regardless of one's economic status. It is however often the less affluent who are most adversely impacted and typically most vulnerable to severe storms. Gauteng province is characterized by high levels of population density as well as intensive infrastructural development, including housing, roads, highway networks, industrial parks and airports, all of which are susceptible to storm damage. Whilst severe storms are not preventable, the key to mitigating such risks lies in the value of timeous weather-related warnings to communities in the path of such storms. Although the concept of such warnings, both locally and abroad is not new, there is nevertheless scope for continual improvement; through improved human processes, elevated awareness as well as improved tools and techniques to identify incipient severe storms. This study will focus on tools and techniques relating to severe thunderstorm identification and how some of these methodologies may be enhanced in a Highveld setting. Of the four classes of thunderstorm, the storm-types associated with multicell- and supercell- type storms have the greatest potential to become severe. In the case of supercell storms, this typically occurs in 9 out of 10 occasions. Supercells are thus a highly significant element to consider when there is a concern regarding the possible development of severe storms. Whilst there is a plethora of thunderstorm parameters relating to thunderstorm severity, by contrast there are very few such indices in mainstream use which have skill in relation to categorization of thunderstorm type, particularly in terms of the distinction between multicell and supercell. This study is concerned with the latter, in other words supercell

identification, through the use of an index derived from upper air radiosonde observations of the current state of the atmosphere. A Modified Supercell Composite Parameter (MSCP) is formulated and the response thereof fine-tuned to provide short-term forecast guidance in terms of identifying pre-storm atmospheric conditions which may be conducive to supercell thunderstorm development. Supercells are often associated with unusual and unexpected storm motion as well as extended storm longevity. In the latter case, two to four hours can usually be expected, although six to eight hours is not unprecedented as an upper temporal bound. From a risk mitigation perspective, consistent and skilful identification of supercell thunderstorms, as well as accurate predictions regarding their movement, presents many challenges to a forecaster. In the opinion of the author, the operational use of a tool such as MSCP to identify high-risk days when supercell storms may be encountered, has the potential to contribute significantly towards severe storm risk mitigation for the public at large.

ACKNOWLEDGEMENTS

The author would like to express his sincere appreciation to the following persons and/or institutions, whose assistance and support contributed significantly towards this research work:

- First and foremost; my study leader, Dr. Liesl Dyson, University of Pretoria.
- My wife Andrea and son Adrian; for their patience and support.
- Mr. John Shewchuck, ERS (USA); for an exceptional level of customer support regarding RAOB software upgrades and code amendments.
- Ms. Karin Oxley and Ms. Anastasia Demertzis, SAWS library staff. Their enthusiasm and helpfulness are highly appreciated.
- Mr. Craig Powell, SAWS RADAR scientist, for use of the photo which appears in Fig. 2.13.
- Mr. Mark Todd (New Zealand MetService); for use of lecture and case-study material.
- Ms. Elke Louw (New Zealand MetService); for information relating to the 16 December 2013 supercell storm near Geraldine, South Island, New Zealand.
- New Zealand Metservice, for permission to use the RADAR image which appears in Fig. 2.19.
- Mr. Steven Shongwe, Ms. Samantha Linnerts and Ms. Coleen de Villiers, for the provision of SAWS meteorological data (surface AWS observations). In addition, a special word of thanks to Ms. Linnerts for upper air data for the 21 October 1999 Heidelberg tornadic storm.
- A further vote of thanks to Ms. Linnerts for numerous GIS-based maps which added much value to this work.
- Ms. Elsa de Jager, for provision of SAWS Lightning Detection Network (LDN) data.
- Ms. Stephanie Landman (SAWS) and Ms. Patience Shibambu (SAWS), for operational NWP implementation of MSCP at SAWS using the WRF and UM models respectively.
- The South African Weather Service, who provided funding for the author's study.
- The Senate of the University of Pretoria.

Table of Contents

LIST OF FIGURES

LIST OF TABLES

LIST OF ABBREVIATIONS

AGL	Above Ground level
AMDAR	Aircraft Meteorological Data Relay
BoM	Australian Bureau of Meteorology
BRN	Bulk Richardson Number
BWER	Bounded Weak Echo Region
CAPE	Convective Available Potential Energy
CAPPI	Constant Altitude Plan Position Indicator
CG	Cloud-to-ground (lightning discharge)
CINH or CIN	Convective Inhibition (the converse of CAPE)
COMET	Cooperative Program for Operational Meteorology, Education and Training
CSIR	Council for Scientific and Industrial Research
dBZ	RADAR reflectivity (unit of)
EBS	Effective Bulk Shear
ECSS	European Conference on Severe Storms
EHI	Energy-helicity index
EL	Equilibrium level (of a sounding)
EMM	Equatorwards of mean storm motion
ERS	Environmental Research Services
ESRH	Effective Storm Relative Helicity
ESRI	Environmental Systems Research Institute
ESSL	European Severe Storms Laboratory
EUMETSAT	European organisation for the exploitation of Meteorological Satellites
FFD	Forward flank downdraft
GPS	Global Positioning System
GZ	Goldilocks zone (relating to proximity sounding schemes)
HMA	Hailmass Aloft (RADAR-derived index)

HP	High Precipitation (supercell type)
ID	Internal Dynamics (thunderstorm movement algorithm)
IGRA	Integrated Global Radiosonde Archive (at NCDC)
IQR	Interquartile range (statistical measure of distribution)
LCL	Lifting condensation level
LFC	Level of free convection
LDN	Lightning Detection Network (South African Weather Service)
LIS	Lightning Image Sensor (NASA remote-sensing satellite)
LM	left-moving (supercell)
LP	Low Precipitation (supercell type)
MATLAB	MATrix LABoratory, a numerical analysis application.
MSCP	Modified Supercell Composite Parameter
MSG	Meteosat Second Generation (satellite), now designated Meteosat 9.
MSL	Height above Mean Sea Level (units specified in accompanying text)
MUCAPE	Most Unstable CAPE
NASA	National Aeronautics and Space Administration
NCAPE	Normalised CAPE
NCDC	National Climatic Data Center (USA)
NOAA	National Oceanic and Atmospheric Administration
NON-SUP	Sample group of 510 non-supercell cases used in ths study
NSSL	National Severe Storms Laboratory
NWP	Numeric Weather Prediction (model, modelling)
NWS	National Weather Service (USA)
ORTIA	Oliver Tambo International Airport
PMM	Polewards of mean storm motion
PPI	Plan Position Indicator (RADAR)
RADAR	RADio Detection And Ranging
RAOB	RAwinsonde OBservation Program

RFD	Rear Flank Downdraft
RGB	Red, Green, Blue composite satellite image
RHI	Range Height Indicator (RADAR)
RM	Right-moving (supercell)
SAWS	South African Weather Service
SAST	South African Standard Time
SBCAPE	Surface-based CAPE
SCP	Supercell Composite Parameter
SI	Systéme International (metric system)
SPC	Storm Prediction Center (USA)
SRH	Storm-relative helicity
STP	Significant Tornado Parameter
SUP	Sample group of 15 supercell cases used in ths study
TITAN	Thunderstorm Identification, Tracking, Analysis and Nowcasting algorithm
TRMM	Tropical Rainfall Measuring Mission (satellite platform)
UM	Unified Model (NWP)
UTC	Universal Time
USA	United States of America
VORTEX	Verification of the Origins of Rotation in Tornadoes Experiment
VORTEX2	*ibid.* (the second field experiment thereof)
VWP	vertical wind profile (especially relating to soundings and hodographs)
WINDEX	Surface wind gust index (McCann, 1994)
WER	Weak Echo Region
ZAMG	*Zentralanstalt für Meteorologie und Geodinamik* (Austrian Institute for Meteorology and Geodynamics)

CHAPTER I : INTRODUCTION

1.1 Background

Southern Africa is a region highly prone to frequent outbreaks of thunderstorms (Gill, 2008) which are often severe in nature (Goliger *et al*., 1997; de Coning & Adam, 2000; Goliger & Retief, 2007). Supercell thunderstorms (Browning, 1962; 1964) are a particular class of thunderstorm which are typically long-lived (Bunkers *et al*., 2006a; 2006b) and usually evolve into severe thunderstorms (Houze, 1993; Burgess & Lemon, 1990; Glickman, 2000).

The Republic of South Africa is located within the greater region of southern Africa (Fig. 1.1) and is bounded by the sovereign countries of Namibia, Botswana, Mozambique and Swaziland. The highland kingdom of Lesotho, though surrounded by South Africa, is also an independent sovereign country. The domain for this study is located predominantly within the Gauteng province (hereafter Gauteng), one of nine such provinces in South Africa. Gauteng lies within a latitudinal band ranging from 25.11 S to 26.90 S, polewards of the Tropic of Capricorn (Fig. 1.1). Gauteng is thus located within a sub-tropical setting, with the majority of rainfall occurring in the summer season (Tyson, 1987; Kruger, 2007) and delivered mostly by thunderstorms (Held, 1973; Dyson, 2009).

Much of Gauteng lies at an elevation of approximately 1500 m above mean sea level (hereafter MSL) as part of a geographically elevated terrain covering a large part of South Africa, commonly referred to as the Highveld. According to Kruger (2004) most of Gauteng is classified as the "Moist Highveld Grassland" climatological region, indicated in Fig. 1.2 as region 11, corresponding to Kruger's classification. Similarly, region 10 in Fig. 1.2 is also associated with the Highveld and is classified as being "Dry Highveld Grassland"

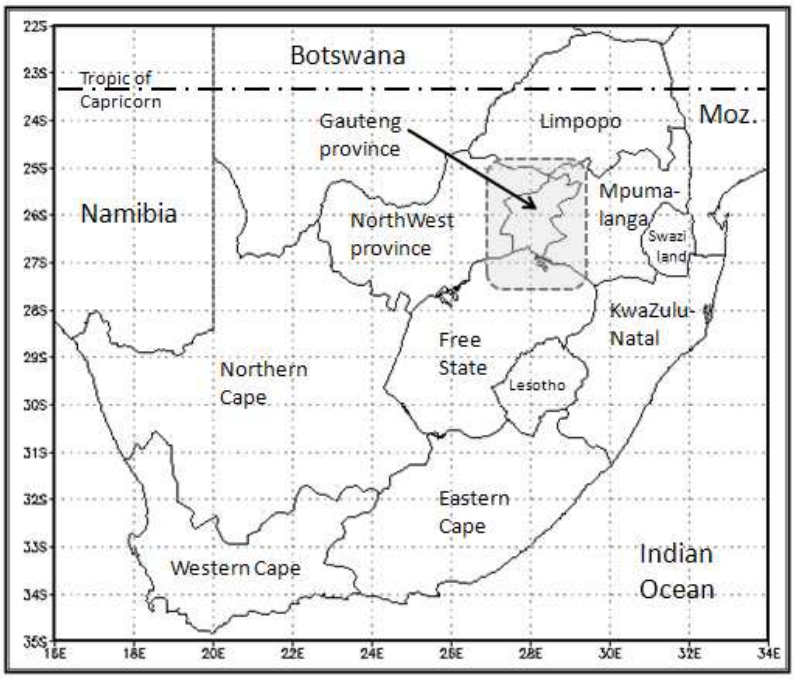

FIGURE 1.1: Geographic location of Gauteng province in South Africa, in relation to adjoining provinces as well as adjacent foreign countries. South Africa lies predominantly in a sub-tropical region of southern Africa, with the Tropic of Capricorn bisecting the northernmost province of Limpopo. At top right of this Fig., the inscription "Moz." indicates the position of Mozambique, relative to South Africa. Source: compiled by this author.

Collectively, last-mentioned two regions can be considered to be the greater Highveld region in colloquial usage. As a consequence of the generally high altitude of the region, the climate is somewhat cooler than would typically be expected, given the sub-tropical latitude of the Gauteng province (Kruger, 2007). Furthermore, average annual precipitation in Gauteng province is of the order of 600 to 800 mm (Kruger, 2004; 2007) whilst a proportionally smaller part of Gauteng, occupying the northern extremity of this study domain northwards of the Magaliesberg mountain range, is classified as being part of the "Central Bushveld" climatological region (Kruger, 2004), annually receiving 500 to 700 mm of rain and indicated as region 2 in Fig. 1.2 following Kruger's classification. The Highveld region is known to experience one of the highest rates of occurrence of thunderstorms as well as lightning within southern Africa (Gill, 2008). Furthermore, Gijben (2012) states that "…the Highveld and eastern escarpment (region) record on average between 10 and 15 lightning flashes per square km per annum."

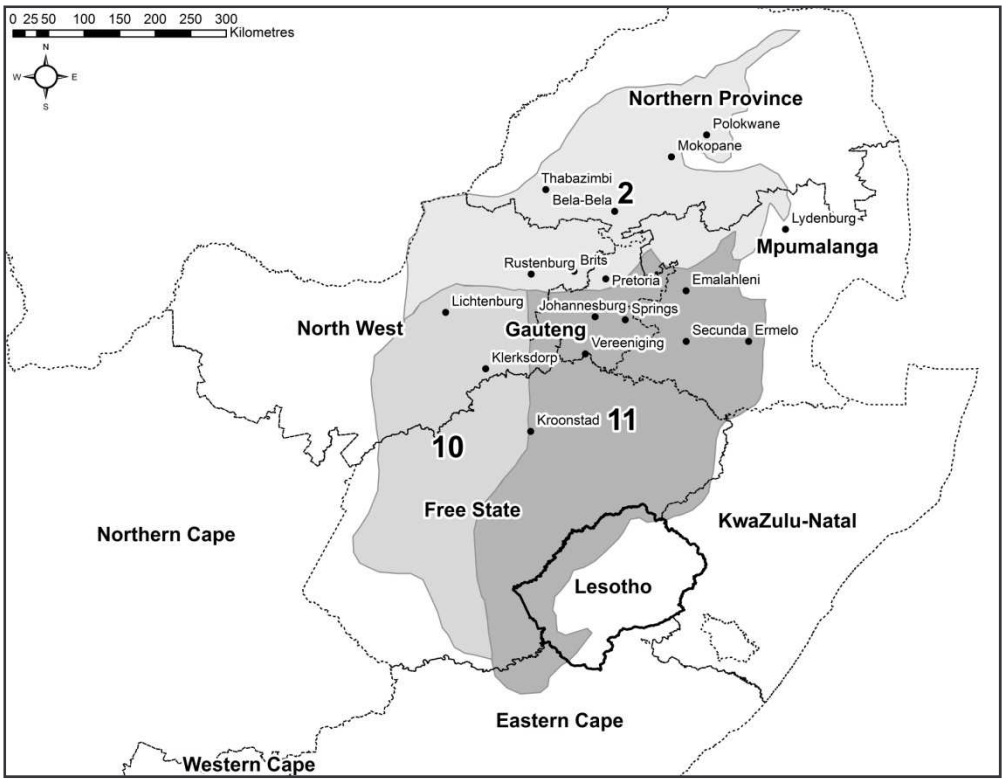

FIGURE 1.2: Map of the Highveld classification of Kruger (2004), indicated as regions 10 and 11. Source: After Kruger (2004). Map generated using ESRI ArcGIS 10.1.

The domain for this study extends across Gauteng in entirety, including the large, heavily-populated and industrialised metropolis encompassed by Pretoria, Midrand and Johannesburg. Situated chiefly within the Highveld region, Gauteng is thus centrally located within a region that is highly prone to frequent thunderstorms, many of which are severe (Goliger *et al*., 1997). The population and infrastructure of the abovementioned metropolitan area are thus clearly at risk in terms of frequent occurrences of severe thunderstorms which may include one or more of strong, damaging winds, large hail (or large amounts of small hail), urban flooding or even tornadoes (SAWS, 2013).

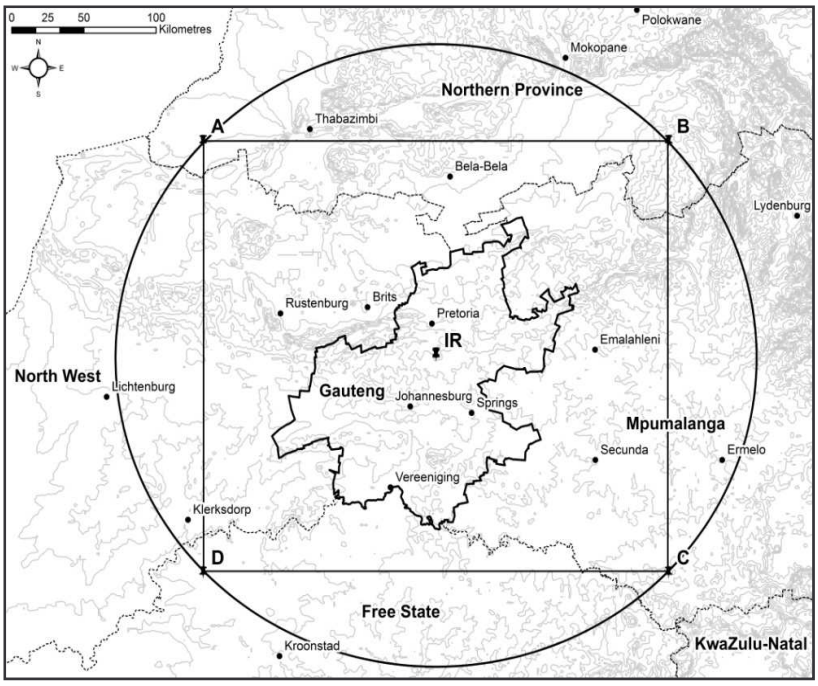

FIGURE 1.3: The study domain centred over Gauteng, including sections of adjacent provinces. The domain is indicated by a 200 range ring (circle) surrounding the Irene RADAR (IR pushpin located just south of Pretoria). The square bounded by ABCD represents the latitude/longitude box domain used for filtering LDN lightning detections. Source: Map generated using ESRI ArcGIS 10.1.

1.2 Motivation for this study

The South African Highveld of which the province of Gauteng is a part, is well-documented in the literature as being a geographic region particularly susceptible to frequent occurrences of thunderstorms (Goliger *et al*., 1997; de Coning & Adam, 2000; Gill, 2008; Gijben, 2012), especially in the summer months (Tyson, 1987). Some of these thunderstorms become severe and are associated with occurrences of one or more of large, damaging hail (Carte & Basson, 1970; Carte & Held, 1972; Held, 1973), strong winds (Goliger & Retief, 2007) and to a less frequent but no less severe extent; tornadoes (D' Abreton, 1991; Goliger *et al*., 1997; de Coning & Adam, 2000).

Burgess & Lemon (1990) determined that 90% of supercell thunderstorms, hereafter termed supercells, can be classified as severe thunderstorms during their lifetime. Furthermore, supercells are by definition significantly longer-lived than regular airmass type thunderstorms (Houze, 1993; Moller *et al*., 1994; Bunkers *et al*., 2006a;

2006b). in addition, Bunkers (2002) determined that 53 of a sample of 60 left-moving supercells across the contiguous United States produced large hail with a diameter of 19 mm or greater. Moller *et al.* (1994) established that most strong or violent tornadoes are produced by supercells in the contiguous United States of America (USA). Goliger & Retief (2007) determined that, together with KwaZulu-Natal province, Gauteng is one of the most tornado-prone provinces in South Africa. This strongly suggests that at least a significant proportion of such southern African tornadoes are likely to have been spawned by supercell thunderstorms if one accepts the results of Moller *et al*. (1994) as being globally applicable.

The Pretoria, Gauteng severe hailstorm of 1 November 1985 exemplifies the destructive power of supercell storms, due in part to the longevity of such systems. This isolated supercell persisted for over four hours and was associated with extensive damage to vehicles and property with a swathe of destruction extending from Pretoria West, through the Pretoria CBD and thence into Groenkloof and Erasmuskloof. In relation to this storm, Terblanche (1985) made particular note of the presence of significant wind shearing with altitude; typical of an atmospheric environment favouring supercell development. The Heidelberg, Gauteng tornado of 21 October 1999 is a further example of a 100 km long track, left-moving storm that was associated with significant human and infrastructure impact, leaving "…40 people injured, 10 people hospitalised, 300 people left homeless and farm dwellings damaged." (de Coning *et al*., 2000b). This storm narrowly missed the large metropolitan area of Johannesburg and in particular, the authors make specific mention that, had this storm been displaced as little as 50 km to the north, "…it would have resulted in the loss of many lives and the destruction of property".

The multiple supercell outbreak of 24 October 2010 documented by Powell *et al*. (2010) saw at least nine supercells identified across Free State, Gauteng and Mpumalanga. The winter supercell outbreak of 23 June 2012 was associated with at least four confirmations of tornadoes at a variety of localities. One such supercell storm during this outbreak spawned a tornado over the Oranjeville and Rose Bay

region of the Vaal dam, killing one person, injuring five others as well as wrecking boats, yachts and holiday homes (Beeld, 2012; Pretoria News, 2012). During the same outbreak, a tornadic supercell near Bethlehem, north-east Free State resulted in an additional fatality (Beeld, 2012). The Viljoenskroon, Free State supercell storm of 28 November 2013, presented in more detail in Chapter 7, is a prime example of a long-lived, long-track supercell storm which eventually migrated into Gauteng and resulted in widespread, devastating hail damage, especially along the Vaal river basin and in Randburg, Gauteng where hail was large enough to break car windows. It is worth noting that on the date in question a number of other thunderstorms across Gauteng also concurrently delivered large, damaging hail of a sufficient size to cause extensive automotive damage. From the above evidence, it is apparent that strong or violent tornadoes as well as large hail are frequently associated with supercells. Due to their generally long-lived nature, typically of the order of several hours (Bunkers *et al*., 2006a; 2006b), supercells are likely to be associated with damage swathes of considerable length and duration (de Coning *et al*., 2000a) as well as significant economic impact (de Coning & Adam, 2000; de Coning *et al*., 2000b). This aspect, relating to human risk and infrastructural impact is also echoed by Pyle (2006) in a southern African study relating to the socio-economic impacts of severe thunderstorms in the Eastern Cape province of South Africa. Furthermore, accurate and reliable predictions of supercell motion are critical from a disaster risk mitigation perspective, especially in the context of communities in the path of such storms (Bunkers *et al*., 2000).

Supercell thunderstorms occur over a wide range of atmospheric instability and wind shear regimes (McCaul & Weisman, 2001; Craven & Brooks, 2004). Consequently short-term predictions of this particular type of thunderstorm can be complex and non-trivial if one is to consider a broad spectrum of parameters and thresholds associated with the formation of supercell storms (Doswell & Schultz, 2006). Furthermore cognizance can be taken that not all thunderstorms become severe *per se*. In a study of 658 thunderstorm hail days in Gauteng province in the period 1984 to 1995, based on 12365 Council for Scientific and Industrial Research (CSIR) hail

survey cards, Rae (2005) determined that only 21% of such hail storms delivered hail that exceeded the category of "grape size" and which would consequently have the potential to cause automotive damage. Conversely one could infer that approximately four out of every five Gauteng hail storms can generally be considered to be non-severe in nature if one considers only occurrences of hail as a contributory factor towards severe storms.

There are a variety of predominantly sounding-based parameters and indices relating to the relative threat of strong winds, tornadoes and hail associated with severe storms in general. The WINDEX index (McCann, 1994) estimates surface gusts resulting from dry downbursts. Hart & Korotky (1991) mention the use of the Energy-Helicity index (EHI) as a tornado prediction index and Thompson *et al.* (2002) similarly configured the Significant Tornado Parameter (STP) for the same purpose. In terms of hail size prediction, Shewchuck (2013) cites Fawbush & Miller's (1953) hail size algorithm used in the RAOB software program. More recently however, the work of Brimelow *et al*. (2002), building on methodology initiated by Poolman (1992), has delivered encouraging results in terms of hail size prediction. Notwithstanding the aforementioned indices which focus strongly on aspects relating to thunderstorm severity, there is by comparison a paucity of index-based information to provide meaningful information relating to skilful discrimination in terms of "storm type" when considering the four major storm types. One particular exception is the Bulk Richardson Number (BRN) which offers some degree of discrimination between supercells and multicells, given the acknowledged overlap of optimum values of BRN for supercells as opposed to multicells (Weisman & Klemp, 1982; 1984).

It is known from Houze (1993) that, of the main classes of thunderstorms described in some detail in Chapter 2, it is the storms associated the multicell and supercell storm-type structures which are generally the most organised, long-lived and likely to be the harbingers of violent destructive phenomena such as very strong surface winds, large hail and tornadoes. It therefore makes sense that if short-term

predictions relating to severe thunderstorms are to be skilful, it is essential that appropriate guidance tools be developed and refined to efficiently discriminate between multicells and supercells. Apart from the BRN mentioned earlier, a further, more recently developed predictive tool incorporating *inter alia* the wind shear component of BRN currently exists in the form of the Supercell Composite Parameter (SCP). It has been demonstrated in USA-based studies that the SCP can skilfully identify pre-storm environments conducive to supercell development (Thompson *et al*., 2002; 2003).

What is specifically envisaged in relation to this study is to mathematically modify and fine-tune the SCP through the formulation of a Modified Supercell Composite Parameter (MSCP), tuned to Gauteng Highveld conditions. Thus it is hoped that the MSCP will provide useful guidance in terms of short-term prediction of weather conditions conducive to the development of supercell storms in the high-altitude Highveld grassland domain of Gauteng province, South Africa.

1.3 Research Aims and Objectives

The main aim of this reseach is to propose a method to provide short-term forecasts of weather conditions which may favour the development of supercell thunderstorms, given that thunderstorms are expected on a particular day. This methodology will be strongly based on existing formulations of the Supercell Composite Parameter (SCP) as declared by Thompson *et al.* (2002; 2003). The aforementioned SCP will be fine-tuned to be more representative of near-storm conditions relating to Gauteng supercells and will be termed the Modified Supercell Composite Parameter (MSCP). In order to achieve this aim, six primary Objectives are pursued in this research work:

Objective 1

Filter and analyse 2007 to 2011 SAWS Lightning Detection Network (LDN) data for South Africa to explicitly determine diurnal "thunderstorm days" where 2 or more CG strokes occurred in the period 09h00UTC to 15h00UTC daily within the study domain.

Objective 2

Using results from Objective 1, compile a corresponding dataset of 2007 to 2011 12h00UTC Irene soundings for "thunderstorm days" so identified. If no representative proximity sounding can be retrieved for a particular thunderstorm day, then that date will be precluded from the dataset. Analyse the intraseasonal variation of selected thunderstorm and SCP parameters for this dataset. Further filter and refine the aforementioned dataset to reflect only austral summer dates, January to March as well as October to December months. To ensure independence of this dataset, remove data for any known supercell dates associated with the SUP dataset identified in Objective 3. The final dataset of 2007-2011 austral thunderstorm days to be termed the NON-SUP (i.e. "non-supercell thunderstorm") sample.

Objective 3

Compile a representative sample of historic Gauteng supercell proximity sounding cases to be designated as SUP (i.e. the "supercell" sample). Generate typical measures of distribution (especially the median and quartiles) for sounding-based thermodynamic variables and parameters (such as CAPE, storm-relative helicity and Bulk Richardson shear) to be used to inform threshold scaling values for MSCP.

Objective 4

Through the use of statistical hypothesis testing and associated distribution tests, compare the SUP and NON-SUP samples and provide statistical inference relating to components of SUP and NON-SUP which are significantly dissimilar in terms of their distributions.

Objective 5

Apply storm parameters identified in Objective 4 to a modified formulation of SCP to be termed MSCP. Each factor of MSCP to be normalised by a threshold value to be

gained from the first quartile (or in the case of negative distributions, the quartile nearest the origin) of the corresponding parameter occurring in the SUP sample.

Objective 6

Apply MSCP to a range of recent Gauteng case-study scenarios to gain an informed impression regarding the operational performance and viability of MSCP in term of providing useful short-term guidance relating to supercell storms. Similarly evaluate the T(2002) and T(2003) formulations of SCP for the same case-studies to provide a means of reference for MSCP assessment.

1.4 Scope of this study

The scope of this research is presented by means of a structured decision-tree flow-chart in Fig. 1.5. Particular attention is drawn to the ring-fencing of the study design, such that the question of whether a supercell storm is likely to be tornado-producing (*i.e.* tornadic) is not formally explored. Similarly, the question of whether the particular supercell is likely to be classified as a severe thunderstorm will not be tested in the study design. These and related aspects are discussed further in the paragraph to follow.

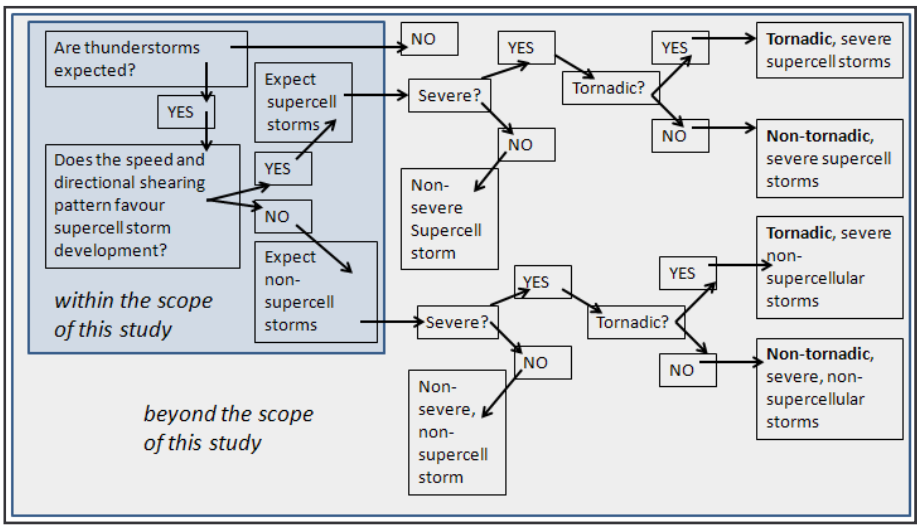

FIGURE 1.5: A decision-tree diagram indicating the possible spectrum of thunderstorm classification when forecasting thunderstorms. The light blue shaded area lies within the scope of this study.

Aspects relating to the severity of thunderstorms will not be explored in great detail. If a particular thunderstorm discussed in this study was known to be classified as a severe thunderstorm, this fact will be introduced anecdotally as a supporting observation. Likewise, with reference to Fig. 1.5 the classification of severe versus non-severe thunderstorm will not be tested in this research design. Similarly, the classification of thunderstorms as being either tornadic or non-tornadic will also not be formally tested. The scope of this study, given certainty that thunderstorms will occur on a given day, is to make predictions based on the prevailing pre-storm environment of that day. Such predictions, through the use of MSCP, would attempt to address the question as to whether or not subsequent thunderstorm development on the given day would be likely to favour the development of supercell type storms. through the use of the MSCP.

At this point, it is appropriate to introduce a caveat; that notwithstanding the abovementioned assertions regarding the scope of this research, particularly in respect of tornadic supercell thunderstorms not being closely investigated, it bears mentioning that a significantly large proportion of the body of scholarly work dealing with supercell thunderstorms also embodies investigation into the sometimes tornadic nature of such storms. The focus in some scholarly work is almost exclusively devoted to this aspect, while in other works less so. As such, and particularly within the literature review presented in the chapter to follow, it is considered an implicit feature that academic narratives relating to supercell storm structure often include some form of discussion regarding tornadoes. It is however hoped that within this research, the body of scholarly work representing current knowledge and thinking surrounding supercell storms in general has been presented in a holistic and balanced fashion with sufficient emphasis on the scope of the study at hand.

1.5 Chapter overview

- Chapter 1 serves to identify both the geographic domain and the climatological setting of this research and provides contextual information regarding the motivation for this study, together with the primary Objectives and the scope of this research work.
- Chapter 2 presents an overview of current and early historic literature alluding to supercell thunderstorms whilst simultaneously positioning supercells within the broad family of thunderstorm nomenclature.
- Chapter 3 provides a thumbnail overview of methodology to be adopted, per data type. Each data type is also briefly discussed in the context of its contribution towards the study as a whole.
- Chapter 4 provides information and discussion regarding the 15 (SUP) supercell cases utilised for this study. Supercell characteristics and criteria, per supercell case, are also presented in logframe format. Additional storm cases which were initially considered for inclusion in the study but however not used, are also briefly discussed.
- Chapter 5 provides a explanation as to how the dataset of 510 non-supercell thunderstorm days was compiled. In addition, research results relating to observational sources of meteorological data in support of this research are also presented in this chapter, stratified per data type.
- Chapter 6 deals with a statistical intercomparison between the SUP and NON-SUP datasets in order to determine which thunderstorm parameters differ most markedly between the two sets. This process ultimately leads to the step by step mathematical formulation of MSCP.
- Chapter 7 is the penultimate chapter and offers five mini case-studies of recent thunderstorm events in the period October to November 2013, illustrating relative performance of the Modified Supercell Composite Parameter (MSCP) within a Gauteng domain, given varying environmental pre-storm conditions. Performance of MSCP is compared with SCP calculated according to Thompson *et al*. (2002; 2003).

- Chapter 8 forms the final chapter of this dissertation and reconciles all the components and findings in the form of a summary of main findings as well as discussion and conclusions surrounding same. Any challenges faced during this study, pertaining to methodology, data availability or otherwise is captured within this chapter, together with insight as to how such challenges were reconciled with the study at hand. This chapter ultimately concludes with a perspective relating to the implications for existing theory surrounding supercell thunderstorms, recommendations for operational implementation of the Modified Supercell Composite Parameter (MSCP) and finally a number of salient suggestions relating to further research opportunities in this regard.

1.6 Summary

This chapter introduced a high-level overview of the research to follow, firstly describing the study domain that was utilised as well as the general climatology and terrain associated with the Highveld region and similarly for the Gauteng province. The particular exposure of this domain to a range of severe weather, particularly that of frequent thunderstorms which often become severe, was also discussed from a southern African perspective as well as globally. This led into a detailed motivation as to why there is a need to have a better understanding surrounding the skilful prediction of, and/or discrimination between, various thunderstorm types, particularly that of supercells. The primary Objectives associated with this study were also introduced, as well as their logical interrelationship. Towards the latter part of the chapter, the scope of the research was also defined, especially in terms of which aspects fall within (or beyond) this research. The chapter concluded with a brief overview of the content to follow in subsequent chapters.

CHAPTER II : LITERATURE REVIEW

This chapter commences with a broad overview of literature dealing with thunderstorms. What processes need to be in place to initiate storms? What constitutes a severe thunderstorm? What thunderstorm types are there and where do supercells fit into this classification? What mechanisms allow supercells to form and how do they form? In addition, the characteristics that define supercells are also discussed as the identification of supercells forms an important component of the forthcoming chapter dealing with methodology. In a similar vein, thunderstorm characteristics which may be associated with supercells but are however not unique to supercells are also discussed in order to further clarify issues surrounding supercell characteristics.

It was stated in the preceding chapter that the SCP and MSCP will form a central theme and activity throughout this work, hence a corresponding section that concludes this chapter contains a detailed discussion focussing on the history of the SCP algorithm, how it was first formulated and how it has evolved with time. The components that feed into SCP, such as Most Unstable Convective Available Potential Energy (MUCAPE) (Doswell & Rasmussen, 1994), storm-relative helicity (SRH) (Davies-Jones *et al*., 1990) and Bulk Richardson shear (the denominator of the Bulk Richardson Number defined by Weisman & Klemp (1982; 1984)) are discussed in terms of their respective influence on SCP. In this context, accurate estimates of supercell storm motion are important as this has an implicit, nested effect on SRH calculations. A complete sub-section is therefore devoted to storm-motion algorithms with a view to establishing the most accurate and preferred algorithm to utilise within this research, according to prevailing literature.

2.1 Thunderstorm initiation

The Oxford dictionary (Fowler & Fowler, 1964) defines a thunderstorm as "…a storm accompanied by thunder and lightning and usually heavy rain or hail". Thunderstorms are also called electrical storms by Glickman (2000) who further defines thunderstorms as being "…invariably produced by a cumulonimbus cloud and (are) always accompanied by lightning and thunder, usually with strong gusts of wind, heavy rain and sometimes hail." Thunderstorms occur across all continents, with the notable exception of the Antarctic (Panneerselvam *et al*., 2004) and are most prevalent over the equatorial, tropical and mid-latitude regions of the world (NASA, 2012). Zipser *et al.* (2006) state that southern African thunderstorms feature strongly as some of the most intense events worldwide, ranked within the upper 1 x 10^{-3} % of a 1998 to 2004 global distribution of remotely-sensed thunderstorms, as inferred from the LIS flash-rate aboard the TRMM satellite.

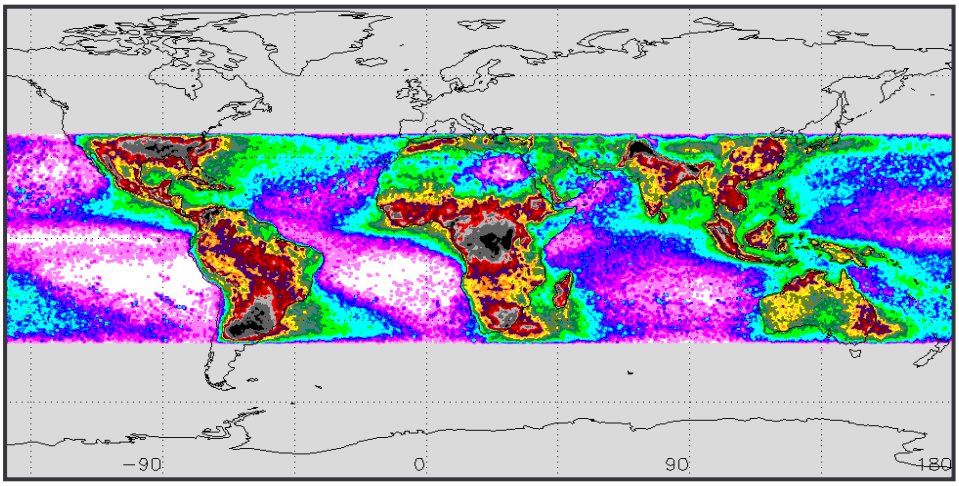

FIGURE 2.1: NASA Lightning Image Sensor (LIS) composite image of satellite-based, remotely-sensed lightning, 1998-2012. Dark grey as well as black shaded regions are indicative of regions most susceptible to lightning. Notably, the purple and white shades over open oceanic areas indicate regions that are almost totally devoid of such phenomena. Source: NASA (2012).

Fig. 2.1 clearly highlights particular continental regions where lightning and by implication, thunderstorms are most populous. By contrast, markedly fewer storms occur over open ocean environments. Parts of South America as well as southern Africa are regions in the southern hemisphere that are especially prone to such

storms. Gill (2008) performed a detailed, high-resolution study of lightning distribution in South Africa for the year 2006 using cloud-to-ground (hereafter CG) lightning data from the SAWS LDN network. Gill (2008) noted the particular and extreme predisposition of the Highveld to the occurrence of thunderstorms, as indicated in Fig. 2.2.

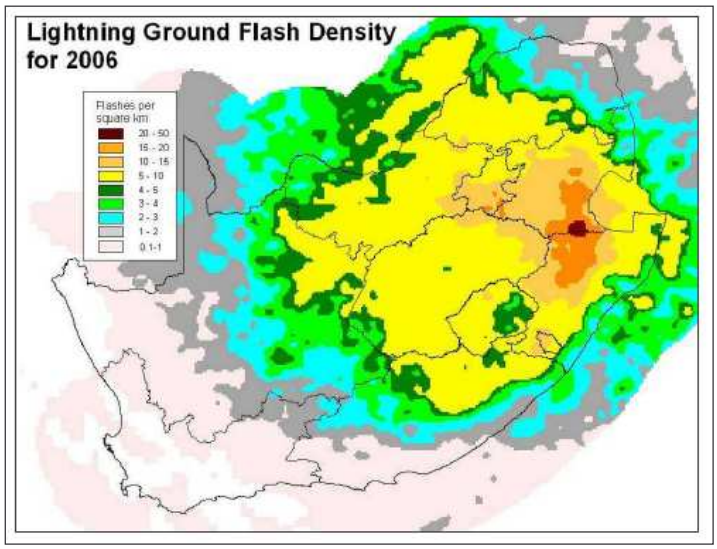

FIGURE 2.2: Lightning ground flash density over South Africa for 2006. Note in particular the extremely high density of flashes on the Highveld. From Gill (2008).

Gill's findings were affirmed in a later study by Gijben (2012) who expanded upon Gill's work and produced a South African lightning climatology for the 2006 to 2010 period. Earlier southern African work by Schulze (1984) also cited by Tyson (1987), regarding frequency of occurrence of thunder as well as that of hail, have much in common with the findings of Gill (2008) and Gijben (2012), highlighting the Drakensberg mountains, Lesotho region as well as the Highveld geographic region collectively as the extreme high risk regions for the occurrence of thunderstorms.

The basic atmospheric requirements needed to support the initiation of thunderstorms are well-established and are discussed by various authors (Maddox, 1976; McNulty, 1978; Doswell, 1987; Johns & Doswell, 1992). For thunderstorm initiation, the following three requirements should be fulfilled: (1) a sufficient supply of moisture should be present in the atmosphere, particularly at the surface as well as within the first few kilometres above ground level (hereafter AGL), (2)

atmospheric instability to enable moist air to rise and reach its lifting condensation level (henceforth LCL) and thence to ascend further in the guise of cumulus cloud and finally (3) the presence of a suitable triggering mechanism to initiate the free ascent of the air parcel.

It is beyond the scope of this work to elaborate in great depth on the generic growth and life cycle of ordinary thunderstorms. Notwithstanding this constraint, a basic background to thunderstorm formation will nevertheless be presented herein to further define and highlight the niche that supercell thunderstorms occupy within the broad family of thunderstorm development in general.

2.2 Thunderstorm types

Of the four major types of thunderstorm, namely single-cell, multicell cluster, multicell line and supercell thunderstorm it is the latter that is the particular focus of this research work. Furthermore it has been stated that the SCP and MSCP will be actively utilised, particularly in Chapter 7 case-studies, in an attempt to skilfully identify pre-storm environments with a predisposition towards supercell development. It thus follows that it will be useful to place supercells in an appropriate context within the literature, especially in terms of what thunderstorm structures and characteristics set supercells apart from the other classes of thunderstorm.

2.2.1 Isolated, single-cell thunderstorms

Byers & Braham (1949), Weisman & Klemp (1986) as well as Houze (1993) have all provided excellent descriptions of the processes controlling the development of small, isolated cumulonimbus or thunderstorm clouds. Importantly, these storms typically form in an environment associated with minimal levels of wind shear, thus restricting the opportunity for the storm to develop spatially separated up- and downdrafts in contrast with other storm types (Houze, 1993). For clarity of

nomenclature, wind shear may equally be referred to as a sheared environment and this implies speed and/or directional shearing in the vertical (Markowski & Richardson, 2006).

Once downdrafts begin to dominate within the single-cell storm, they interfere with the remaining updraft regions, consequently leading to the rapid demise of the storm. This process explains the relatively short lifetime of such single-cell thunderstorms, often of the order of 25 to 45 min (Houze, 1993). Weisman & Klemp (1986) state that whilst severe weather may indeed occur in association with single-cell storms, such events are usually short-lived. This viewpoint is also supported by Houze (1993), who adds that multicell and supercell thunderstorms are the dominant sources of significant thunderstorm-related damage, such as strong winds, violent tornadoes and large hail.

2.2.2 Multicell cluster thunderstorms

Byers and Braham (1949) are universally acknowledged as being the initiators of the three stage life-cycle of a thunderstorm; from first initiation to maturity and thence the dissipative stage. Byers and Braham are also cited regarding conceptualisation of the structure of multicell thunderstorms (Houze, 1993; Weisman & Klemp, 1986). It is noteworthy that Houze (1993) describes single-cell storms as being the building blocks for multicellular storm structures.

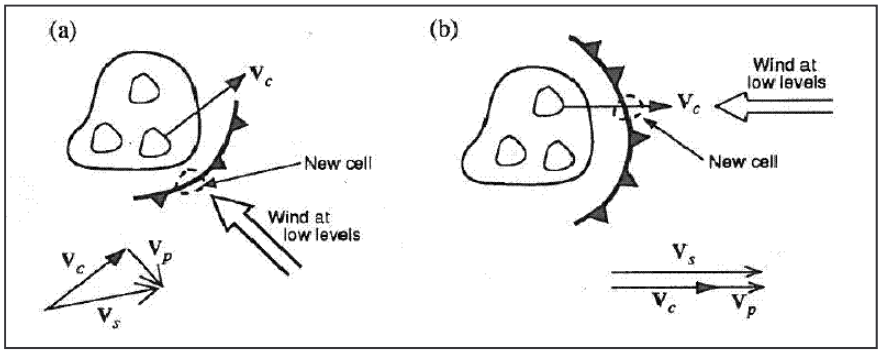

FIGURE 2.3: Conceptual plan view of multicell propagation and overall movement, according to whether the low-level inflow occurs (a) laterally, relative to cell motion, or in opposition to cell motion, as in (b). Barbed boundary in each of (a) and (b) corresponds to low-level outflow emanating from the storm complex. From Houze (1993).

Furthermore, Houze states that multicell cluster storms can be conceptualised as an agglomeration or clustering of single-cell storms, where the individual single-cells within this grouping still have a short life-cycle. Under particular conditions of low-level airflow interacting with cold outflow from the clustering of single-cells, low-level convergence areas can be initiated on the inflow side of the storm cluster, thus allowing for re-invigorated, fresh convective development along the upwind side of the storm cluster, as can be inferred from a multicell cross-section view presented in Fig. 2.4 whilst a plan view of two contrasing examples of multicell development are shown in Fig. 2.3 (a) and (b) respectively. In Fig. 2.3 (a), V_c and V_s indicate the storm cell velocity and the overall storm cluster velocity respectively. Furthermore, It will be seen in (a) that the low-level inflow is at a normal to the cell velocity vector V_c . As fresh cells continually develop along the cold outflow boundary on the inflow side, storm propagation (V_p) occurs in vector opposition to the orientation of low-level inflow. The vector sum [V_c + V_p] is thus the netto resultant vector V_s as viewed by an observer from a perspective above the storm. Similarly in Fig. 2.3 (b), following the same naming convention as in (a), the low-level inflow is in direct opposition to the cell movement, thus allowing for a multicell setup where the propagation vector V_p enhances the overall motion of the storm complex. In (b), as with example (a), the storm-complex motion vector V_s = [V_c + V_p]

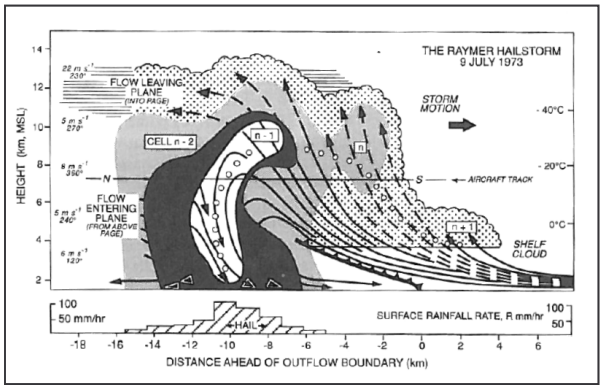

FIGURE 2.4: Schematic cross-section diagram of an observed multicellular thunderstorm complex near Raymer, Colorado, 9 July 1973. Storm motion is oriented from left to right, while low-level inflow enters the storm from bottom right of the image. As in the hypothetical multicell plan view in Fig. 2.3, the barbed boundary is the 'head' of the cold, density-current outflow spreading out at the base of the complex, deflecting the inflow stream into vertical uplift. The white core region was measured to exceed 50 dBZ and was associated with downward hail trajectories. Note the overhang towards the inflow side. Newest cells typically develop in the vigorous updraft region at right of image, whilst oldest cells occupy the left side of the complex. From Houze (1993), reproduced from Browning *et al*. (1976).

Notably, within the context of this research, it is important to mention some aspects of multicell storm structure and behaviour that are similar to those of supercells. Weisman & Klemp (1986), when discussing the overall motion of a multicell storm-complex, state that "The storm's motion as a whole, however, may deviate substantially from the mean wind direction, owing to the discrete redevelopment of cells." Furthermore, they mention that multicell storms may exhibit great longevity, due to the cyclic regeneration of fresh storm cells. Multicell storms can often become severe, being associated with hail and even short-lived tornadoes triggered by outflow boundary interactions, again according to Weisman & Klemp (1986). Heavy rain and flash-flooding are also likely to be associated with this storm type, especially when overall storm movement V_s is very low. In particular, two aspects are especially noteworthy here. Firstly, multicell storm complexes can exhibit deviant motion, as do supercells. Secondly, it is acknowledged that overall storm longevity of multicell complexes can be significant. Supercells storms are also associated with great longevity, however the distinction is that in the latter case, it is the individual storm cell that is sustained thoughout. Taking cognizance of the above, deviant motion and longevity alone are insufficient criteria upon which to classify a storm as being a supercell as these qualities are not unique only to supercells. Concepts relating to supercell identification criteria will however be revisited in Chapter 3 to follow.

2.2.3 Multicell line thunderstorms

Under certain favourable meteorological conditions, groups of thunderstorm cells become linearly aligned in unbroken or semi-continuous lines, commonly referred to as squall lines. Squall line thunderstorm features can typically extend laterally over distances of a few hundred kilometres. An in-depth analysis of the particular conditions favouring the development of squall line storms is beyond the scope of this research work. It is however useful to present a brief overview of the structure and structural features associated with multicell line storms in order to contrast this thunderstorm class with thunderstorm features typically associated with supercells. Squall line thunderstorms are grouped under the family of multicell thunderstorms,

although the structure of multicell line thunderstorms differs somewhat from that of multicell clusters described in the preceding section in 2.2.2. A typical plan and cross section view of a multicell line storm is provided in Fig. 2.5 (a) and (b) respectively. A significant defining feature of the structure of multicell line storms is the well-defined gust front which occurs along the leading edge of such storm complexes and which is often associated with strong downburst type wind events. This leads to so-called straight-line wind damage which is typical of such storm complexes. Tornadoes are also sometimes encountered in association with the gust front (Knupp *et al*., 2014). The outflow boundary of a typical single cell thunderstorm often manifests itself as an expanding radial feature, emanating from the base of the parent storm, however by contrast the primary outflow boundary associated with multicell line storms is focussed at the leading edge of the approaching storm complex, as shown in Fig 2.5.

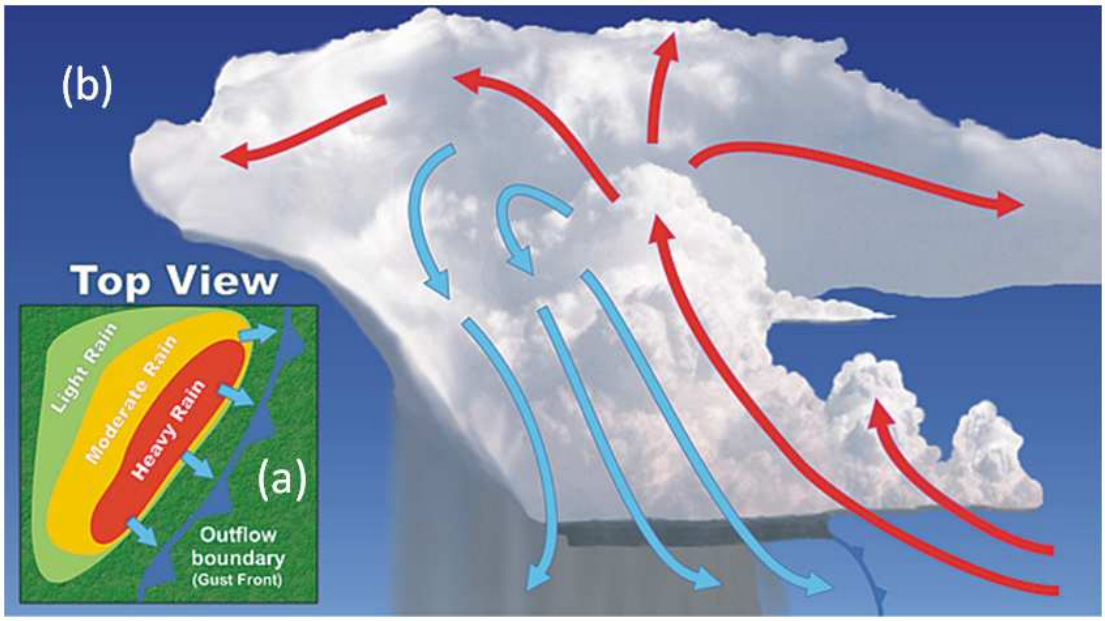

Figure 2.5: Plan view (a) and cross section view (b) of a typical multicell line storm, also commonly known as a squall line. Note how the outflow boundary is oriented on one side of the storm complex, forming a marked gust front along the leading (approaching) edge of the storm. From NOAA / NWS online resources at http://www.srh.noaa.gov/jetstream/tstorms/tstrmtypes.htm

2.2.4 Supercell thunderstorms

Supercell storms comprise the final class of thunderstorm types and as such are generally the most long-lived and organised of the four broad classes of thunderstorm (Houze, 1993). Glickman (2000) defines a supercell thunderstorm as "…an often dangerous convective storm that consists primarily of a single, quasi-steady rotating updraft…" and furthermore that "…it may exist for several hours and usually forms in an environment with strong vertical wind shear". Another statement attributable to Glickman is that "…severe weather often accompanies supercells, which are capable of producing high winds, large hail and strong, long-lived tornadoes…"

2.3 Severe thunderstorms

The National Severe Storms Laboratory (NSSL, 2014) as well as the National Weather Service (NWS) in the USA defines a severe storm as being the occurrence of a thunderstorm, accompanied by one or more of the following weather phenomena (Johns & Doswell ,1992):

- Large hail, greater than 19 mm diameter.
- Strong, damaging winds with measured gusts reaching or exceeding 26 m s^{-1}
- Any tornado, regardless of intensity thereof.

In terms of a suitable definition of a severe thunderstorm, the Australian Bureau of Meteorology (hereafter BoM) makes use of a similar definition to that of NSSL, but with the ancillary criterion of flash flooding (BoM, 2013). In South Africa, the South African Weather Service (SAWS) follows the same criteria as NSSL but with the distinction of two additional criteria, notably "significant urban flooding" and "large amounts of small hail" respectively (SAWS, 2013). In the research conducted for this dissertation the severe storm criteria as used by SAWS are applied when reference is made to the severity of any particular storm occurring within a southern African domain.

2.4 Supercell thunderstorms in general

Over a period spanning more than 50 years of the recent past, supercell storms have featured prominently in scientific literature, with the term supercell being first adopted by Browning (1962; 1964). A supercell thunderstorm is a storm with a deep, vertically extensive and persistent mesocyclone (Burgess & Lemon, 1990; Doswell & Burgess, 1993).

Historically there has been much debate relating to the defining characteristics of supercells (Doswell & Burgess, 1993), especially in terms of the relative merits of utilising particular observational or RADAR-derived criteria (Lynn, 2002). Furthermore, early work on conceptual models of supercells focussed strongly on supercells being prolific producers of tornadoes (Rotunno & Klemp, 1985). Schmid *et al*. (1997) documented case studies of supercells in Switzerland, particularly nowcasting implications thereof. Wang *et al.* (2008) conducted a comprehensive investigation of Taiwanese supercell cases wherein mention is made of supercell occurrences in France, citing Dessens & Snow (1993) as well as pre-monsoonal supercell events in India (Singh, 1981). Furthermore, Wang also cites Barnes (2001), asserting that supercells are "nearly nonexistent" in tropical regions due to a climatological lack of vertical wind shear.

In terms of supercell events within the southern hemisphere, Sills *et al.* (2004) explored a case-study of an Australian tornadic supercell storm event during the Sydney 2000 Olympic Games whilst Allen (2012) documented a multiple supercell event in the Melbourne, Australia area on Christmas Day 2011, with some of the latter storms being associated with tornadoes. Held (1978; 1981) is well-known for his work on severe hail storms in South Africa but he is equally acknowledged as a contributor to RADAR-based supercell case-studies in southern Brazil (Held *et al.*, 2006; 2010), utilising *inter alia* the TITAN storm tracking algorithm (Dixon & Wiener, 1993). An additional austral case of interest was reported by Louw (2014) who documented RADAR observations of a tornadic supercell near Geraldine, New

Zealand, exhibiting in particular a well-defined bounded weak echo (BWER) region (refer Fig. 2.19). There are numerous southern African references relating to the spectrum of extreme weather phenomena associated with severe thunderstorms, such as damaging hailstorms (Carte & Basson, 1970; Carte & Held, 1972; Held, 1978; Visser & van Heerden, 2000), severe winds (Goliger & Retief, 2007) as well as tornadoes (D'Abreton, 1991; Goliger *et al.*, 1997; Goliger & Milford, 1998; de Coning & Adam, 2000; Visser, 2001). Literature by southern African authors relating particularly to supercell thunderstorms includes Steyn & Hudak (1982), who documented RADAR-observed characteristics of a left-moving Highveld supercell storm between Steynsrus and Heilbron on 22 January 1982 in the Free State. Furthermore, de Coning *et al.* (2000a) investigated a long-lived supercell on the Highveld near Bethlehem, north-east Free State on 29th December 1997. Todd (2009) presented RADAR analysis of a particularly long-lived, left-moving supercell storm that developed near Potchefstroom on 5th November 2008. Pyle (2006) thoroughly documented the socio-economic aspects of severe thunderstorms in the Eastern Cape province of South Africa, making brief mention of supercells as well as the potentially devastating consequences of severe weather associated with such storms.

Tyson (1987) holds that occurrences of supercells in South Africa are fairly rare, an opinion echoed by Admirat *et al.* (1985), at least in terms of supercells maintaining a quasi-steady state. In addition, when referring to the general reported occurrence of supercells on the "South African Transvaal Highveld", Admirat *et al.* (1985) indicate "Few cases". More recently, the installation of a Doppler-enabled RADAR network across South Africa has enabled the routine identification and analysis of severe thunderstorms, especially in relation to typical characteristics associated with supercells.

There is recent southern African evidence of instances of multiple supercell thunderstorms occurring during so-called supercell outbreaks when as many as nine storms exhibiting RADAR-identified supercell-type characteristics were documented

over South Africa within a single day on 24 October 2010 (Powell *et al.*, 2010). Whilst Galway (1977) offered a basic and often-cited categorical classification of tornado outbreaks, a similarly accepted universal definition of an outbreak of supercell storms does not currently exist and remains elusive (Edwards *et al.*, 2004a). Notwithstanding this, the term supercell outbreak is introduced in this research in a colloquial context, largely to illustrate that such groupings of supercell phenomena are not only possible but are indeed encountered and documented from time to time in a southern hemisphere domain. The Christmas Day 2011 supercell outbreak in Melbourne, Australia (Allen, 2012) is one further such austral example. Yet another South African Highveld supercell outbreak case of great significance is that of 23 June 2012 (Loots, 2012), when a number of supercell storms occurred over the Free State and Gauteng during the passage of an intense winter cold front. Some of the supercell storms spawned tornadoes, with at least four individual tornadoes being confirmed photographically. According to Galway (1977), this type of event could be classified as a "small-sized" tornado outbreak.

2.5 Supercell Identification and structure

2.5.1 Supercell formation

Houze (1993) states that although the supercell storm is of a comparable size to a multicellular storm, the supercell cloud structure, air motion and processes controlling precipitation, are all "…dominated by a single storm-scale circulation consisting of one giant updraft-downdraft pair." There are two separate mechanisms whereby supercell thunderstorms may evolve and the nature of vertical wind shear plays a key discriminatory role as to determining which of the two processes will more readily be followed (Weisman & Klemp, 1986). The first mechanism involves thunderstorm growth within an environment that is characterized by well-defined speed and directional shearing within the lower few kilometres of the atmosphere closest to the surface. For the southern hemisphere, the most frequently

encountered orientation of shearing is an anti-clockwise tendency in wind direction, with increasing altitude. Supercell formation in the southern hemisphere is also possible but more uncommon when the shear orientation exhibits a clockwise shear tendency, resulting in atypical supercells which are discussed in more detail in sections to follow. For northern hemisphere supercells developing in a directionally sheared environment, the opposite holds true, with clockwise shearing being the typical climatological state of the atmosphere. The second mechanism whereby supercells evolve is typified by splitting storms developing in a unidirectionally sheared environment.

Weisman & Klemp (1982; 1984) experimentally determined that there is an optimum range of shearing that will favour supercell development and that under circumstances where shearing magnitude exceeds this optimum range, multicells will generally be favoured. The research conducted by Weisman & Klemp thus led to the development of the Bulk Richardson Number (also referred to as BRN or equivalently "R"). A representation of BRN versus storm type is indicated graphically in Fig. 2.6. Broadly speaking, increasing shear is directly proportional to a larger BRN. Whilst strong shearing favours multicells, there is a large region of overlap in BRN between supercells and multicells, given similar shearing scenarios and it is acknowledged that supercells and multicells occur along a continuum of shearing magnitude (Doswell & Burgess, 1993) and furthermore that multicells can evolve into supercells (Houze, 1993). Observational results have shown that BRN can discriminate well between supercells ($10 < BRN < 40$) and multicells ($BRN > 30$). It should be noted in Fig. 2.6 that there is a degree of overlap between BRN values associated with supercells and multicells. In other words the two categories are not mutually exclusive with respect to their respective range of optimal BRN values (BRN is indicated as "R" in Fig. 2.6).

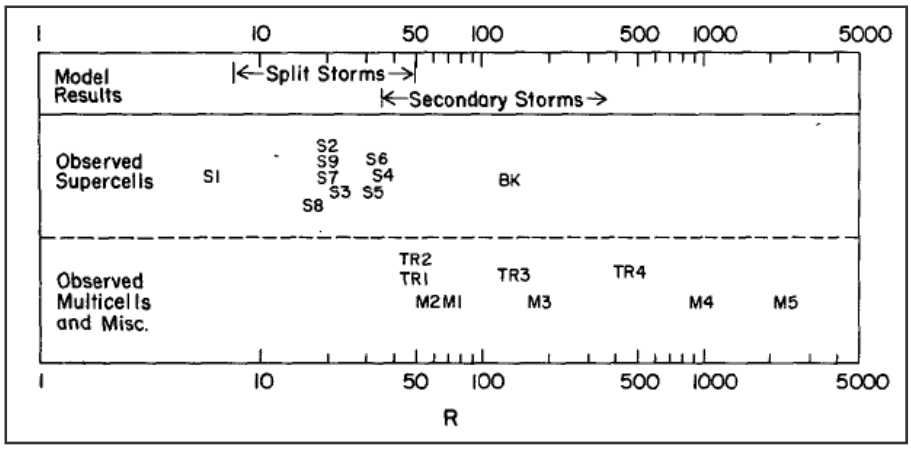

FIGURE 2.6: Richardson Number R (equivalent abbreviation BRN also in common use) as calculated for a series of documented storms. Numerically modelled results at top of Figure. Observed supercells indicated by 'S' prefix whilst 'M' prefix indicates multicell cases. Tropical events indicated by 'T'. From Weisman & Klemp (1982).

Cotton & Anthes (1989) as well as Houze (1993) provide an explanation about the dynamic process of storm splitting in a unidirectionally sheared environment. If one visualises a pre-storm environment where the lower layers are increasingly speed sheared, without measurable directional shear, as in Fig. 2.10 (a), the lowest layers near the surface are exposed to a shearing vector which induces a rolling or overturning motion in a roll or tube-like section of air, with the orientation of the tube at a normal to the shear vector, and the direction of overturning in the same direction as the shear vector orientation. Any local disturbance, such as hilly topography or localised heating imbalances, inevitably leads to lift and deformation in the vortex roll. Notably the local or relative vorticity of the roll has thus been shifted from a horizontal orientation into a vertical orientation, allowing for the rotation of two air columns in the vertical, each with an opposing spin. The thunderstorm inflow process often allows for the ingestion of large volumes of warmer, moist air with a largely horizontal vorticity to enter the thunderstorm updraft with the spin orientation shifted into the vertical, resulting in a helical spin within the updraft (Houze, 1993; Klemp, 1987). Furthermore Klemp (1987) states that numerical models as well as Doppler RADAR data confirm that linear tiling of horizontal vorticity is an important mechanism for the formation of in-cloud vertical vorticity, within convective clouds that form in significantly speed sheared environments. Houze (1993) mentions that, apart from the linear aspect of vorticity conversion from the horizontal into the vertical, there are also significant non-linear

effects, such as vortex stretching and associated conservation of angular momentum that need to be considered when regarding the dynamics of the rotating updraft.

For many years opposing theories existed as to the exact cause or trigger to initiate the splitting of thunderstorm cells containing rotating cores. RADAR-observed storm splitting events were observationally reported by Achtemeier (1975). Klemp & Wilhelmson (1978a) argued that precipitation drag in the cloud interior was the cause of the split. Conversely, a theory put forward by Schlesinger (1980) as well as Clarke (1979) was that mid-level entrainment of colder air was the cause. However, following numeric modelling experiments such as Klemp & Wilhelmson (1978a) it is now generally accepted that "…it is the vertical pressure gradient associated with the eddies on the updraft flanks that is responsible for the (storm) splitting…" (Houze, 1993).

Houze elaborates further by emphasising that, as the helical rotating updrafts on either flank of the storm intensify, a pressure minimum within the core of the updraft vortex intensifies in sympathy with the increase in angular velocity around the vortex. Furthermore, the magnitude of upward vertical velocity is promoted and also enhanced through vortex stretching, thus maintaining the updraft and further promoting increased low level inflow to feed the updraft. As the updrafts on the flanks of the storm intensify and begin to dominate the storm structure, mid-level entrainment of cooler, denser air is enhanced on the upshear side of the storm, combining with precipitation products. Consequently, the centroid of the storm becomes increasingly dominated by downdrafts as the storm splits and the flanks become increasingly spatially separated, again according to Houze (1993).

2.5.2 Conceptual models of supercell structure

Apart from the distinction of being credited with inventing the name "supercell", Browning (1962; 1964) was also the first to conceptualise models describing supercell formation and structure. Academic work relating to supercell

thunderstorms invariably records the historic contribution that conceptual models have made to the overall body of understanding relating to supercell thunderstorms (Lemon & Doswell, 1979; Weisman & Klemp, 1986; Burgess & Lemon, 1990; Doswell & Burgess, 1993).

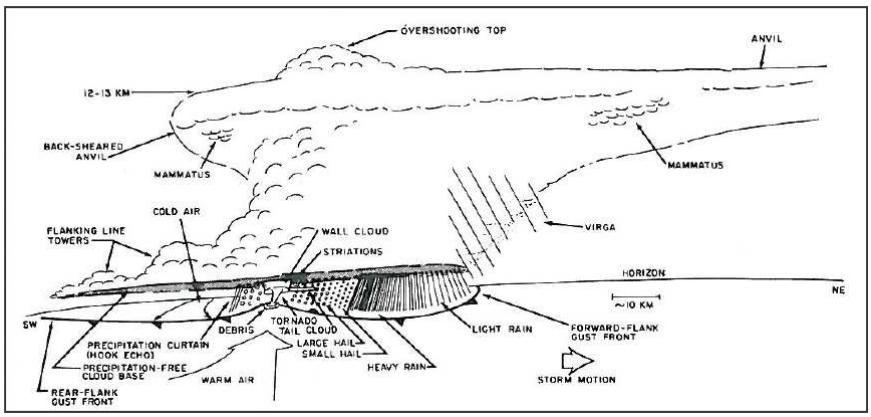

FIGURE 2.7: Conceptual sketch of the side view of a typical northern hemisphere supercell storm, together with typical thunderstorm and supercell thunderstorm distinguishing features. Based on U.S. NSSL publications and unpublished work by H.B. Bluestein, reproduced in Houze (1993).

It is relevant to mention that despite recent advancements in Doppler RADAR remote sensing of thunderstorm mesocyclones (Doviak & Zrnic, 2006), conceptual models still occupy a useful role in aiding and supplementing visualisation of the development and evolution of such thunderstorms, particularly from a three-dimension perspective (Visser, 2001). In the context of meteorological phenomena, the Austrian national *Zentralanstalt für Meteorologie und Geodinamik* (ZAMG, 2013) state that a conceptual model describes essential features of a meteorological phenomenon and identifies the principal processes taking place.

The early work of Browning (1962, 1964) relating to the conceptual modelling of supercell thunderstorms is seminal as it associated observed thunderstorm features, such as hook echoes and weak echo regions (hereafter WER) with a concept of which unique mechanisms and features, such as inflow orientation and updraft location, were typically associated with the formation of supercell storms. An excellent illustrative example of a conceptual model of the storm splitting process, presented in a discrete sequence of stages, is shown in Fig. 2.10, from Houze & Hobbs (1982) and reproduced in Houze (1993). Note in particular, in Fig. 2.10 (b) the collapsing

core and associated surface gust front and outflow, flanked on either side by strong, counter-rotating updrafts. This scenario was observed in the splitting storm at Harrismith, Free State province, on 15 November 1998 (Visser, 2001) in Fig. 2.9. It is useful to clarify that whilst this case-study is a good illustration of a splitting storm conceptual model, incidentally with the leftmost cell being tornadic for a brief space of time, Visser nevertheless remarks that in this particular case there is only limited or partial evidence to suggest that the tornadic storm cell was a supercell storm. Whilst the presence of counter-rotating mesocyclones in the 15 November 1998 case was inferred by Visser through animated analysis of RADAR reflectivity fields, he concedes that no well-developed weak echo regions (WER) were observed.

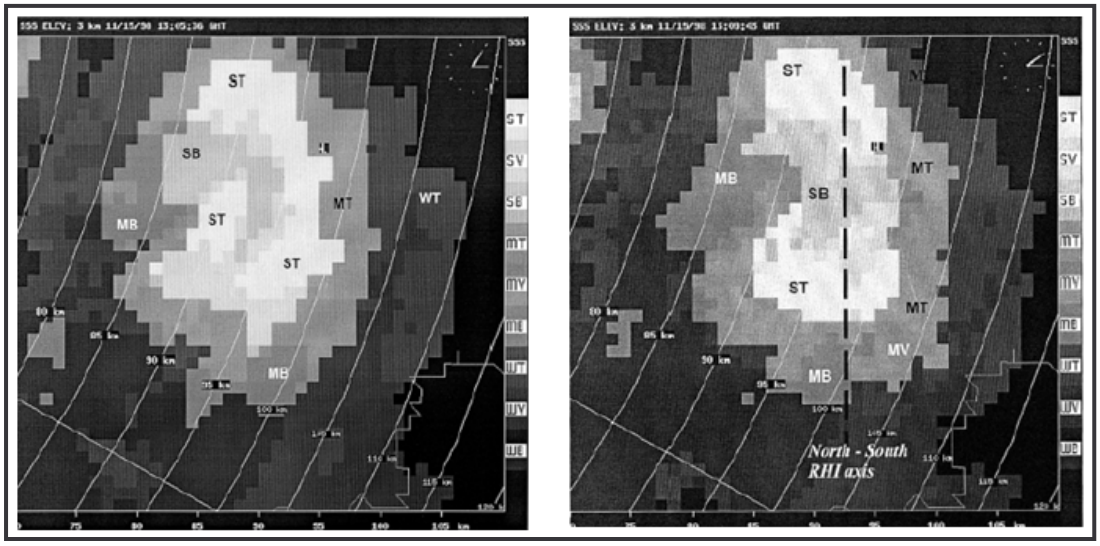

FIGURE 2.8: (a) and (b) Storm-splitting process observed during the 15 November 1998 Harrismith tornado incident utilising the SSS (Visser, 2001) visualisation of TITAN (Dixon & Weiner, 1993) at 13h05UTC in Fig. (a) and the corresponding following scan in Fig. (b) at 13h09 UTC. The northernmost storm intensified; developing a tornado near Harrismith (top right of image), approximately 90 km ESE of Bethlehem where this particular RADAR is located. The southernmost storm decayed soon afterward. Note the north to south cross-section transect line in Fig. (b), with reference to the corresponding RADAR cross-section in Fig. 2.9 . Reproduced from Visser (2001).

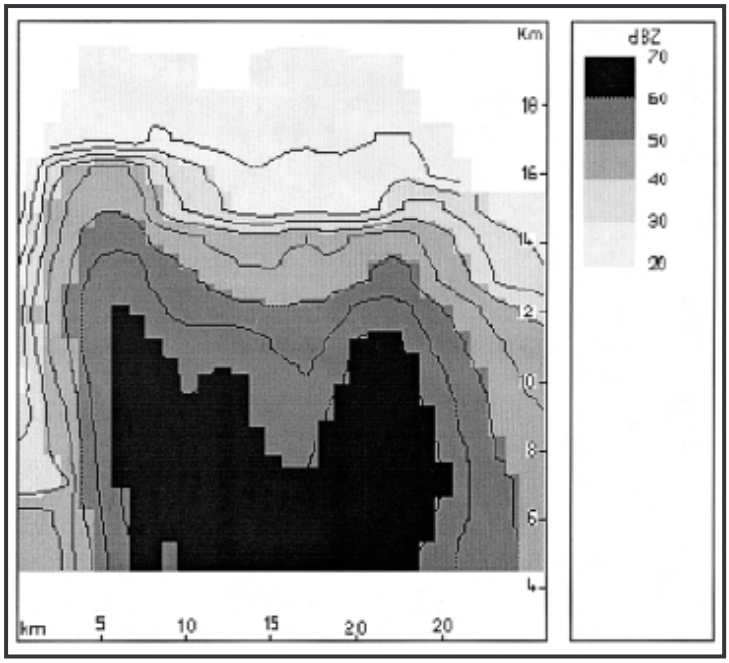

FIGURE 2.9: Continuing from the PPI RADAR view in Fig. 2.8 (b), a Range-Height Indicator (RHI) cross-section of the RADAR reflectivity (*dBZ*) at 13h09 UTC, revealing extensive peaks of cloud tops at left (north) and right (south) respectively. The region of lower reflectivity in the middle of the image corresponds to a central collapsing region, dominated by downdrafts. From Visser (2001).

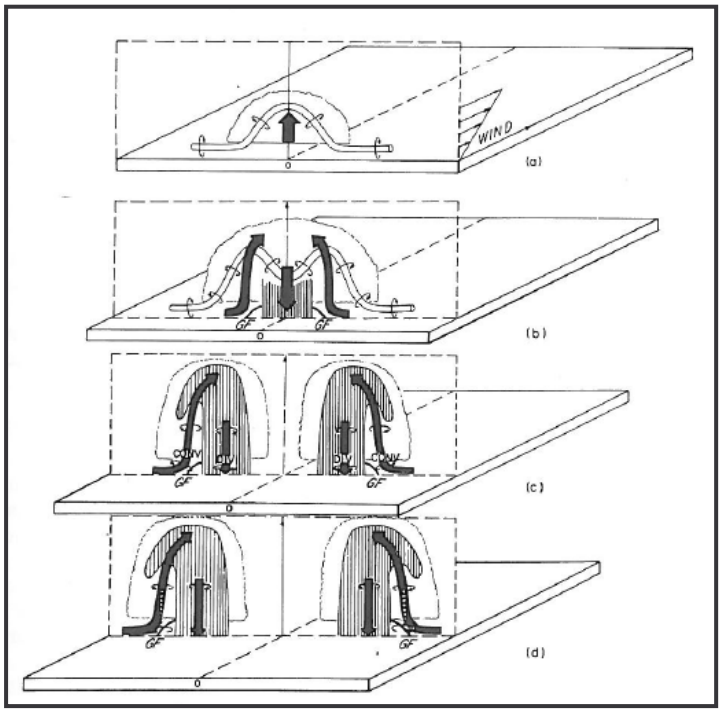

FIGURE 2.10: Schematic diagram (a) through (d) of the evolution of vorticity regions within a developing supercell prior to, during and after the storm splitting process. In particular, compare the region of descending downdrafts in diagram (b) to the RADAR cross section in Fig. 2.9 from Visser (2001). Diagrams (a) to (d) from Houze (1993) after Houze & Hobbs (1982).

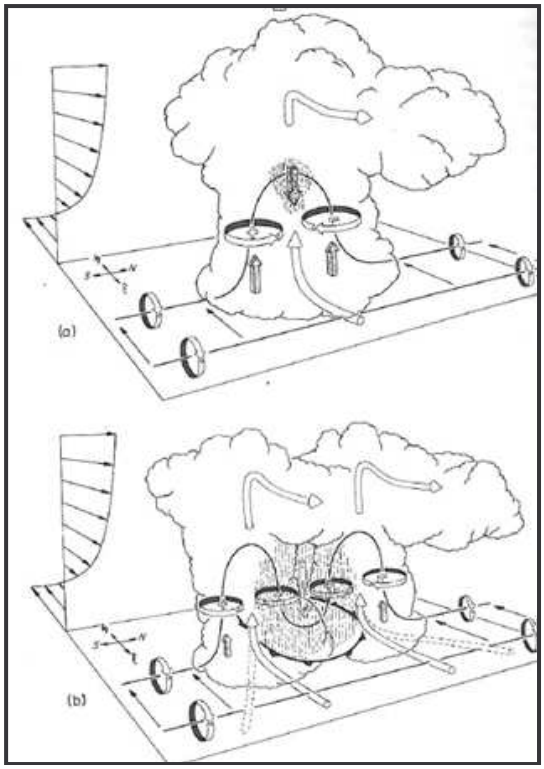

FIGURE 2.11: Conceptual schematic (northern hemisphere orientation) indicating in (a) low-level easterly winds overlaid by higher altitude westerly winds (north is to right of image) inducing a horizontal vortex roll which interacts with thunderstorm updraft, thus inducing rotation within the vertical as the vortex roll is ingested into the storm. In (b) the splitting stage is subsequently reached, where the collapsing core, dominated by downdrafts and rain products wedges in-between the two thunderstorm cells. The barbed line near the surface, at the head of the descending outflow, marks the cold outflow boundary. Compare to Fig. 2.9 from Visser (2001) elsewhere in this chapter. From Cotton & Anthes (1989) after Rotunno (1981), adapted by Klemp (1987).

2.5.3 Supercell characteristics

At the current time there is no standardised, universally accepted definition of a supercell which includes a list of the necessary and sufficient characteristics thereof. Notwithstanding this statement, a number of authors have proposed such lists (Doswell & Burgess, 1993, Moller *et al*. 1994, Lynn, 2002) and there is broad commonality and a fair degree of agreement regarding criteria for supercell identification. This aspect will be considered in more detail in Chapter 3 where the application of supercell characteristics to this particular study will be discussed. The following sub-sections expand on the history and background of the more commonly encountered supercell characteristics.

2.5.3.1 Persistent rotating updraft

There is universal acceptance of the requirement that a supercell thunderstorm must have a deep, persistent rotating updraft (Browning, 1964; Weisman & Klemp, 1984; Doswell & Burgess, 1993; Moller *et al*., 1994; Bunkers *et al*., 2000). In relation to the question of vertical extent of the rotating updraft, Bunkers *et al*. (2000) argue that rotation should ideally be observed through a layer of 2000m to 8000 m AGL whilst Doviac & Zrnic (2006) state that for a given storm, the vertical extent of mesocyclones can extend through the entire troposphere. Bunkers *et al*. (2000) also mention that in terms of temporal persistence the dipole of rotation (with respect to radial velocity) should persist for at least a matter of tens of minutes, in agreement with Moller *et al.* (1994). Regarding the horizontal spatial scale of such a thunderstorm cyclone or mesocyclone Doviac & Zrnic (2006) state that it is much smaller than that of a tropical or extra-tropical cyclone and is also typically of the order of a few kilometres in diameter.

The presence of a wall cloud feature (Fujita, 1960a; Forbes & Bluestein, 2001) embedded in the base of the thunderstorm is a further visual cue to confirm the presence of a mesocyclonic circulation within the storm. A wall cloud is a region where the cumulonimbus cloudbase is significantly lowered by approximately 200 m or more and furthermore may seem cylindrical or elliptical in cross-section. The swirling, orbital circulation of the mesocyclone can often be observed visually, particularly in the case of High-Precipitation (HP) supercells (Doswell & Burgess, 1993) although Forbes & Bluestein (2001) caution that clear evidence of rotation is not always visually observed in a wall cloud feature. Doviac & Zrnic (2006) also state that tornadoes associated with supercells are always preceded by either RADAR or visual confirmation of a mesocyclone and as such are spawned by the mesocyclone. In the absence of Doppler RADAR confirmation, the unequivocal visual observation of a persistent and clearly-defined thunderstorm wall cloud feature is thus significant in terms of confirming the presence of a mesocyclone and by implication a supercell thunderstorm. Southern hemisphere photographic examples of a wall cloud are presented in Fig. 2.12 and Fig. 2.13 respectively. The former case being associated

with the 25 December 2011 Melbourne, Australia supercell (Allen, 2012) whilst the latter occurred in association with the Bapsfontein, Gauteng supercell storm of 19 October 2013 in South Africa.

FIGURE 2.12: A striking example of a cumulonimbus wall cloud feature associated with one of the Christmas Day supercell storms of 25 December 2011 in Melbourne, Australia. Source: Allen (2012), AMOS Bulletin. Image © Brad Hannon.

FIGURE 2.13: A South African example of a well-defined wall cloud (with a hook feature in the mid-foregound, at right) associated with a supercell thunderstorm near Bapsfontein, Gauteng, Saturday 19 October 2013 at 14h15UTC. (Photo perspective is towards the south-east, from a point approximately 12 km ESE of the Irene RADAR). Compare to corresponding 3 km CAPPI scan in Fig. 2.16. Image © Craig Powell.

2.5.3.2 Hook echo

The hook echo feature (van Tassel, 1955; Forbes, 1981; Markowski, 2002) associated with supercells may be identified using the RADAR reflectivity field (Doviak & Zrnic, 2006) but will only be revealed at low RADAR elevation angles and also at relatively short horizontal range separation from the RADAR, due in part to the curvature of the earth. Cotton & Anthes (1989) state that the hook echo feature wraps around the weak echo vault (Chisholm & Renick, 1972). Thus the hook echo will be found in close association with the periphery of the base of the weak echo region, where the rear flank downdraft (RFD) curls back towards the low level inflow feeding the main updraft core, as seen in the plan view diagrams reproduced in Fig. 2.15 (a) and (b) (Lemon & Doswell, 1979; Weisman & Klemp, 1987). It is also notable that Cotton & Anthes (1989) argue that due to the evolutionary continuum between multicell and supercell thunderstorms, hook echoes may indeed be seen in intense multicell storms, but that such a feature would most ikely be a transient feature, unlike supercells where the hook echo would be more persistent from one RADAR scan to another (Doviak & Zrnic, 2006) and would be identifiable in at least a few consecutive scans.

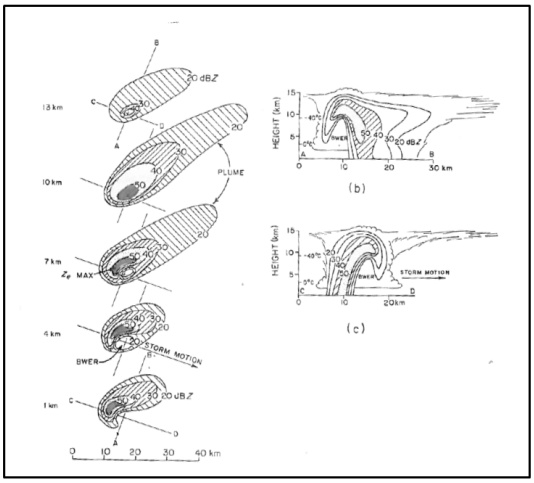

FIGURE 2.14: Orientation in this series of CAPPI scans is relative to a northern hemisphere storm. Note the Bounded Weak Echo Region (BWER) on the inflow side of the storm at 4 km altitude, whilst extensive, low reflectivity anvil "blowoff" can be seen at 7 km and higher. In (b), a cross section through A-B (at 1 km altitude) and similarly in (c), a cross-section through C-D (also at 1 km altitude) suggests the typical RADAR reflectivity cross-sectional appearance of a supercell, with the overhang of the BWER "leaning out" towards reference points A and D respectively. Originally from Chisholm & Renick (1972), reproduced by Weisman & Klemp (1986). Compare the BWER to a real-life RADAR cross-section example of the Potchefstroom supercell of 5 November 2008 (Northwest province, South Africa) in Fig. 2.18.

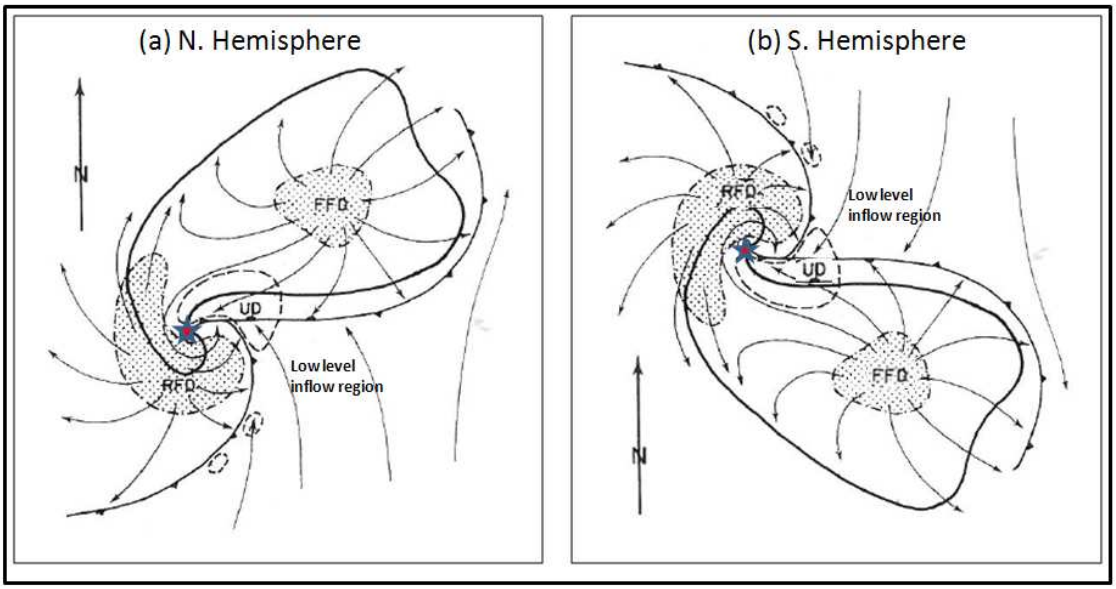

FIGURE 2.15: A conceptual model of a plan view of a supercell thunderstorm in (a) the northern hemisphere and (b) the corresponding diagram for the southern hemisphere, which has been rotated through 180 degrees along the equatorial axis to form a "mirror image" of diagram (a). In the figure, RFD and FFD refer to the preferred location of the rear flank downdraft and forward flank downdraft respectively. Source: (a) From Weisman & Klemp, 1986; after Lemon & Doswell, 1979. Diagram (b) adapted for the southern hemisphere by this author.

For typical northern hemisphere supercell cases it is relevant to mention that the orientation of the hook feature will be on the southern, equatorward, side of the storm as seen in Fig. 2.15 (a), whilst by contrast a typical southern hemisphere supercell will present this feature on the northern, equatorward, side of the storm as indicated in Fig. 2.15 (b). Furthermore, attention is drawn to the correspondence between the southern hemisphere conceptual model presented in Fig. 2.15 (b) and that of RADAR CAPPI plan view of two southern African case-study examples of supercells near Bapsfontein, 19 October 2013 (Fig. 2.16) and near Potchefstroom, 5 November 2008 (Fig. 2.17), where the location of the hook echo, indicated as "H" in the respective RADAR images, in relation to the "low-level inflow notch" can clearly be identified in accordance with the aforementioned conceptual model.

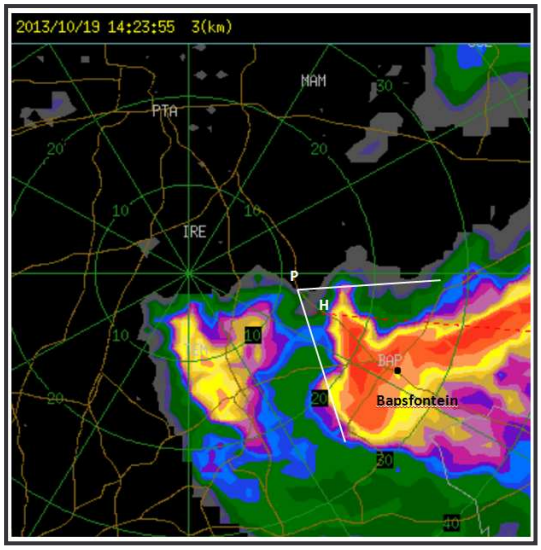

FIGURE 2.16: Irene S-band RADAR 3 km CAPPI reflectivity scan of the supercell thunderstorm near Bapsfontein, Gauteng, Saturday 19 October 2013 @ 14h23UTC, 8 minutes after the photo taken in Fig. 2.13. (Photo perspective towards the south-east, from a point approximately 12 km ESE of the Irene RADAR, as indicated by "P"). A prominent hook echo ("H") dominates the thunderstorm structure, with a BWER on the northern (equatorward) side of the storm. Image provided by C. Powell, SAWS. RADAR visualisation: TITAN software (Dixon & Weiner, 1993).

Doswell & Burgess (1993) also advise that in the context of RADAR-based supercell identification there are a variety of thunderstorm reflectivity features that might masquerade as, or falsely give the impression of, being a hook echo. Unavoidably there is much subjectivity related to RADAR identification of a hook echo, analogous in some respects to the interpretation of a Rorschach image (Rose *et al.,* 2001). Consequently Doswell & Burgess (1993) state that a RADAR analyst should strive to be as objective as possible and to consider additional supporting information as well as concurrent observations of supercell features such as WER or BWER when considering RADAR diagnosis of supercells, given a preliminary diagnosis of a hook echo feature.

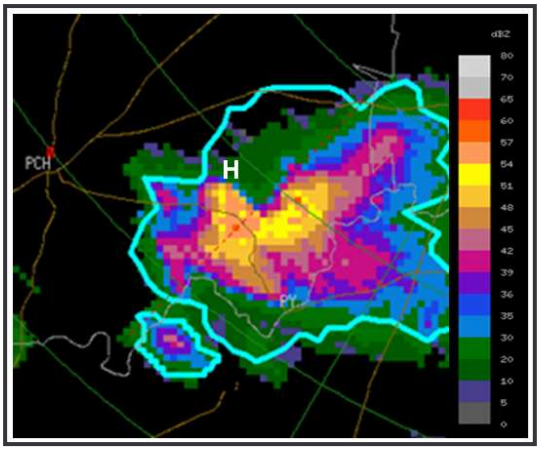

FIGURE 2.17: Supercell thunderstorm with well-defined hook echo feature ("H"), east south-east of Potchefstroom (indicated by PCH icon) on 3 km CAPPI reflectivity scan Irene C-band RADAR at 13h34UTC 05 November 2008. Light blue border represents boundary limits of the storm as determined by TITAN. The hook feature "H", on the NW side of the storm, corresponds closely with the 54-57 *dBZ* contour in this image. The storm was about 125 km distant from the RADAR at this time. Reflectivity scale (*dBZ*) at right of image. An image of the BWER from the same storm appears in Fig. 2.18. Source: SAWS Irene C-band RADAR, TITAN software. Dixon & Weiner (1993).

2.5.3.3 Bounded Weak Echo Region

The term bounded weak echo region (hereafter BWER) is attributable to Chisholm & Renick (1972). Glickman (2000) defines a BWER as being "A nearly vertical channel of weak RADAR echo, surrounded on the sides and top by a significantly stronger echo." Furthermore Glickman states that the bounded weak echo region is also referred to as a "vault", citing Browning & Ludlam (1962). Furthermore, the BWER occurs at mid-levels of convective storms at altitudes of 3000 to 10000 m AGL and has a horizontal diameter of a few kilometres.

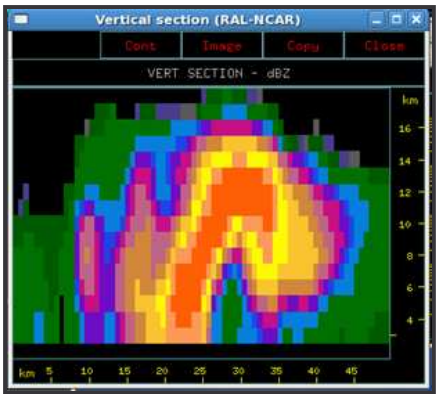

FIGURE 2.18: RADAR reflectivity cross-section of Potchefstroom supercell storm of 5 November 2008, Indicating a classic BWER at 13h47 UTC. Reflectivity of 50+ *dBZ* (in red) extends right up to 13-14 km in the overhang region. Source: SAWS Irene C-band RADAR, TITAN software. Dixon & Wiener (1993).

Weisman & Klemp (1984) utilised numeric modelling methods to determine that the spatial location of the BWER would be closely associated with the gradient of strong updrafts. Cotton & Anthes (1989) also recall the Browning & Ludlam (1962) hypothesis that the BWER is caused by air rising so rapidly within the strong updraft that there is insufficient time for RADAR-identifiable hydrometeors to form.

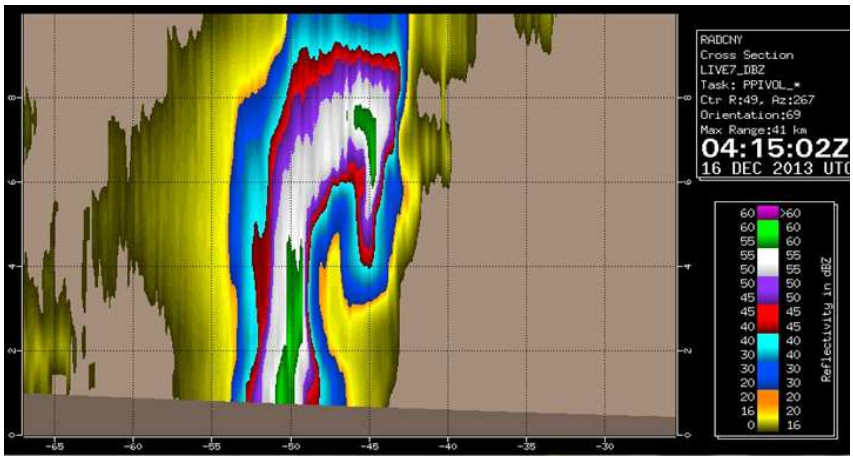

FIGURE 2.19: A RADAR reflectivity cross-section of BWER of supercell storm at 04h15UTC (16h15 local New Zealand time) near Geraldine (SE of Christchurch), New Zealand, 16 December 2013. BWER was approximately 44 km away from the RADAR, located on the north-eastern, inflow side of the storm. Source: New Zealand Metservice, image provided by E. Louw, Metservice (Louw, 2014).

Furthermore, Glickman (2000) defines a weak echo region (WER) as being "A region of weak RADAR echo that is bounded on one side and above by strong echo." The default location for a WER, or BWER, is on the low-level inflow side of the storm, where the inflow region feeds the strong updraft. In Fig. 2.14 (a) an idealised plan view of successive horizontal CAPPI slices of RADAR reflectivity (*dBZ*) through a typical supercell, indicates the low-level manifestation of the BWER is revealed as an inflow notch at the 1 km and 4 km CAPPI levels. Similarly in Fig. 2.14 (b) and (c) vertical cross-sections though this idealised conceptual model of a supercell, displays the classic high-reflectivity overhang or dome that spills over the very top of the BWER. A comparison of the conceptualised BWER in Fig. 2.14 (c) with a RADAR cross-section (Fig. 2.18) of an intense Southern African supercell case at Potchefstroom, 5 November 2008, shows remarkable similarity between the conceptualised and actual structures, despite the Potchefstroom storm being a southern hemisphere case.

2.5.3.4 Supercell motion and the concept of deviant motion

Concepts relating to thunderstorm motion were variously investigated in the period preceding 1960 (Byers 1942; Brooks, 1949; Byers & Braham, 1949; Newton & Katz, 1958). For northern hemisphere storms it was generally observed that non-severe storms moved parallel to the mean wind whilst larger, more severe storms were longer-lived, moved slower and to the right of the mean wind. Maddox (1976) introduced the 30R75 concept for northern hemisphere storms. In plain language the expression 30R75 simply represents a shorthand code or acronym, suggesting that predicted supercell motion would be 30 degrees to the right of the mean flow, with a vector magnitude of 75% of the mean storm speed. To arrive at the 30R75 concept, Maddox (1976) expanded on earlier work by Fankhauser (1971) as well as that of Marwitz (1972a). Colquhoun (1980) approached the question of supercell motion by applying an updraft versus downdraft mass equalisation scheme; based on ten subjectively selected severe storm proximity soundings. This method was, however, constrained by numerous rigid assumptions and did not enter popular usage. Davies & Johns (1993) subsequently utilised 31 right-moving supercell proximity soundings and modified the Maddox (1976) approach through the application of a dichotomous stratification based on the mean environmental wind speed within the lowest 6000 m AGL layer. For fairly weak winds Davies & Johns (1993) used the Maddox algorithm "as is" whereas for stronger flow above a subjective threshold of 15 m s^{-1}, the predicted supercell motion would become 20 degrees to the right of the mean flow, with 85% of mean wind speed. In other words 20R80 in accordance with the coding convention explained earlier. In subsequent work, Davies (1998) expanded on the Davies & Johns (1993) algorithm by adding a further option to accommodate very slow moving storms, allowing for the possibility of 80R60 (*i.e.* 80 degrees to the right, at 60% of mean wind speed).

All of the preceding methodologies regarding supercell movement have an unavoidable limitation, in that they are not Galilean invariant (Bunkers *et al*., 2000). Galilean invariance was first postulated by Galileo Galilei (Galilei, 1632), stating that

the laws of motion remain the same in all inertial frames of reference. Galilean invariance with respect to storm motion implies that one would arrive at identical shear-relative storm motion results, irrespective of where the hodograph lies with respect to the origin (Ramsay & Doswell, 2005). Historically, two supercell storm motion methodologies have evolved which are indeed Galilean invariant and are thus considered in the context of this research to be preferable to earlier, pre-1998 methods by their respective authors. Firstly, Rasmussen and Blanchard (1998) developed an algorithm based on 45 supercell proximity soundings, where for the first time, the effects of shear within the boundary layer, estimated to be the first 500 m AGL, as well as deep shear up to 4000 m AGL were considered. Secondly, Bunkers *et al.* (2000) also developed a Galilean invariant algorithm which has become known as the Internal Dynamics (hereafter ID) approach, or more popularly, "the Bunkers scheme". In this approach, Bunkers and collaborators were inspired by earlier work of Rotunno & Klemp (1985) and investigated a dataset of 130 right-moving supercells. A number of subsequent studies (Ramsay & Doswell, 2005; Zeitler & Bunkers, 2005) have corroborated the reliability and robustness of the Bunkers approach, versus alternative methodologies; affirming that the ID algorithm is indeed both superior and preferable to the various supercell storm motion methodologies discussed earlier.

2.5.3.5 Atypical supercells

Typical northern hemisphere supercells can be expected to move to the right of the mean flow whilst southern hemisphere supercells typically move to the left of the mean flow. It is however possible to occasionally encounter supercells which do not conform to this expectation. The storm splitting process allows for both a left-moving as well as a right-moving supercell to evolve from a bow echo structure. In the northern hemisphere, the right-moving cell will normally be favoured to evolve and develop further, whilst the left-moving cell typically decays and dissipates soon after the storm split has occurred. In the southern hemisphere, the converse typically applies, with the left-mover typically being favoured to evolve further. From

time to time the northern hemisphere left-mover, and its southern hemisphere right-mover counterpart, will continue to develop and evolve. This type of occurrence can be expected when the shearing flow is unidirectional in the vertical, a situation typically associated with multicellular storm development, when neither the left nor the right-mover is particularly favoured (Weisman & Klemp, 1984; 1986). There appears to be increasing academic interest in left-movers, or atypical supercells, in the literature (Edwards *et al*., 2004b; Edwards & Hodanish, 2004; Lindsey & Bunkers, 2005; Bunkers & Stopkotte, 2007; Blanchard, 2011)

Left-movers (and their southern hemisphere right-mover counterparts) are more likely to be associated with occurrences of large hail and strong, non-tornadic wind damage and are less likely to be tornadic in nature, at least according to northern hemisphere studies (Monteverdi *et al.*, 2001; Dostalek *et al*., 2004; Edwards & Hodanish, 2004; Edwards *et al*., 2004b). The results of Brown & Meitin (1994) suggest that 10% of northern hemisphere left-moving supercells are tornadic, whilst by contrast Bunkers & Stopkotte (2007) are even more conservative and suggest a corresponding percentage as low as 1%.

Another means of encountering unconventional supercell movement is driven by an anticyclonic shearing profile within the lowest few kilometres AGL in the pre-storm environment. Edwards & Hodanish (2004) documented a severe left-moving supercell which developed under anticyclonic shearing conditions whilst Blanchard (2011) used an anticyclonic supercell case study to draw particular attention to the significance of atypical hodographs and their potential operational use by forecasters to anticipate the development of such atypical supercells by a matter of hours or even up to a day ahead. Furthermore, Blanchard (2011) acknowledges the standpoint of Doswell (1995) and emphasises the need for effective situational awareness to correctly identify and anticipate similar pre-storm environments in an operational nowcasting context.

2.5.3.6 Lightning and the supercell mesocyclone

Numerous studies have been conducted relating to the spatio-temporal distribution and evolution of electrification within supercells (MacGorman *et al*., 2002; Lang *et al.,* 2004; Calhoun *et al*., 2013). One of the more significant discoveries to arise has been that of the phenomenon of "lightning holes" (MacGorman *et al.,* 2002) where the superposition of total lightning and RADAR data led to the discovery that, whilst the periphery of the mesocyclone may well be associated with frequent and intense lightning discharge, the core of the mesocyclone is often characterised by a general absence of lightning activity. In many cases, this spatial discontinuity of discharge is so marked that it is manifested in plan view as a circular gap or hole, hence the term "lightning hole", also referred to by Calhoun *et al*. (2013) as "a lightning ring around a lightning hole". This discovery is highly significant, both from a research as well as an operational perspective as it potentially adds an additional tool to the range of measures by which supercells may be identified. Lang *et al*. (2004) extended this model to include the BWER feature, holding that the BWER was similarly characterised by an absence of lightning, although more recently Murphy & Demetriades (2005) have countered this viewpoint, stating that the patterns of lightning distribution are more complex than earlier studies suggest. Calhoun *et al*. (2013) also offer that the lightning hole is a relatively transient feature (duration ≤ 20 minutes) that is roughly co-located with the BWER but typically not of the same shape as the BWER and of the order of 7 km to 12 km in horizontal extent. Other relevant results offered by Murphy & Demetriades include (1) the finding that the manifestation of such "lightning holes" occurs cyclically, with a period of about 15 minutes, (2) "lightning holes" are best observed in slower-moving supercells and (3) that such features can successfully be identified even given a lightning data resolution as low as 2x2 km for 2D spatial plots. Lastmentioned finding opens the possibility for such holes to be identified from 2D plots, rather than 3D plots used in the studies cited above.

Whilst it was mentioned that SAWS LDN lightning network data was used for the current study, in terms of identifying "thunderstorm days", this particular LDN network senses and records cloud-to-ground (CG) discharges only and as such is a subset of overall or total lightning activity. The latter includes intra-cloud as well as "cloud to clear air" discharges and it is total lightning upon which the abovementioned studies are based, thus making the SAWS LDN data network, in its current configuration, unsuitable for such an application. However, should the SAWS LDN network be upgraded at a future time to have the capacity to sense and display total lightning activity, the phenomenon of "lighting holes" could prove to be a robust means of identifying and tracking supercell storms in a separate but complimentary manner to that of RADAR.

2.5.4 Features not limited only to supercells

2.5.4.1 Overshooting top

The observation of an overshooting top feature associated with a cumulonimbus thunderstorm cloud is indicative of the presence of a vigorous updraft. Glickman (2000) defines an overshooting top as "A domelike protrusion above a cumulonimbus anvil, representing the intrusion of an updraft though its equilibrium level." In addition, he asserts that "Tall and persistent overshooting tops are frequently observed with strong or severe thunderstorms…" The presence of a strong updraft may hint strongly at a tendency or a predisposition for such a storm to exhibit severe thunderstorm characteristics (Bedka *et al.*, 2011) however he cautions that this relationship has only conclusively been demonstrated in 16% of cases for a very large dataset using geostationary satellite data.

The question as to whether the aforementioned updraft associated with an overshooting top is indeed rotating helically in the mid-levels of the storm, deeming said storm to be mesocyclonic (Houze, 1993) and hence supercellular would require

additional supporting information other than naked eye observation of an overshooting top before a categorical declaration could be made as to the supercellular nature of said storm (Doswell & Burgess, 1993). For example, Doppler RADAR imagery of the storm would conclusively confirm the existence of a mesocyclone (Doviak & Zrnic, 2006).

In summary, an overshooting top merely hints at a likelihood that the storm may be severe or has the capacity to become severe. While the overshooting top is the visible by-product or consequence of a vigorous updraft, this feature alone is insufficient evidence to suggest classification of the storm as being a supercell.

2.5.4.2 Thunderstorm longevity

Burgess *et al.* (1982) state that the average lifespan of a supercell thunderstorm is one to two hours. This fits well with Weisman & Klemp (1986) who state that "A supercell usually reaches its mature, quasi-steady phase within 90 minutes…". In 2006 studies focusing on long-lived supercells, Bunkers *et al.* (2006a; 2006b) selected a lifespan of four hours as the lower threshold for their dataset of long-lived supercells but were careful to emphasise that the threshold of four hours was arbitrarily chosen. Furthermore, they emphasise that there is no universally accepted formal definition of a long-lived supercell. Edwards (2006) documented a number of Mexican supercells with lifespans of six to seven hours, hinting at the likely upper bounds of longevity for supercell storms. An exceptional example of a long-lived southern African Highveld supercell was documented by Clark (2004) wherein a deviant left-moving supercell was tracked on the Irene C-band RADAR on 27 October 2004, moving north-east across Gauteng from 11h36UTC to 18h43UTC, an overall storm duration slightly exceeding seven hours. Hail corresponding to golf ball size was reported at most localities in the path of said storm.

Bunkers *et al.* (2006a) state that a distinction in nomenclature is required between a long-track supercell and a long-lived supercell. In the former case, the storm could

merely be carried along at a brisk ground-relative speed due strong airflow aloft, whilst the temporal lifetime of the storm however might not be markedly longer than that of a typical supercell. In addition, another significant finding of Bunkers *et al.* (2006a) is that that long-lived supercells tend to be more isolated and discrete in relation to spatial separation from other storms as opposed to shorter-lived supercells.

2.5.5 Supercell types

In the context of this research, it is not essential to explore in great depth the different sub-types of supercells, however, it is useful to briefly mention that these variations or sub-types of supercells do exist. Doswell & Burgess (1993) emphasise that despite the three main classes listed below, supercells may nevertheless manifest themselves as one or more of a number of variational hybrids of these classes. The three sub-types of supercells are namely Classic-, High precipitation (HP) and Low precipitation (LP) supercells and are briefly described in the sections to follow.

2.5.5.1 Classic Supercell

The Classic supercell is the familiar textbook manifestation of the supercell, with a RADAR plan view that, in appearance, is somewhat reminiscent of a kidney-bean or perhaps a cashew nut, as replicated in Fig. 2.20 (a) This type of storm can deliver large hail and moderate to strong tornadoes, due to well-developed FFD and RFD features, combined with fairly strong mid- to upper-tropospheric flow according to Doswell & Burgess (1993). Typically whilst there may be precipitation visible at the base of the storm, it is generally not of a heavy nature. Classic supercells are readily identifiable on RADAR and are often associated with a full range of severe weather, including strong to violent tornadoes. In the opinion of Doswell & Burgess (1993), if a hook echo is indeed identifiable, the PPI RADAR reflectivity (dBZ) thereof is usually quantifiably lower than that of the precipitation core in contrast to that of the HP supercell.

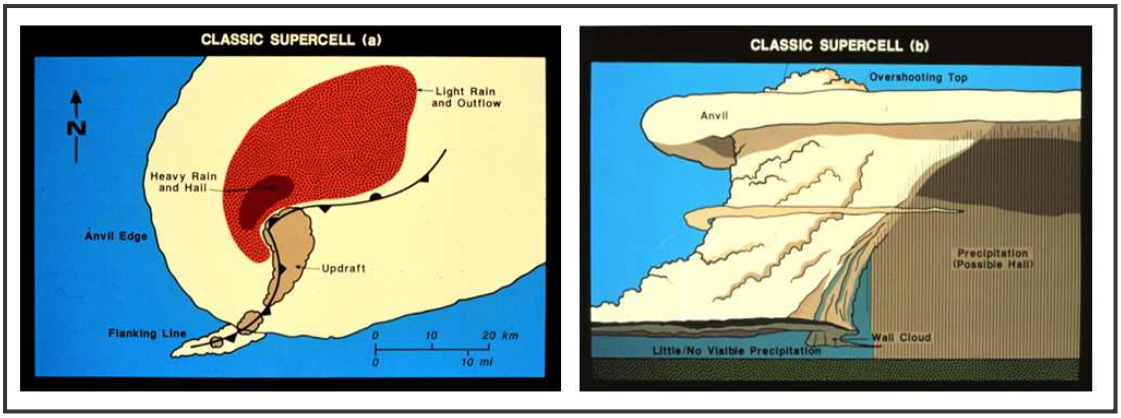

FIGURE 2.20: (a) At left an idealised plan view of a Classic supercell. At right (b) the corresponding side view of the storm. From Doswell & Burgess, 1993.

2.5.5.2 High precipitation (HP) Supercell

HP supercells characteristically form in more moist environments and are notable for significant rainfall in close association with their mesocyclone (Doswell & Burgess, 1993). They also found that in the USA, HP supercells are the most commonly encountered supercell sub-type. In the case of an HP storm, visual confirmation of a wall cloud is often impaired by the presence of *virga* and/or stratus fractus cloud. They suggest that RADAR assessment of such storms will readily and conclusively confirm the presence of a mesocyclone as there are many hydrometeors to enhance overall RADAR reflectivity. The hook echo (Forbes, 1981) feature is often well-defined. Furthermore, the level of RADAR reflectivity (*dBZ*) is often similar to that of the precipitation core (Doswell & Burgess, 1993). An idealised plan and side view of an HP supercell is presented in Fig. 2.21 (a) and (b) respectively.

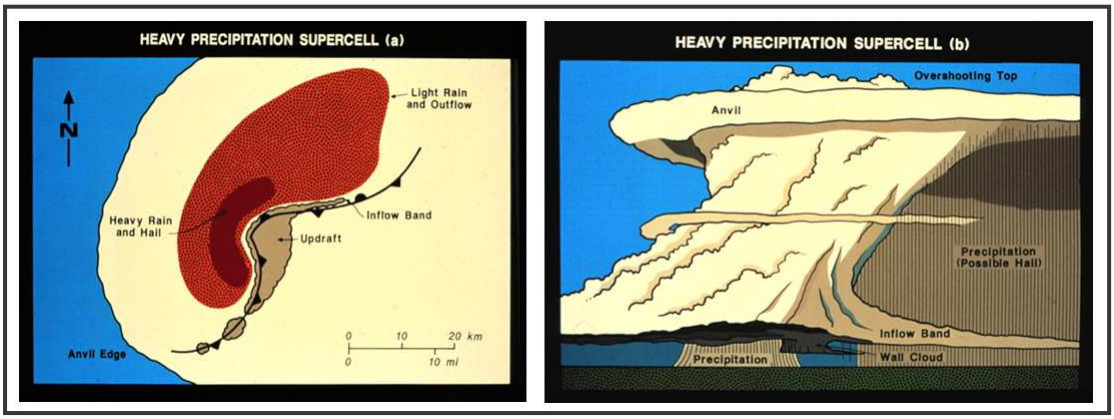

FIGURE 2.21: (a) At left an idealised plan view of a heavy/high precipitation (HP) supercell. At right (b) the corresponding side view of the storm. From Doswell & Burgess, 1993.

2.5.5.3 Low precipitation (LP) Supercell

This type of supercell is associated with a generally drier atmosphere and is often encountered near the surface dryline (Doswell & Burgess, 1993). This type of supercell typically has a more elevated cloudbase as can be seen in Fig. 2.22(b), with *virga* (precipitation fallstreaks) correspondingly being more distinctive and clearly identifiable. This type of supercell is generally associated with precipitation that is less heavy than in the HP supercell type or in the Classic type (Bluestein & Parks, 1983). LP supercells are frequently non-tornadic and often non-severe, despite rotation being present in the mesocyclone. Classic RADAR characteristics traditionally associated with supercells, such as a hook echo (Forbes, 1981) are often lacking in this supercell sub-type (Doswell & Burgess, 1993).

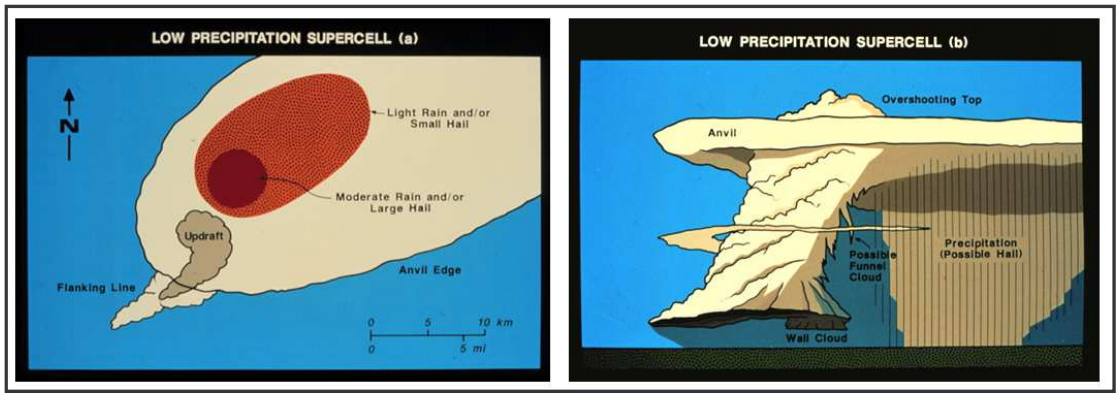

FIGURE 2.22: (a) At left an idealised plan view of a low precipitation supercell. At right (b) the corresponding side view of the storm. From Doswell & Burgess, 1993.

2.6 Hodographs

Hodograph plots of upper air sounding profiles have long been utilised to aid and inform better understanding surrounding the nature of the prevailing speed- and directional shearing profile for a pre-storm environment and to predict or guide the most likely nature and type of thunderstorm development to be expected (Doswell, 1991) as well as the movement thereof (Bunkers *et al*., 2000).

A hodograph may be visualised in the mind of the reader as being representative of an overhead, plan view of the sounding launch site, with the four primary compass points orientated such that North is uppermost on the page. Each wind vector retrieved from the sounding profile, possessing information both in terms of wind speed as well as wind direction, is then plotted on this common axis system. Each vector is represented as a scaled arrow and each vector, from the initial surface wind measurement upwards, is successively plotted on the hodograph using a common origin (0,0) each time a new vector is plotted. This representation can be visualised in Fig. 2.23 (a) where a hypothetical hodograph is presented, with each wind vector shaded in green. When the vector arrowhead tips of each vector are joined, as in Fig 2.23 (b), represented by red dots joined by solid line segments, this becomes the hodograph trace itself.

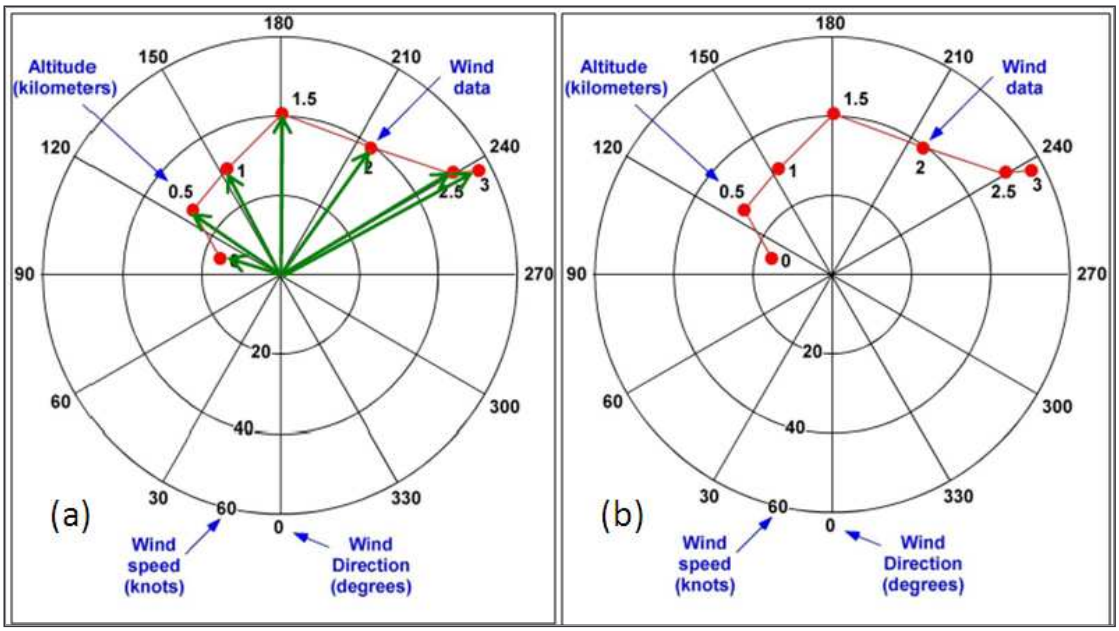

FIGURE 2.23: Construction of a hypothetical northern hemisphere hodograph typically based on upper air sounding or NWP data, showing successive scaled wind vectors represented as green arrows plotted with a common origin in (a). The hodograph trace is formed by simply connecting each arrowhead to its adjacent partner, starting with the surface wind vector, following each vector in turn, up to the final wind reading. The hodograph trace is indicated as a succession of red line segments, interspersed with red dots as in (b). From U.S. NWS, Louisville, Kentucky, USA. Link: http://www.crh.noaa.gov/images/lmk/Hodographs_Wind-Shear.pdf

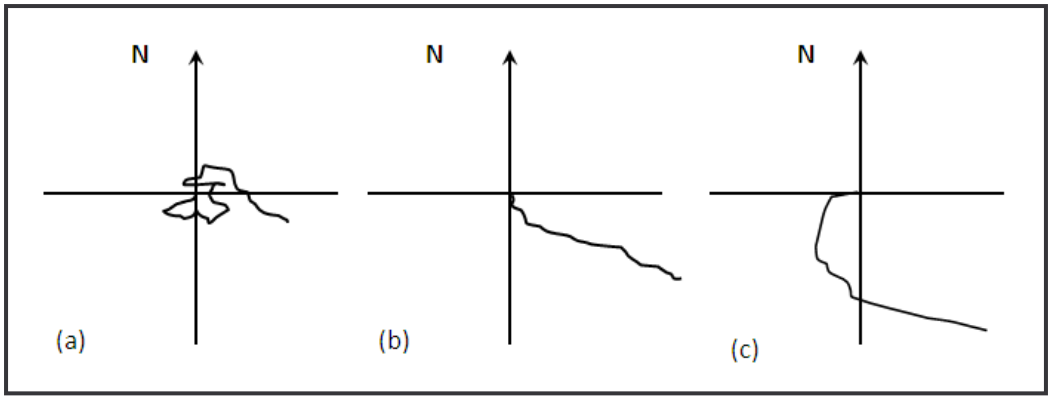

FIGURE 2.24: Hypothetical hodographs, orientated relative to the southern hemisphere, with North towards top of page, indicating typical hodograph profiles which would favour: (a) single cell, airmass thunderstorm, (b) multicell thunderstorm and (c) typical sickle-shaped shearing profile that is characteristic of supercell storms. Originally from McNulty (1995), after Chisholm & Renick (1972), adapted and re-orientated relative to the southern hemisphere by this author.

There is much that can be inferred graphically from such a representation, adding value to the overall picture of speed and directional shearing within the vertical wind profile (VWP). The hodograph is thus a plot of vertical wind shear from one level to the next. Fig. 2.24 is a textbook-type representation of typical hodographs associated with the main thunderstorm types introduced in Chapter 2, with Fig. 2.24 (c) indicative of the typical sickle-shaped shearing profile to be expected in association with a southern hemisphere supercell.

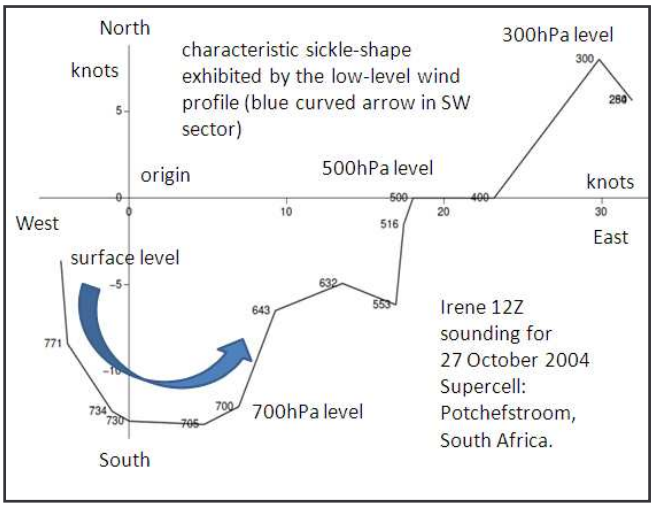

FIGURE 2.25: Irene, Gauteng 12h00UTC 27 October 2004 Hodograph, representative of a typical southern African Highveld supercell storm sounding, with a classic sickle-shape profile, self-evident in the south-western and south-eastern quadrants. Numeric inscriptions on the hodograph trace represent (decreasing) air pressure values (hPa) corresponding with each successive wind observation. This sounding corresponds to the date of the 2004 Potchefstroom supercell case. Data and hodograph image source: University of Wyoming. Link: http://weather.uwyo.edu/upperair/africa.html

In the case of northern hemisphere hodographs, the equivalent profiles in each case of (a) to (c) would simply be represented as a mirror image rotated along the equatorial or West-East hodograph axis. Fig. 2.25 displays a typical southern hemisphere case-study example of a supercell type of profile, from the midday Irene sounding performed on the day of the 27 October 2004 Potchefstroom supercell and has much in common with the corresponding conceptual pattern offered in Fig. 2.24 (c).

2.7 Components of the Supercell Composite Parameter

The Supercell Composite Parameter (SCP) was first developed at the NOAA/NWS Storm Prediction Center (SPC) in the USA by Thompson *et al.* (2002) to identify areas of supercell potential through a combination of several thermodynamic thunderstorm parameters. In order to better understand the rationale behind the composition of SCP, it is now appropriate to introduce each of the three factors of SCP in turn. The SCP formula and its various iterations are then introduced thereafter in section 2.7.4.

2.7.1 Convective available potential energy

Convective Available Potential Energy (hereafter CAPE) from Moncreiff & Miller (1976) is defined in equation (1):

$$\mathrm{CAPE} = g \int_{Z_{LFC}}^{z_{EL}} \left(\frac{T_{v_p} - T_{v_e}}{T_{v_e}} \right) dz \qquad (1)$$

where:

g is acceleration due to gravity (≈ 9.8 m s^{-2})

T_v is virtual temperature with respect to the parcel (V_p subscript)

T_v is virtual temperature with respect to the environment (V_e subscript)

z_{LFC} is the height (LFC) for the lower boundary of the integral

z_{EL} is the upper boundary of the integral, at the equilibrium level (EL)

dz implies integration in the vertical, with respect to Z (altitude)

In equation (1), one considers the virtual temperature between the level of free convection (hereafter LFC) and the upper, equilibrium level (EL) of a hypothetical parcel of air as it is raised along an appropriate saturated adiabat. The difference between the virtual temperature of the parcel and that of the environment is expressed as a relative proportion (quotient) of the virtual temperature of the environment. This quantity is then integrated with respect to z, extending from the LFC, up to the EL. CAPE is often, albeit mistakenly, thought of as being a quantification of buoyancy but it is more correctly an expression of the relative potential of the column to be conditionally unstable, on condition that the parcel attains the level of free convection to enable free, unimpeded ascent.

Most Unstable CAPE (MUCAPE) represents a variation on the standard definition of CAPE as presented in equation (1) and is defined as the largest resultant CAPE that can be calculated within the lowest 300hPa of a particular upper air sounding for a particular parcel (Doswell & Rasmussen, 1994). In an iterative approach, starting at the surface, data pairs of temperature (T) and dewpoint (T_d), measured at particular pressure levels, are lifted to their local condensation level (LCL). If free ascent can be established, then a CAPE integral is performed. This process is then repeated for all (T,T_d) data pairs throughout the lowest 300hPa of the sounding. The greatest individual CAPE resultant determined in this manner is then deemed to be MUCAPE. As such, MUCAPE has a desirable quality in that the iterative approach allows one to overcome the hurdle of low-level inversions, which often prevent or severely inhibit, free ascent taking place.

In the context of temperature profiles within the troposphere, an inversion is simply a rise of temperature with increasing altitude, in contrast with the typically-

encountered phenomenon of a lowering of temperature with increasing altitude. Such inversion features act as obstacles which inhibit or negate the free ascent of air. Through the calculation of MUCAPE, one is thus able to simulate, to a fair degree, CAPE that would have been calculable via the standard method in (1), should low-level capping inversions not have been present. However, on the other hand, it can be argued that MUCAPE can produce overly-optimistic estimates of CAPE, especially in circumatances where capping inversions are particularly well-defined.

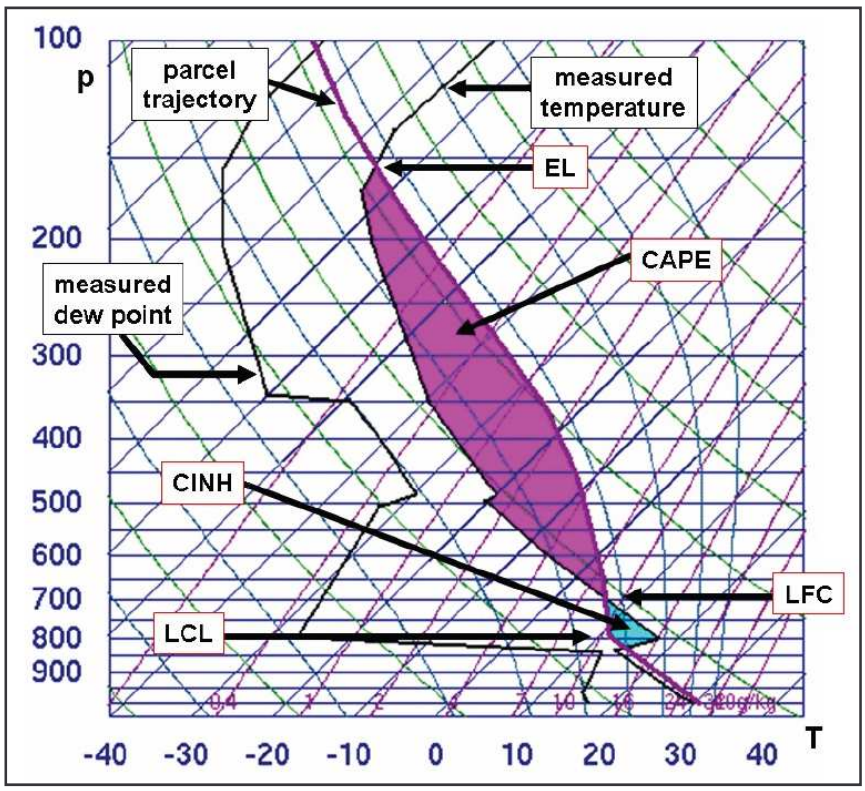

FIGURE 2.26: A skew-*T* / log-p sounding diagram, indicating the location of lifting condensation level (LCL), level of free convection (LFC), negative CAPE or CAPE deficit region also known as CAPE inhibition (CINH) indicated in solid light blue, the positive CAPE region indicated in solid purple. The equilibrium level is also indicated (EL). Temperature (*T*) in degrees C along the horizontal axis. A logarithmic pressure (p) scale (hPa) indicated in the vertical. LCL and LFC positions in this representation are relative to the observed surface *(T, T_d)* pair, delivering a surface-based CAPE (SBCAPE) value if there is no intervening inversion. Source: From Dahl (2006), originally adapted from University of Wyoming online site at: http://weather.uwyo.edu/upperair/sounding.html

Surface Based CAPE or SBCAPE (Doswell & Rasmussen, 1994) is calculated similarly to equation (1) but with the substitution of z_{LCL} (in other words, the height of the local condensation level) instead of z_{LFC} as the lower bound and the expression thereof is provided in (2). In the event that LCL and LFC coincide, then positive CAPE

may thus be integrated, however, if a capping inversion separates LCL from LFC as in the example in Fig 2.26, then SBCAPE is identically zero. Hence SBCAPE is often perceived as being too conservative for realistic estimates of CAPE.

$$\text{SBCAPE} = g \int_{z_{LCL}}^{z_{EL}} \left(\frac{T_{v_p} - T_{v_e}}{T_{v_e}} \right) dz \qquad (2)$$

where:

g	is acceleration due to gravity (≈ 9.8 m s^{-2})
T_v	is virtual temperature with respect to the parcel (V_p subscript)
T_v	is virtual temperature with respect to the environment (V_e subscript)
z_{LCL}	is the height (LCL) for the lower boundary of the integral
z_{EL}	is the upper boundary of the integral, at the equilibrium level (EL)
dz	implies integration in the vertical, with respect to Z (altitude)

Another variation of CAPE is Normalised CAPE (hereafter NCAPE) defined by Blanchard (1998). Utilising CAPE calculated with the virtual temperature correction T_v (Doswell & Rasmussen, 1994) and integrating from the level of free convection (LFC) up to the equilibrium level (EL). This form of CAPE calculation is equivalent to the classic formulation presented in (1) earlier, however with the distinction that Blanchard divided the resultant CAPE by the vertical distance in metres over which the integration took place. In other words, the difference in altitude between the lower and upper bounds of the integral. Through the application of NCAPE, Blanchard sought to compare various shapes of CAPE integral profiles on a more equal footing. The rationale was that a CAPE integral which presented a “short and fat” profile could be compared against a different CAPE profile which might appear “tall and skinny” on an aerological diagram. In the case of the former, one would encounter a smaller [$z_{EL} – z_{LFC}$] combined with large contributions by [T_v (parcel) – T_v (environment)] whilst conversely the latter would be typified by smaller, more conservative values of [T_v (parcel) – T_v (environment)], accumulated over a greater [$z_{EL} – z_{LFC}$]. While Blanchard’s approach in terms of reconciling these two numeric

extremes was certainly innovative, NCAPE remains less popularly utilised than other forms of CAPE presented in this work. Bearing in mind that the standard unit of CAPE is Joule per kilogram (J kg^{-1}), the corresponding units of NCAPE are J kg^{-1} m^{-1} or equivalently $m\ s^{-2}$ which, in the latter case, according to Blanchard is an expression of acceleration. Therefore, division of (1) by the term $[z_{EL} - z_{LFC}]$ results in NCAPE, symbolically formulated as:

$$\text{NCAPE} = g\,[z_{EL} - z_{LFC}]^{-1} \int_{z_{LFC}}^{z_{EL}} \left(\frac{T_{v_p} - T_{v_e}}{T_{v_e}} \right) dz \qquad (3)$$

2.7.2 Storm-relative helicity

In the discipline of atmospheric science, Lilly (1985) is credited with elevating the concept of helicity into mainstream use by exploring the hypothesis that "…these (supercell) storms owe their long life, stability and apparent predictability to the helical nature of their circulation." Lilly cites earlier fundamental work by Betchov (1961) as well as mentioning that the term "helical cyclogenesis" was introduced by Levitch & Tzvetkov (1984). In 1990, Davies-Jones and collaborators further expanded upon Lilly's theme by introducing the concept of helicity occurring within a storm-relative framework, thus resulting in the quantity now known as storm-relative helicity or equivalently SRH (Davies-Jones *et al*., 1990).

Before embarking on a description of the formulation of SRH, it will be useful to first explore the relative influence and orientation of forces associated with vorticity on a local, storm-scale. Firstly consider a vorticity vector ω , which can be expressed in terms of the contribution of ω as vorticity components orientation in Cartesian coordinates (x,y,z) as represented by the right hand side of (4).

$$\begin{aligned}\boldsymbol{\omega} \equiv \nabla \times \mathbf{v} &= \left[\left(\frac{\partial w}{\partial y} - \frac{\partial v}{\partial z}\right), \left(\frac{\partial u}{\partial z} - \frac{\partial w}{\partial x}\right), \left(\frac{\partial v}{\partial x} - \frac{\partial u}{\partial y}\right)\right] \\ &\approx \left[-\left(\frac{\partial v}{\partial z}\right), \left(\frac{\partial u}{\partial z}\right), 0\right] = \mathbf{k} \times \frac{\partial \mathbf{v}_h}{\partial z} = \boldsymbol{\omega}_h,\end{aligned} \tag{4}$$

where:

V = (u, v, w) is the wind velocity vector

ω is the vorticity vector

k is the vertical unit vector

$\mathbf{V}_h$ is the horizontal wind velocity

$\boldsymbol{\omega}_h$ is the vorticity in a horizontal plane

∂/∂z[$\mathbf{V}_h$] is the incremental change of of the horizontal wind $\mathbf{V}_h$ with height (z); commonly termed the shear vector

In equation (4) Dahl (2006) argues that, in a hypothetical pre-storm environment where vertical velocities are negligible; the vorticity of the domain, as conceptualised in Fig 2.27 will be dominated by vorticity contributions restricted to the (x,y) horizontal plane of the Cartesian system. Dahl also mentions that, in terms of the comparative scale of vorticity components, the background, earth-relative sources of vorticity in the vertical are approximately 50 times smaller than background sources of vorticity in a horizontal plane. In (4) Dahl therefore approximates ω to be adequately represented by variations in the vertical of the u and v horizontal wind components. Equivalently ∂/∂z[u] and ∂/∂z[v] respectively, or ∂/∂z[$\mathbf{V}_h$].

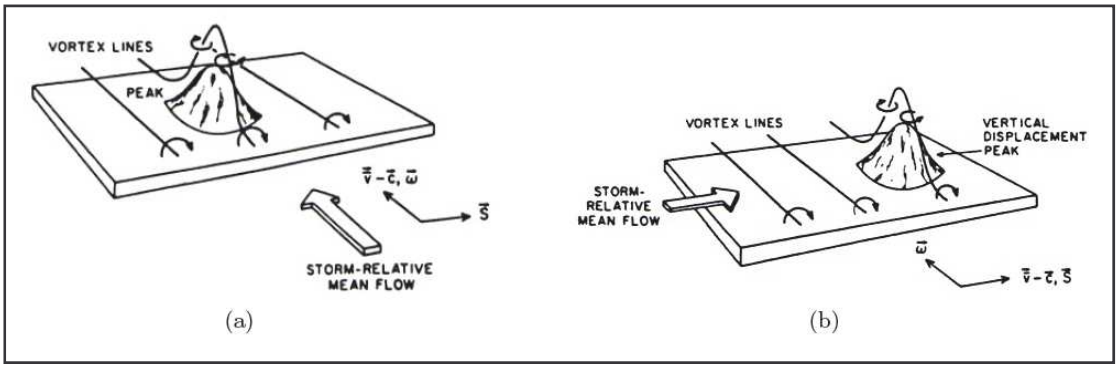

FIGURE 2.27: Vortex lines on an isentropic surface being deformed by an obstacle (convective updraft) to the initial unperturbed flow, in the case of (a) streamwise vorticity and (b) crosswise vorticity. Compare the similarity of (a) in this figure to Fig 2.10 (a) Source: Adapted from Davies-Jones (1984).

In the two contrasting examples offered in Fig. 2.27, the relative contribution of streamwise vorticity to long-lived supercells is explored graphically by means of a conceptual model. In (a) as well as (b), the environment is characterised by a speed-sheared low-level flow, with wind speed increasing aloft, resulting in overturning of the low-level environment, from left to right in each of (a) and (b). This field is then punctuated by a fresh updraft which warps or deforms the initial flow. It can readily be determined that for the example in (b), storm-relative mean (in)flow which is oriented in the same direction as the shear vector does not accumulate vertical vorticity. The vertical vorticity rather tends to accumulate around the flanks of the updraft feature.

By contrast, in the particular case (b) where the mean storm-relative inflow is oriented at a normal (i.e. 90 degrees in opposition) to the low-level shear vector, the inflow is induced to twist in a helical fashion. This helical path associated with spinning motion is analogous to a bullet exiting from a rifled gun barrel, with a spin orientated along an axis parallel to the gun barrel. This particular setup allows for the generation of a favourable vorticity maximum, collocated with the updraft, on the upwind, inflow side of the updraft. Low-level horizontal inflow with a helical twisting tendency thus has the potential to be ingested into the predominantly vertical thunderstorm updraft, setting the stage for a storm-scale updraft with a tendency to rotate horizontally around a vertical axis, otherwise known as a mesocyclone.

Shifting focus to the formulation of SRH as defined by Davies-Jones *et al*. (1990), some familiar components can be identified in equation (5). The quantity $\boldsymbol{\omega}_h$, or vorticity within a horizontal plane, was introduced in (4). Similarly the prevailing wind velocity within horizontal plane *h* was also described and declared as $\mathbf{V}_h$ with components *u* and *v* respectively. A new quantity, namely the storm motion vector **C** appears in (5), with the storm-relative wind defined as the vector difference $(\mathbf{V}_h - \mathbf{C})$. It should now become self-evident as to why it was critical within this work to (a) introduce the topic of 'effective storm-motion estimates' and (b) to discuss in detail

the various algorithms dealing with the estimation of supercell storm motion. Unless one is investigating an historic case-study, where the actual storm motion may be determined explicitly, the quantity **C** is typically unknown and requires careful estimation. As mentioned elsewhere, the storm motion algorithm utilized for this work was the Internal Dynamics scheme (Bunkers *et al*., 2000), otherwise known as the "Bunkers scheme". At the current time, this particular scheme has been shown to be superior to other alternative schemes (Ramsay & Doswell, 2005; Zeitler & Bunkers, 2005) and is thus the preferred default storm motion algorithm.

$$SRH = \int_0^h (\mathbf{v}_h - \mathbf{c}) \cdot \boldsymbol{\omega}_h dz \tag{5}$$

where:

$\mathbf{V}_h$ is the horizontal wind velocity

$\boldsymbol{\omega}_h$ is the vorticity in a horizontal plane

C is the storm motion vector which, in the absence of actual storm motion, is usually estimated

($\mathbf{V}_h$ – **C**) is the vector difference between $\mathbf{V}_h$ and **C** and represents the storm-relative wind

From (5), the definition of SRH may be further expanded, with the substitution of the alternative expression for $\boldsymbol{\omega}_h$ presented in (4) where $\boldsymbol{\omega}_h$ is quantified in terms of a vector cross product of **k** with the shear vector ∂/∂z[$\mathbf{V}_h$] thus $\boldsymbol{\omega}_h$ = **k** X ∂/∂z[$\mathbf{V}_h$] where **k** is a placeholder unit vector. Re-arrangement of the terms in (5) results in (6) below, which is the familiar, generalised expression for SRH with integration being performed through height *h*.

$$SRH = -\int_0^h \mathbf{k} \cdot (\mathbf{v}_h - \mathbf{c}) \times \frac{\partial \mathbf{v}_h}{\partial z} dz \tag{6}$$

Note that many sources also use the alternative expression storm-relative environmental helicity (SREH) to indicate SRH. While SRH is typically integrated over the first 3km AGL, in other words, *h* = 3000m AGL in (6), in accordance with Davies-Jones *et al*. (1990), it is also useful and feasible to calculate SRH through vertical sections of the lower atmosphere other than 0-3km AGL. For example Rasmussen (2003) proposed an upper boundary of *h* = 1000m AGL when discussing tornado predictands. In this current work, SRH will be calculated for three separate near-ground layers, namely 0-1km AGL, 0-2km AGL and 0-3km AGL.

2.7.3 Bulk Richardson shear

Weisman & Klemp (1982, 1984) showed that the complex relationship between instability, storm type and wind shear, and the overall or collective influence of these factors on supercell development, can be better understood through the use of the Bulk Richardson Number (hereafter BRN), as defined in equation (7). In equation (7), U_0 is the average wind encountered within the lowest 500 m AGL, whilst $\bar{U}$ is the density-weighted mean wind over the lowest 6 km AGL of the profile (Weisman & Klemp, 1986).

$$\mathrm{BRN} = \frac{\mathrm{CAPE}}{\frac{1}{2}\left(\overline{U} - U_0\right)^2} \tag{7}$$

where:

$\bar{U} = \bar{U}_{6000}$ is the density-weighted mean wind within the lowest 6km AGL

$U_0 = \bar{U}_{500}$ is the average wind in the lowest 500m AGL

$U = [\bar{U} - U_0]$ a shorthand notation appearing in subsequent SCP formulas

The denominator of BRN is also commonly termed the Bulk Richardson shear component (hereafter BRN shear). BRN shear represents a quantification of the west- to east-oriented speed shear in the vertical within the atmospheric column and is deemed to be an important ingredient regarding longevity of storms, particularly multicells and supercells (Houze, 1993).

$$\text{BRN shear} = (\tfrac{1}{2}U^2) = 0.5\,[\bar{U} - U_0]^2 \qquad (8)$$

where:

$\bar{U} = \bar{U}_{6000}$ is the density-weighted mean wind within the lowest 6km AGL

$U_0 = \bar{U}_{500}$ is the average wind in the lowest 500m AGL

$U = [\bar{U} - U_0]$ a shorthand notation appearing in subsequent SCP formulas

note: some sources use $\bar{U}_{500}$ and $\bar{U}_{6000}$ in the notation used for BRN shear. For clarity, both equivalent forms of notation are provided above.

It is relevant to mention that wide debate surrounds the question of an appropriate and effective depth for the quantification of 'deep layer shear' to discriminate effectively between supercell and non-supercell shearing profiles. While Marwitz (1972a) recommended use of shear thoughout "…the entire cloud column…", by contrast some authors favour 4000m (Rasmussen & Wilhelmson, 1983), 5000m (Houston *et al*., 2008) or even 7500m (Weisman & Klemp, 1986). In particular, the Houston *et al*. (2008) study was the first to investigate and quantify which such thickness would be optimal. In their opinion, 5000m is the best thickness AGL in order to successfully distriminate between supercell and non-supercell shearing profiles. Notwithstanding the results of Houston and co-authors, Rasmussen & Blanchard (1998) as well as Thompson *et al*. (2003) convincingly demonstrated that 6000m, as an upper bound of deep shear, is a strong discriminator between supercell and non-supercell shearing. For this research, 6000m was used, in line with Rasmussen & Blanchard (1998). In the context of this research, the decision to use 6000m was also found to be attractive as it would facilitate ease of comparison of

MSCP with Thompson *et al.* (2002; 2003). Whilst the engaging question of optimal shear thickness falls beyond the scope of this work, it was felt that there is nevertheless significant opportunity to pursue this particular aspect, within a uniquely southern African context, via further studies subsequent to this work.

2.7.4 Evolution of the Supercell Composite Parameter

According to Thompson *et al.* (2002) the SCP is defined as:

$$\mathbf{SCP_{2002}} = [\ (\text{MUCAPE}/1000) * (\text{SRH}_{0\text{-}3\text{km}}\ /150) * (\ (\tfrac{1}{2}U^2)\ /40\ )\ ] \qquad (9)$$

where:

MUCAPE is the most unstable CAPE in the lower 300hPa of the atmosphere, expressed in units of J kg^{-1} (Joule per kilogram)

$SRH_{0\text{-}3km}$ is storm-relative helicity, for a surface to 3km AGL layer as per Davies-Jones *et al*. (1990), expressed in units of $m^2\ s^{-2}$

$\frac{1}{2}U^2 = 0.5\ [\bar{U} - U_0]^2$ is the Bulk Richardson shear component (BRN shear), expressed in units of $m^2\ s^{-2}$

In (9) note that the units of each empirically derived scaling value are 1000 J kg^{-1}, 150 $m^2\ s^{-2}$ and 40 $m^2\ s^{-2}$ respectively

The SCP in equation (9) can be referred to as a composite index (Glickman, 2006) as it is a composite of three distinct meteorological indices. Examples of other similar composite indices relating to severe thunderstorms are the EHI (Hart & Korotky, 1990) and the STP (Thompson *et al.*, 2002). In the context of short-term prediction of severe thunderstorms, composite indices have become increasingly popular amongst meteorologists in the last few decades (Doswell & Schultz, 2006). EHI was one of the first indices to combine an estimation of relative instability within the atmosphere (represented by CAPE), together with a deep layer shear term, represented in this particular instance by storm-relative helicity (SRH). EHI was specifically designed as a tornado forecast parameter (Hart & Korotky, 1990). In general however, Doswell &

Schultz (2006) urge that a degree of care should be applied when meteorologists consider the design of new formulations of composite indices and that these should not be formulated in a haphazard fashion. Consequently the design of MSCP for this study is based strongly on the adaptation or fine-tuning of existing SCP composite index formulations by empirical means, rather than defining a new, hitherto unknown composite index.

Following initial work on SCP (Thompson *et al.*, 2002) further refinement of the SCP algorithm was explored, leading to the formulation of an updated and refined SCP (Thompson *et al.*, 2003), wherein SCP is re-defined as in equation (10) below:

$$\mathbf{SCP_{2003}} = [\ (\text{MUCAPE}/1000) * (\text{SRH}_{0\text{-}3\text{km}}/100) * (\ (\tfrac{1}{2}U^2)/20\ )\ ] \qquad (10)$$

where:

the respective quantities and units of measurement in (10) are as per SCP_{2002} provided in equation (9)

In Thompson *et al.* (2003), a dataset of 413 proximity soundings was used to compare to hourly NWP output from the Rapid Update Cycle (RUC-2) NWP model. Comparison between equations (9) and (10) reveals that the normalisation factor for SRH changed from 150 $m^2 s^{-2}$ (Thompson *et al.*, 2002) to 100 $m^2 s^{-2}$ (Thompson *et al.*, 2003), whilst Bulk Richardson shear similarly changed from 40 $m^2 s^{-2}$ to 20 $m^2 s^{-2}$. These changes in Thompson *et al*. (2003) were informed by use of the first quartile of the distribution of parameters from the 413 proximity soundings as a threshold or normalisation factor. The normalisation factor for MUCAPE however remained constant at 1000 J kg^{-1} in both Thompson *et al. (*2002) and Thompson *et al.* (2003).

In Thompson *et al.* (2003), the authors draw attention to a limitation in the original formulation of Thompson *et al.* (2002). They state that only right-moving supercells were investigated in the original dataset used for Thompson *et al.* (2002). Furthermore, the authors acknowledge the findings of Bunkers (2002) that hypothetical left-moving supercells which may form in an anticyclonic shearing

regime would lead to SRH values of an opposing polarity, which by implication would change the polarity of SCP. In other words, positive as well as negative values of SCP are possible globally.

It is important to note that Thompson *et al*. (2002; 2003) are central to this body of research and will be cited recurrently in forthcoming chapters, both in terms of narrative as well as references in tabular format. For brevity and to simplify discussion, especially when comparisons of various SCP formulations are presented in Chapter 7, the two Thompson *et al*. (2002; 2003) references will henceforth simply be referred to as T(2002) and T(2003) respectively.

In later work regarding formulation of SCP, the concept of effective bulk shear (EBS) was introduced (Thompson *et al.*, 2004a). Similarly in Thompson *et al.* (2004b), the concept of effective storm-relative helicity (ESHR) was also defined, leading ultimately to Thompson *et al.*, (2007) wherein SCP is re-defined as equation (11).

In Thompson *et al.* (2007), both ESHR and EBS are defined as being relative to an effective inflow layer where it is argued *inter alia* (Thompson *et al.*, 2004a, 2004b, 2007) that a constant 0-3 km thickness of atmosphere is not consistently appropriate for all storm types. Furthermore, it is argued that some storms in a moist near-ground environment associated with a small dewpoint depression value will consequently have a lower convective cloudbase whilst storms in a drier sub-cloudbase environment will tend to have a much higher convective cloudbase. Thompson *et al.* (2007) argue that in the latter case, elevated thunderstorms have an impaired opportunity to develop rotation through a large portion of the 0-3 km AGL layer, with much this layer residing in the drier sub-cloudbase environment. By contrast, it is further argued (Thompson *et al.,* 2007) that storms with a much lower cloudbase have a more effective inflow layer as the majority of the 0-3 km layer is occupied by deep, moist convection. Thompson, *et al.* (2004a) define effective storm-relative helicity (ESHR) as SRH which is constrained by an effective inflow base and effective inflow top respectively where the vertical extent of the SRH integral is

determined by the most unstable parcel meeting constraints set by permutations of CAPE vs CIN pairs of +(-)100 J kg^{-1}, +(-)250 J kg^{-1} , +(-)500 J kg^{-1} respectively, where CIN is defined as convective inhibition in the atmospheric profile. Similarly effective bulk shear (EBS) is defined as "…the vertical shear though a percentage of the "storm depth" as defined by the vertical distance from the effective inflow base to the equilibrium level associated with the most unstable parcel (maximum θ_e value) in the lowest 300hPa" (Thompson *et al.*, 2007). The new quantities of effective SRH (ESRH) and effective bulk shear (EBS) are incorporated in the revised 2007 version of SCP in equation (11) hereunder:

$$\mathbf{SCP_{2007}} = [\ (\text{MUCAPE}/1000) * (\text{ESRH}/50) * (\ \text{EBS}/20\ )\ ] \qquad (11)$$

where:

MUCAPE is the most unstable CAPE in the lower 300hPa of the atmosphere, expressed in units of J kg^{-1} (Joule per kilogram)

ESRH is "effective storm-relative helicity" expressed in units of $m^2\ s^{-2}$ and fully described in the narrative of this chapter

EBS is "effective bulk shear" , fully described in the narrative, expressed in units of $m^2\ s^{-2}$

In (11) note that the units of each empirically derived scaling value are 1000 J kg^{-1}, 50 $m^2\ s^{-2}$ and 20 $m^2\ s^{-2}$ respectively

2.8 Summary

The main points relevant to this study which arose in this chapter include:

- The T(2002) and T(2003) formulations of SCP appear to be well-suited to use as a basis for this proposed study, with both such formulations of SCP having a similar structure but differing only in terms of the normalisation factors

used. By contrast the Thompson *et al*. (2007) form of SCP appears to be too complex to (a) utilise as part of this modular SCP study design and (b) difficult to compare against other formulations of SCP. Hence the 2007 formulation of SCP will not be utilised in this study.

- As stated by Doswell & Rasmussen (1994) there are a number of methods whereby CAPE can be summated and it would be prudent to experimentally test some of these. For example SBCAPE, MUCAPE, NCAPE as the CAPE component of SCP, when considering an MSCP formulation within this study.
- Similarly, SRH as originally formulated by Davies-Jones *et al*. (1990) may be calculated for atmospheric layers other than the first 3 km AGL, as proposed by Rasmussen (2003) who suggested the use of a surface to 1 km layer. Within this study, a suitable design for MSCP could easily accommodate investigation of each of 0-1 km SRH, 0-2 km SRH and 0-3 km SRH. These three SRH integrals form part of the standard output of the RAOB sounding visualisation and analysis program (Shewchuck, 2013).
- The literature study revealed that, implicit in the formulation of SRH, the vector of estimated storm motion **c** introduced in equation (5) and (6) has a significant influence on the resultant SRH. With reference to the study at hand, it was critical that various storm motion algorithms were listed and assessed during the literature study. The importance of the concept of Galilean Invariance in the context of this study was also introduced and explained. It became clear that the Bunkers storm motion algorithm (Bunkers *et al*., 2000) also known as the "Bunkers scheme" would be the preferred scheme to use within this study, both in terms of acknowledged accuracy as well as popular usage thereof. The RAOB program allows for user-definable storm motion selection, including the Bunkers scheme.
- Apart from SCP and BRN, there do not appear to be any other alternative indices or published methodologies to effectively discriminate "storm type" and in particular, the storm type of "supercell", as proposed in this study. Whilst BRN (Weisman & Klemp, 1982; 1984) has been available for some time, it is acknowledged in the use of BRN that there is a large degree of

overlap between the categories of “multicell” and “supercell”. Thus the relevance of SCP as a more refined predictor of the “supercell” storm type is further emphasised.

- In terms of the criteria associated with supercells and in particular, necessary and sufficient criteria to justify a storm being declared a supercell, it is noteworthy that at the current time there is no universally accepted standard for such criteria, although there is much agreement and common ground amongst authors in terms of this aspect. Hence it will be important, within the scope of this study and in forthcoming chapters, to clearly specify the supercell criteria applied to each supercell case.
- A final point relates to the acknowledged existence of atypical supercells which may form under conditions of anticyclonic shear. In a similar fashion to T(2002) this study will utilise a dataset of supercells associated with typical, cyclonic shearing. Within the scope of this study, it must however be kept in mind that any mathematical formulation of SCP or MSCP as the case may be, should at least allow for MSCP to be defined for circumstances when SRH > 0 m^2 s^{-2} as in the case of an anticyclonic shearing profile (relative to the southern hemisphere) within the lower few kilometres of the surface. In other words, anticyclonic shearing in the input conditions to MSCP should not result in a mathematically undefied result for MSCP.

CHAPTER III : DATA TREATMENT AND METHODOLOGY

This chapter provides background information regarding the various data types that were instrumental in conducting this research. This is discussed in relation to how the data was sourced as well as issues surrounding the quality of said data. In particular, the role and function of each data type will be discussed, relative to the various objectives of this study. In some cases it was required to prepare datasets in a sequential manner, so as to allow further subsequent analysis. In such cases, careful planning was required in order for analysis to proceed in a structured fashion.

3.1 Proposed universal naming convention

In this research the following naming convention is proposed regarding the deviant movement of supercell thunderstorms, regardless of whether said storm is a northern or southern hemisphere candidate. In Table 3.1, supercell motion resulting from a typical cyclonic shearing profile will simply be referred to as being equatorwards of mean storm motion (hereafter termed EMM). Conversely, the less common anticyclonic form of deviant motion (due either to an anticyclonic shearing profile or due to the anticyclonic member of the storm splitting processes) will be referred to as being polewards of mean storm motion (hereafter termed PMM). In the southern hemisphere, EMM or deviant left movement is the typical default supercell storm movement. Conversely, deviant right movers associated with PMM movement is the storm movement encountered less frequently than the former. In the northern hemisphere, as per Table 3.1, this situation is reversed.

TABLE 3.1: Comparison per hemisphere of relative supercell thunderstorm motion. Greyed out areas correspond to universal descriptors of supercell motion, irrespective of whether the thunderstorm is in the southern or northern hemisphere. Table compiled by the author.

TABULATION OF RELATIVE ORIENTATION OF SUPERCELL MOTION

	NORTHERN HEMISPHERE		SOUTHERN HEMISPHERE	
"typical" deviant motion	equatorwards of mean storm movement	right of mean	left of mean	equatorwards of mean storm movement
anticyclonic deviant motion	polewards of mean storm movement	left of mean	right of mean	polewards of mean storm movement

Supercell thunderstorm movement: relative to hemisphere within which the storm develops and also relative to the local mean environmental storm movement

3.2 Optimal sizing of study domain

Accurate supercell thunderstorm analysis relies strongly on investigation of low-level (inflow notch, hook echo) and mid-level (weak echo regions, overhang as well as mesocyclonic rotation in the case of a Doppler-enabled RADAR) features, whilst the TITAN storm-tracking algorithm (Dixon & Wiener, 1993) will only provide accurate short-term predictions if the predominant portion of the vertical extent of the storm is in direct “line of sight” of the RADAR. Hence, in the context of the study at hand, it was important to strike a balance between a domain that would be large enough to sample a sufficient number of supercell cases but equally a domain that would not be too spatially extensive, where the efficiency of the RADAR, as a storm analysis tool, could be compromised. The 200 km range-ring of the Irene RADAR was conveniently used as the boundary of the domain for this study. Whilst the RADAR in question is indeed capable of radiating a sweep of up to 300 km, a more conservative maximum range of 200 km was selected. One of the main reasons supporting this choice stems from the unavoidable limitation of RADAR, relating to the curvature of the earth. Whilst the RADAR beam would faithfully identify storms at distances of beyond 200 km, the beam would only scan the upper regions of the storm as alluded to above.

3.3 Radiosonde soundings and RAOB software

3.3.1 Sourcing of radiosonde data

Data from radiosonde balloon ascents performed at the South African Weather Service (SAWS) Irene Weather Office located in the Gauteng province was used exclusively for this study, both in terms of the SUP supercell dataset as well as the 2007-2011 NON-SUP non-supercell dataset. Proximity sounding criteria as described in section 3.3.3 were adopted, in keeping with the proximity sounding approach used in similar studies such as Brooks *et al*. (1994). SAWS sounding data were sourced from the searchable online archive of the University of Wyoming, USA at http://weather.uwyo.edu/upperair/africa.html. (UWYO, 2014). There was only one exception regarding the uniform and consistent use of sounding data sourced from UWYO and this related to one of the supercell cases in the SUP dataset, namely the case of 21 October 1999, where the data was not retrievable from UWYO. In this particular case, the original standard level and significant level data as well as corresponding winds were sourced from SAWS and the sounding data manually reconstructed in a CSV format that was RAOB-readable.

3.3.2 Radiosonde instruments

The radiosonde instruments used to compile the NON-SUP sample of 2007-2011 non-supercell thunderstorm days were the IMA BAT-16G radiosonde instrument manufactured by INTERMET (Intermet, 2014). This instrument is a miniaturised weather station with a launch mass of only about 250 g, sampling tropospheric atmospheric variables from the surface, right up to regions well beyond the tropopause, at altitudes where air pressure falls below 100 hPa, corresponding to an altitude of approximately 16000 m for mid-latitude stations such as Irene. It is however common for ascents to reach 25000 to 26000 m, where local conditions would be a near-vacuum, at approximately 20 hPa. As such, the radiosonde is a

highly robust, precision instrument that needs to reliably operate at air temperatures as low as -90 °C and simultaneously be able to register pressures ranging from 1080 hPa to 3 hPa. Temperature resolution for the IMA BAT-16G is 1 x 10^{-2} °C with an in-flight accuracy cited to be 3 x 10^{-1} °C provided pressures exceed 100 hPa (Intermet, 2014). Relative humidity (RH) is sensed at a resolution of 1%, with an accuracy of within 5%. Atmospheric variables of air pressure, air temperature and RH are sensed onboard by the instrument and transmitted back to the surface tracking station via microwave signal within a frequency range of 1680 MHz (Intermet, 2014). The instrument includes a GPS transmitter, enabling accurate spatial tracking to within six metres of the absolute position of the instrument in flight, thus allowing for calculations of spatial displacement and ultimately wind direction and speed information. The soundings performed in South Africa typically use a 500 g latex balloon filled with hydrogen gas, allowing for positive lift of approximately 1200 g and an ascent rate of approximately 360 m min^{-1}, resulting in ascents that typically last for 70 to 75 minutes. Of the radiosonde data used for the SUP supercell sample, ascents performed prior to 2007 utilised the VAISALA RS92-SGP, GPS-enabled radiosonde instrument which has very similar operational performance and sampling accuracy to the data cited above (Vaisala, 2014). A single exception was the upper air data relating to the 1 November 1985 case, being the earliest case in the SUP supercell dataset and was retrieved using the VAISALA RS21 radiosonde device, which pre-dated GPS technology. In this case the upper air wind vectors were determined trigonometrically utilising the relative displacement of the instrument from the launch site, measured from one minute to the next. The data for the SUP supercell dataset numbering 15 cases was exclusively based on midday soundings, with only two exceptions, when 00h00UTC soundings, preceding the normal noon sounding time by approximately 12 hours, were used due to non-availability of corresponding noon soundings. Given the paucity of Gauteng supercell events, it was considered to be important to preserve as many such events in the dataset as possible. The only modification applied to the aforementioned soundings was to substitute the original surface temperature and dewpoint reading with a pair of values more representative of diurnal surface conditions at 11h00UTC, as close as

possible to launching time. Surface temperature (T) and dewpoint (T_d) observations at 5 minute intervals from the Automatic Weather Station (AWS) at the upper air site were utilised for this purpose and are correspondingly shown in Table 3.2 for the two cases in question.

Table 3.2: Surface temperature and dewpoint values as measured at 11h00UTC at the respective launch site, for two supercell cases where 00h00UTC soundings were used.

Date (YYYYMMDD)	Locality	Automatic Weather Station data at launch site	Temperature, deg C at 11h00UTC	Dewpoint, deg C at 11h00UTC
20101024	Marble Hall	Irene weather office	30.7	15.1
20111002	Brits	Irene weather office	16.8	12.6

3.3.3 Proximity soundings

Brooks *et al*. (1994) cite Darkow (1968; 1969) as having been one of the pioneers of the concept of proximity soundings. Furthermore, they contrast the approach of Darkow with later work relating to proximity soundings, with such contrasts discussed in detail later within this section. The work by Brooks and collaborators is significant, in that it offers detailed discussion regarding the factors which influence the use of such proximity datasets as well as associated benefits and drawbacks which may arise; given particular choices at the outset of any study utilising such data. It is thus highly relevant, in the context of this study, that cognizance should be taken of the opinions of Brooks and co-authors. In particular, they mention three main factors that need to be considered when planning to use a proximity dataset. One of these factors relates to the issue of appropriate choice of spatial horizontal separation of the sounding from the event. In general, one would prefer to select events that are not too distant from the sounding site. The second of these factors is the temporal aspect, in that if one acknowledges that the atmosphere is in a continual state of flux, particularly within the planetary boundary layer (PBL), that it is undesirable for an inordinate amount of time to elapse between the sounding and the event itself. These first two spatio-temporal factors are not yet subject to any

internationally agreed criteria and there is much variation in the literature, in terms of appropriate choice of both factors, however, in the opinion of Brooks *et al*. (1994), the exact numerical choice of these first two factors is fairly arbitrary.

Once again, citing Darkow, mention is made of the three criteria that were applied in constructing a proximity sounding dataset, namely (1) that the sounding site should be within 80 km of the event (a tornado in this particular case), (2) the event should occur within 45 minutes before and 60 minutes after the sounding release time and (3) the sounding and the event should both be sampled from the same airmass. Brooks and collaborators emphasise the importance of "balance" when contemplating such a dataset. If, in the opinion of Brooks *et al*. (1994), one is too restrictive in defining the spatio-temporal bounds, as in the Darkow case, one has little scope to produce a large dataset. At the other extreme, the restrictions should not be sufficiently lax as to result in an overly-large dataset. Furthermore, in their opinion, the most important, tertiary factor is the question of representivity of the airmass, with their acknowledgment that the compilation of such datasets is "...potentially more complex than it might appear to be." (Brooks *et al*., 1994).

Central to this is the difficult question of what criteria to apply when considering preclusion of certain soundings, *i.e.* which soundings to include and which not to include? This also serves to highlight the importance and relevance of well-defined, rigorous quality-control of soundings. If a proximity dataset is to explore issues relating to the free convection of a parcel of air, as in this study, then one must be confident that each such sounding can allow free convection to take place.

In the Brooks *et al.* (1994) study, a spatio-temporal proximity sounding constraint of 160 km and a 2 hour time-window, with 60 minutes either side of the sounding launch time, was selected in determining the proximity sounding dataset while Craven & Brooks (2004) used 185 km and a three hour window either side of the sounding time, totalling six hours. Dyson *et al.* (2014) favoured a 100 km radius in their Gauteng-based study of sounding-derived parameters associated with heavy

rainfall and restricted their interest to midday soundings only. In a 2005 study of tornadoes in Alberta, Canada, Dupilka & Reuter (2006a; 2006b) selected events within 200 km of a single sounding site and a corresponding 24hour time window. Last-mentioned authors also make mention of the question of "right-sizing" a proximity dataset, so as to avoid either too few or too many events within the study sample. In a 2010 study, Potvin *et al*. proposed a more structured and tailored approach to the spatio-temporal question of right-sizing a proximity sounding study and proposed the term "Goldilocks Zone" (GZ) to refer to an optimal choice of proximity sounding design. They favoured 40 to 80 km and a two hour temporal window, although notably this choice related to a study specifically focussing on the near-storm environments of significant tornadoes as an ancilliary feature of some thunderstorms rather than classification of thunderstorm type as in this study. Arguably in the latter case, the spatio-temporal bounds need not be excessively restrictive so as to limit the overall size of the dataset, another mitigative factor conceded by Potvin *et al*. (2010). In the particular study at hand, a spatial criterion of 200 km around the Irene RADAR was chosen, closely in line with Craven & Brooks (2004).

Another factor that was taken into account was that due to the curvature of the earth, RADAR cross-section images of thunderstorms would not be able to register the lower-level features of a thunderstorm, especially in the case of a supercell, where some significant features, such as hook echoes will only be registered within the 1 to 3 km AGL CAPPI scans. In terms of temporal restrictions, a 6 hour time window from 09h00UTC to 15h00UTC was selected (approximately 1.5 hours prior to launch of the balloon sounding, extending to 4.5 hours thereafter) was selected. Whilst it is acknowledged that for Irene, Johannesburg and ORTIA that the diurnal maximum of precipitation frequency occurs after 18h00UTC according to Rouault *et al*. (2013), it was felt that from a proximity sounding perspective, there would be undue risk associated with extending the upper temporal bound into the evening hours as there would be reduced confidence in the overall representivity of the noon proximity sounding. Furthermore, in a study of long-lived supercells, Bunkers *et al.*

(2006a, 2006b) found that, especially for isolated, discrete supercells, there was a marked tendency for such development to occur early in the diurnal cycle, thus favouring a temporal bias in the proximity sounding design to the midday to late afternoon time-window, rather than extending the temporal window into the evening hours.

3.3.4 RAOB software

The 2013 version of RAOB (Version 6.3) available at http://www.raob.com/ was used both to display as well as to process upper air sounding data for this study. The following user-defined configuration and setup was selected as the default setting for RAOB for the duration of this study:

- The virtual temperature (T_v) correction was applied to all surface lifted parcels as urged by Doswell & Rasmussen (1994); to ensure a more accurate representation of the energy available for lifted parcels. Parcel lifting in the absence of this correction, using ordinary, uncorrected air temperature (T) generally results in weaker, less energetic parcel lift.
- The Bunkers Internal Dynamics (ID) storm motion algorithm (Bunkers *et al.*, 2000) was used consistently, as it is acknowledged to be superior to other methods (Ramsay & Doswell, 2005) and has become standard practice for this method to be used as the default storm motion algorithm in preference to other alternative storm motion algorithms that pre-date the ID method.
- 6 km AGL depth of shear selected for Bulk Richardson Number (BRN) and Bulk Richardson shear calculations. This is the standard setting for RAOB, in line with similar such studies and was consequently not manipulated or adapted in any way.
- MUCAPE calculations require use of virtual temperature (T_v) and parcels lifted from LFC to EL level.
- SBCAPE calculations however use a surface-based lifted parcel which is lifted to LCL, without a correction for virtual temperature (T_v).

3.3.5 Quality control of sounding data

A range of quality control (QC) also known as quality assurance measures were conducted on the upper air data. Durre *et al.* (2006) cite Schwartz & Doswell (1991), stating that poor or ineffective QC measures can significantly bias or compromise sounding datasets due to errors of one or more of observation, transmission and processing problems. They state that in terms of QC measures, there is a choice between two broad styles of QC measures which may be applied, namely either a decision-making algorithmic approach or alternatively a sequential series of independent tests. The approach used in this study followed the latter style, as applied at the Integrated Global Radiosonde Archive (IGRA) and reported on by Durre *et al.* (2006), whilst the particular tests which were applied and listed herein were customised to be relevant to the study at hand. The nature of the tests applied in this work corresponds closely with the comprehensive IGRA tests documented by Durre *et al.* (2006) in their Table 3, especially in terms of "fundamental sanity" of the sounding, internal consistency, repetition of values and data completeness. However unlike Durre *et al*. no climatological checks were performed for this study. In contrast to Potvin *et al*. (2010) where outliers either less than the 2.5% percentile or larger than the 97.5% percentile were actively removed, no extreme outlier events were filtered from the plotted box and whisker distributions of thermodynamic parameters for this study, unless said case was obviously suspect, as in 3 December 2009 where CAPE = 7000 J kg^{-1} was initially calculated due to an incorrect dewpoint of T_d = 22 °C.

For this study, the following seven QC measures were applied to each individual sounding within an initial dataset of 757 soundings of interest as well as the SUP supercell sounding dataset. Following the application of QC measures, the dataset of 757 soundings was further reduced to 664 soundings. In terms of QC measures, each point in the list below represents an independant test, where, in the case of critical missing data, the sounding would fail the test and be withdrawn from the dataset. Only soundings which passed all tests successfully were retained in the dataset. In

some cases, if the error was obvious and self-apparent, the error would be corrected to allow the sounding to pass that particular test.

The seven QC tests for this study were as follows:

1) Removal of spurious data artefacts, also known as data spikes, which did not fit the temperature and dewpoint profile. Usually this phenomenon relates to a temporary loss of signal between the radiosonde and the ground station.

2) Removal from the data record of any occurrences of elevated superadiabatic rate of temperature change in the environmental temperature profile as per guidelines of Slonaker *et al*. (1996) and Potvin *et al*. (2010). It should be noted that near-surface superadiabats are neither uncommon nor unusual in hot, dry settings as encountered on the Highveld in summer. The intention therefore was to screen out superadiabats occurring at levels other than at the surface.

3) Each sounding dataset was required to have a full complement of data points relating to significant levels in addition to data points at standard, mandatory pressure levels. Mandatory pressure levels for the pressure range 850 to 200 hPa are 850, 700, 500, 400, 300, 250 and 200 hPa respectively (WMO, 1996). If the sounding had only standard pressure levels present then it was precluded from the master sounding dataset. Similar radiosonde or NWP-based atmospheric studies have been performed solely utilising the relatively coarse resolution of mandatory pressure levels or alternatively at fixed isobaric intervals as in Davies (2004). However for this particular study, it was essential to incorporate the finescale vertical resolution of the significant level data, especially when considering the important role of accurately sampling the meteorological conditions of air temperature, dewpoint temperature, wind speed and wind direction within the planetary boundary layer to determine such quantities as SRH within the first 3000 m AGL.

4) It was preferable that the sounding dataset had no missing data for wind direction and wind speed, especially within the lowest 3000 m AGL. This was

especially important as missing readings could adversely impact on accuracy of parameters which use wind as a variable.

5) Data per sounding had to be available up to and including 200 hPa (+- 12000 m AMSL). An air parcel raised from the LFC needs to arrive at the EL for CAPE integrals to be accurately integrated. Incomplete soundings in the dataset would have resulted in greatly truncated or impaired estimates of CAPE and would have compromised or biased the overall results.

6) The surface meteorological parameters all had to be present with no missing parameters. In particular, air temperature (T), dewpoint (T_d), wind direction and wind speed for the first data level were of critical importance. Missing wind data at this level would have resulted in the RAOB software program being unable to calculate BRN and hence BRN shear. The latter is an essential input component for calculations of SCP.

7) Apart from the checks listed above, each sounding of the dataset was plotted graphically in RAOB and visually scrutinised for additional features that appeared highly unusual and/or not in line with typical thermodynamic profiles of radiosonde soundings.

One caveat bears mentioning, especially in relation to Test (3) and relates to the presence or absence of the 850 hPa pressure level for each sounding. Due to the relatively high altitude of the Irene station, at approximately 1523 m MSL, the surface pressure for Irene is often either slightly above or below the 850 hPa mandatory pressure level. Hence data for this particular pressure level is occasionally absent in the dataset however this is quite normal for Highveld-based stations.

As this study design relied strongly on the simulation of deep convection being triggered by free ascent of a lifted parcel, based on the radiosonde sounding profile, it was necessary to screen out any such sounding profiles where it is was apparent that the profile was indicative of a pre-existing deep, saturated layer throughout the column. Similarly, particular soundings were precluded if the balloon travelled

vertically through a convective cell (cumulus or cumulonimbus), which would equally result in a saturated profile though a deep atmospheric layer. Under such circumstances, the parcel lifting method becomes an inappropriate analysis technique.

3.4 Lightning Detection Network (LDN) data

SAWS LDN network data (Gill, 2008) was utilised as a critical component of this study, in order to confidently determine if one was dealing with a "thunderstorm day" (or not) and therefore whether the particular day should be included or not included in the master dataset of Gauteng "thunderstorm days", 2007-2011. The LDN data sourced from SAWS was continuous for the entire period in question, however the data files covered virtually all of South Africa, requiring further filtering to isolate the Gauteng domain chosen for this study. The most practical solution was to utilise a mask or sub-area, covering the Gauteng domain and corresponding closely to the 200 km range-ring of the Irene RADAR. Consequently a latitude/longitude square was declared as indicated in Fig. 3.1, with the vertices (corners) of the square circumscribed by the 200 km range-ring (*vide* Fig. 1.3 in Chapter 1). Whilst each vertex of the box (A, B, C and D in Fig. 3.2) is exactly 200 km distant from the RADAR, each side of the square is roughly 283 km, while in the direction of the four main compass points, the sides are 141.42 km from the RADAR.

The SAWS LDN network measures cloud-to-ground (CG) discharges and operates on the principle of sferics (Gill, 2008), where radio disturbances initiated by lightning discharge are intercepted by a network of receiving stations which triangulate both the time and relative position of each discharge (Gill, 2008). Spatio-temporally, the system is extremely accurate, with an estimated error of only 500 to 1000 m for the majority of South Africa (Gill, 2008). It should be noted that the current LDN as operated by SAWS does not sense intra-cloud lightning discharges. Lightning stroke data was first filtered to isolate strokes within the domain per 24 hour day. In this

manner, 989 thunderstorm days out of a possible total of 1826 days were identified in this period, with a criterion of 2 or more strokes being required as a lower threshold requirement, in accordance with methodology adopted by Reap (1986). Of this number, 61 storm days were discarded due to missing or incomplete 12h00UTC sounding data.

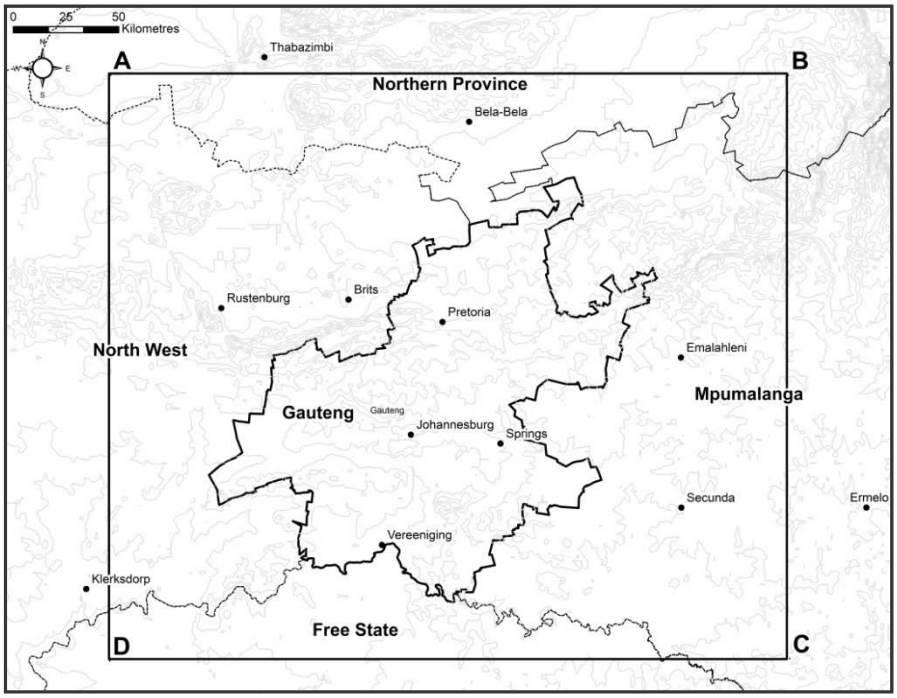

FIGURE 3.1: A map, relative to Gauteng province, indicating the boundaries of the box domain (as indicated by ABCD) used to isolate daily lightning strokes to identify thunderstorm days for the 2007-2011 period. Source map generated using ESRI ArcGIS 10.1.

Of the 928 remaining days, these were processed in the following manner: In order to screen out thunderstorm events which may have been initiated the previous evening, persisting into the early hours of the following day, it was decided to further filter the dataset to reflect only such lightning occurrences within a 6 hour time-window of 09h00UTC to 15h00UTC, broadly in line with the proximity sounding approach of Brooks *et al*. (1994) and Craven & Brooks (2004). This second phase of filtering using, as before, a minimum of two or more strokes resulted in a further 171 storm days being precluded as they fell beyond the time-window of interest, yielding a total of 757 thunderstorm days. However, once rigorous quality control (QC) of radiosonde data had been taken into account, the final number of viable 2007-2011 thunderstorm days to be utilised for the study was further reduced to N = 664 days.

As will also be seen in Chapter 5, the dataset of 664 Gauteng thunderstorm days ultimately required further trimming in order to transform the dataset into one which was representative of 2007 to 2011 Gauteng thunderstorm days only for austral summer months of October to March. Consequently, once the winter months of April to September were edited from the dataset of 664 storm days, 535 austral summer thunderstorm days remained. A further 25 cases were removed later due to QC of RAOB output, where missing values compromised the usefulness of certain case dates, thus leaving (535 - 25) = 510 thunderstorm days as a final list. This dataset was thus termed the NON-SUP, or non-supercell dataset and is further explored in Chapters 5 and 6 to follow.

To summarise, for the purposes of the dataset of 664 thunderstorm days, a particular day during the period 1 January 2007 to 31 December 2011 would be considered to be a "thunderstorm day" if, for the square latitude/longitude box domain as described above, at least 2 (two) or more CG strokes were registered by the LDN system within the six hour time-window of 09h00UTC to 15h00UTC. This would be conditional to a suitable Irene proximity sounding being available, as described in detail in Chapter 3.3. If, however, no such proximity sounding could be retrieved, that particular day would be precluded from further consideration in the study. A "thunderstorm day" was similarly defined for the NON-SUP dataset of 510 austral summer thunderstorm days, but restricted only to 2007 to 2011 thunderstorm activity within the the months of October to March, inclusive.

3.5 Supercell identification: RADAR and visual characteristics

3.5.1 The need for a supercell database

No comprehensive climatology of South African supercell storms, or for that matter southern African Highveld supercell storms, currently exists. Goliger *et al.* (1997) prepared and presented a climatology of South African tornado cases, some of which

may have been supercell storms. However, it is acknowledged by Rotunno & Klemp (1985) that not all supercell storms are tornadic.

Burgess & Lemon (1990) determined that 90% of supercell storms are severe at some point in the life-cycle of a supercell storm. In a similar vein, Stumpf (2003) asserts that between 70% to 90% of rotating storms produce severe weather. On this basis, it was decided to focus on a careful analysis of severe storm reports at the SAWS, particularly at the SAWS National Forecast Centre (NFC), Pretoria, South Africa. If one accepts at least moderate levels of vigilance and awareness on the part of NFC severe storm analysts, it is arguable that a significant number of historic supercells would have been identified as having been severe enough to warrant a severe storm alert even if the identity of the storm, as being of the supercell type, may have been overlooked at the time. However, notwithstanding this, it was known that quite a number of severe storm cases were additionally identified as being supercells, concurrent to nowcast alerts being issued.

It is appropriate to emphasise at this point that the listing of supercell storms generated for this study should not be viewed as a climatology of Highveld supercell storms. The supercell database cases mentioned and actively used within this research work are rather at best a *capita selecta* of an undetermined climatology of Highveld supercells.

3.5.2 Supercell characteristics and criteria applied

Supercell events were identified primarily via reports, presentations and articles written by SAWS forecasters and scientists and supported in most cases by either C-band or S-band RADAR data sourced from SAWS. Supplemental information was also gleaned from SAWS operational diaries, often with detailed notes relating to extreme weather events and associated weather-related warnings.

All 15 supercell storms used within the SUP supercell sample of this study were selected on the basis of the spatial criterion of being within 200 km of the Irene site. Notwithstanding that there is no standardised, universally accepted definition of a supercell which includes a list of the necessary and sufficient characteristics thereof, it was nevertheless essential to define such a list for the purposes of this study. Therefore, with due regard to the position of Doswell & Burgess (1993), Moller *et al*. (1994) as well as Lynn (2002), this author proposes the following:

A thunderstorm will be classified as being a supercell storm if one or more of the following criteria are observed and/or fulfilled:

1) RADAR observed mesocyclone (Burgess & Lemon, 1990) persisting for at least two or more adjacent volume scans (i.e 12 or more minutes) of radial velocity, suggesting a persistent couplet of opposing velocity. Alternatively, an equivalent conclusion may be drawn regarding the presence of a mesocyclone from the visual observation of a wall cloud feature (Fujita, 1960a). Rotation may or may not be observed in the wall cloud feature.
2) A bounded weak echo region (BWER) (Chisholm & Renick, 1972) or weak echo region (WER) in a cross-section of the reflectivity (dBZ) field, coincident with the low-level inflow region of the storm.
3) A *bona fide* and persistent hook echo feature (Van Tassel, 1955 ; Forbes, 1981) typically manifested in the 3 km CAPPI reflectivity, provided that the storm is not further than approximately 100 km from the RADAR, which would otherwise preclude observation of such a low-level feature due to the curvature of the earth.

Additional supporting features which in themselves are not uniquely associated with supercells, but when considered in addition to one or more of (1), (2) and (3) above could aid in overall diagnosis, include:

1) Storm longevity: Generally supercells are long-lived and typical lifetimes meet or exceed 1.5 hours and even approach six to eight hours in extreme cases.

Individual longevity can be difficult to determine when storms are not isolated, however in the case of isolated storms, storm longevity can be a strong indicator of supercell-type storm behaviour and should ideally be assessed in relation to additional supporting information.

2) Deviant motion: Although this is considered by many to be a classic supercell characteristic, as indeed it is, two caveats require mention. Firstly, most but not all supercells exhibit deviant motion, which may be to the left or right of mean flow, depending on the (cell-splitting) history of the cell as well as the prevailing shear regime. Secondly, in the case of airmass thunderstorms developing on the periphery of an anticyclone, it is typical for newer, weaker cumulus cells to exhibit similar movement, under the influence of primarily 700 to 600 hPa winds, whilst more mature, taller storms are more influenced by 500 to 400 hPa winds, often allowing for motion that is to the left of the smaller cells. Whilst this is indeed “deviant motion” in the broad sense of the word, it is usually not indicative of classic supercell-type storm development.
3) Pronounced low-level speed and directional shearing, typically backing with altitude: often termed deep, persistent shear (Davies-Jones, 1984; Brooks *et al.,* 1994) is a good indicator of likely supercell potential, but should be considered in association with points 1, 2 or 3 in the primary list above. Ordinary, non-supercell airmass storms can still develop within such a sheared environment
4) Storm-splitting on RADAR: The storm-splitting process can be a strong indicator of incipient or imminent supercell development, in one or both of the cells. Often, the equatorward member is favoured at the expense or demise of the poleward element however this can also result in failed supercells which may collapse and dissipate soon after the split (Visser, 2001).

3.6 Statistical assessment of supercell and non-supercell samples

A key activity associated with this study will be to assess and quantify the nature of the distribution of the SUP dataset as well as that of the NON-SUP dataset. It is known from the preceding sections of the current chapter, that the SUP dataset of supercells within a 200 km radius of the Irene facility has a relatively small sample size of $n_1 = 15$. Conversely for the NON-SUP sample of 510 austral thunderstorm days within the Gauteng area, 2007 to 2011, from a statistical point of view is a relatively large sample size of $n_2 = 510$ days.

Firstly, the general nature of the distribution of the SUP dataset will be explored and presented in Chapter 4 to follow, primarily by means of box and whisker plots (Tukey, 1977). Secondly and in a similar fashion, the NON-SUP dataset will be explored in Chapter 5.

In Chapter 6, statistical parameters and measures of distribution relating to each of the SUP and the NON-SUP datasets will be determined. This will be important as it will lead into further statistical analysis where it will be investigated whether the distributions can be associated with the normal distribution. Investgation relating to normality of one or more distributions will be performed with the use of cumulative probability plots, with respect to the variable of interest in order to assess the presence or absence of linearity in the plotted variable.

Aspects relating to the independence and variance of the SUP and NON-SUP datasets will similarly be discussed in Chapter 6, especially in relation to hypothesis testing and ultimately the selection of thunderstorm variables to form the basis of the modified Supercell Composite Parameter (MSCP). Furthermore, a range of parametric tests and non-parametric tests will be employed in Chapter 6 to investigate the normality of the datasets in question.

3.7 Summary

A range of datatypes used within this study were introduced, as well as methodology employed in relation to each datatype. The relation of various datatypes toward one another was also discussed in the context of this study. Certain data would require pre-treatment prior to other components of the study. A universal naming convention was proposed, in respect of supercell storm movement. The particular choice of geographic domain was explained, while aspects relating to QC of upper air data as well as proximity soundings were similarly presented.

A key component of this study, namely the identification criteria relating to supercells was also presented in some detail, with acknowledgement that general agreement regarding a universal definition of supercell criteria is not yet in place. The chapter concluded with a broad overview of methodology to be followed regarding statistical analysis of the SUP supercell sample as well as the NON-SUP non-supercell sample, particularly intercomparison thereof, which will be conducted in detail in Chapter 6.

CHAPTER IV : THE SUPERCELL SAMPLE DEFINED

4.1 Supercell cases

A map of the geographic locations of the 15 supercell cases is provided in Fig. 4.1, whilst the associated geographic co-ordinates for said sample are listed in Table 4.1. In accordance with the proximity sounding criteria for this study, all 15 supercell cases within this group occurred within a radius of 200 km from the Irene RADAR site, as per the rightmost column in Table 4.1. Occasionally more than one supercell storm was noted within the domain on the same day. For the purposes of this study, such days counted only as one realisation of a supercell event.

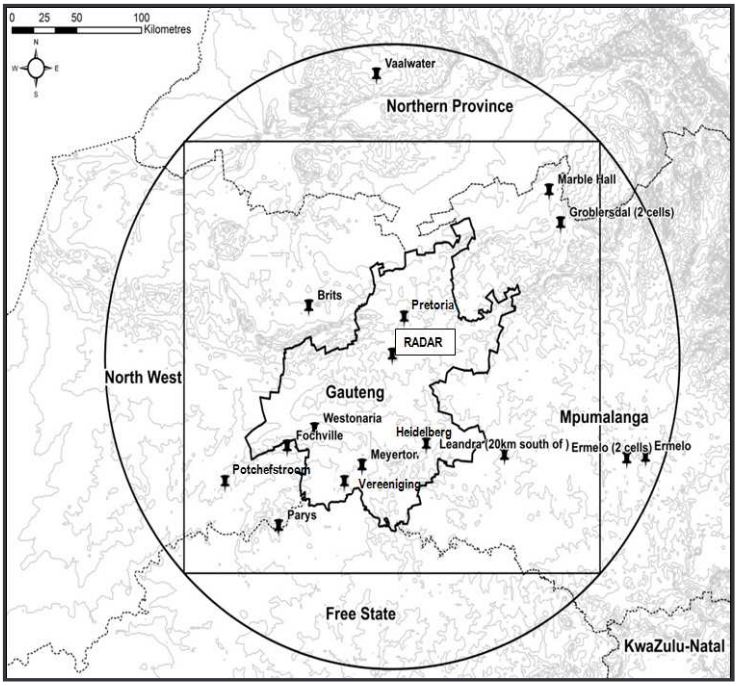

FIGURE 4.1: The study domain centred over Gauteng and including sections of adjacent provinces. The domain is indicated by a 200 km range ring surrounding the Irene RADAR (pushpin icon labelled "RADAR" at centre of image). Black pushpin icons denote locations of the 15 SUP supercell cases used in this study. Source map generated using ESRI ArcGIS 10.1.

In terms of the 15 cases used for the SUP supercell sample, as reflected in Table 4.1, the majority of the cases were based on the corresponding 12h00UTC proximity soundings. However, for two particular events on the list, namely the Marble Hall

and Brits events, the 12h00UTC upper air data was either missing or too corrupted to utilise and consequently 00h00UTC sounding data of 12 hours prior to midday were used. In these particular cases, the sounding was modified to simulate midday conditions by substituting an appropriate surface temperature and dewpoint pair (T, T_d), drawn from the corresponding 13h00SAST (11h00UTC) surface observation at Irene, as described in Chapter 3.

TABLE 4.1: Chronological listing of 15 supercell cases used as the SUP supercell sample for the study domain. All cases were within a 200 km radial distance from the Irene RADAR facility.

No.	Date YYYYMMDD	Location	Province	Latitude (South)	Longitude (East)	Distance to Irene radar (km)
1	19851101	Pretoria	Gauteng	-25.73	28.01	20
2	19991021	Heidelberg	Gauteng	-26.64	28.39	70
3	20001205	Vereeniging	Gauteng	-26.66	27.92	93
4	20041027	Potchefstroom	NorthWest	-26.70	27.10	140
5	20071006	Westonaria	Gauteng	-26.34	27.67	80
6	20071007	Groblersdal (2 cells)	Limpopo	-25.15	29.38	141
7	20071008	Leandra (20km south of)	Mpumalanga	-26.49	28.99	105
8	20071019	Fochville	NorthWest	-26.44	27.48	95
9	20071106	Vaalwater	Limpopo	-24.29	28.10	190
10	20071116	Ermelo	Mpumalanga	-26.50	29.97	195
11	20081105	Parys	Free State	-26.90	27.42	130
12	20091107	Meyerton	Gauteng	-26.55	28.00	80
13	20101024	Marble hall	Limpopo	-24.96	29.30	108
14	20101105	Ermelo (2 cells)	Mpumalanga	-26.51	29.84	185
15	20111002	Brits	NorthWest	-25.63	27.63	52

4.2 Supercell criteria

In line with the criteria relating to supercells defined in the methodology of Chapter 3, the thunderstorm and supercell features associated with each case were logged accordingly in Table 4.2. It will be recalled from Chapter 3 that for the purposes of this study, the necessary and sufficient criteria for a storm to be considered as being a supercell is/are one or more of the following (1) clear evidence of a mesocyclone, either in terms of Doppler RADAR radial velocity couplet or visual observation of wall cloud (Fujita, 1960a), (2) A RADAR-observed BWER or WER and (3) a well-defined hook echo feature. As stated in Chapters 2 and 3, with respect to supercell diagnostics, additional storm features such as (i) deviant motion (ii) notable longevity (iii) low-level shearing and (iv) RADAR-observed storm-splitting may be associated with supercells but are not sufficient evidence in isolation from criteria (1), (2) and

(3). In Table 4.2, the greyed-out column represents cases pre-dating the availability of Doppler RADAR data, in which case radial velocity information was not available.

TABLE 4.2: Supercell criteria and characteristics associated with the SUP supercell case sample. Note that greyed out cells indicate cases pre-dating the availability of Dopper-enabled RADAR radial velocity data.

Case	Date YYYYMMDD	Place	deviant movement	signif l/l shearing (speed and/or dir)	BWER or WER	mesocyclone (radar)	mesocyclone obs (wall cloud)	Hook echo	notable longevity
1	19851101	Pretoria	NO	•			•		•
2	19991021	Heidelberg	•	•				•	
3	20001205	Vereeniging	•		•				
4	20041027	Potchefstroom	•	•	•		•		•
5	20071006	Westonaria	•		•				
6	20071007	Groblersdal	•		•				•
7	20071008	Leandra (20km south of)		•			•		
8	20071019	Fochville	•		•				
9	20071106	Vaalwater/Waterberg	•	•	WER				•
10	20071116	Ermelo	•					•	
11	20081105	Parys/Carletonville	•		•			•	•
12	20091107	Meyerton			•	•		•	
13	20101024	Marble Hall+IR (2 cells)	•	•	•	•		•	
14	20101105	near Ermelo (2 cells)	NO	•	•				
15	20111002	Brits	•		•	•			•

For cases from 2009 onwards, radial velocity information was indeed available to allow potential identification of radial velocity couplets, indicative of mesocyclonic rotation. However in one particular pre-2009 instance for the 8 October 2007 Leandra case, this author witnessed a wall cloud feature in association with the storm in question, making photographic record thereof, as shown in Fig. 4.2 (Rae, 2007b). In the case of the 6 November 2007 Vaalwater/Waterberg case in Table 4.2, the storm was 190 km away from the RADAR and only a weak echo region (WER) could be inferred. Interestingly, *bona fide* hook echo features could only be identified in a few of the cases but this was not unexpected, as it was stated in Chapter 2 that, due to the low-level nature of this storm feature, the hook echo is not identifiable at great distances from the RADAR. Deviant motion was notable in

many cases, however, again in accordance with the supercell criteria defined for this study, this feature alone was not considered to be strong enough evidence to classify the storm as being a supercell. Furthermore, not all supercells exhibit deviant motion, as exemplified by the Ermelo, 5 November 2010 event, where observed motion did not deviate markedly from the prevailing mean flow. The Viljoenskroon supercell of 28 November 2013, presented in fair detail in Chapter 7, was similarly not associated with a track that showed any significant deviation from the mean flow on the day in question.

FIGURE 4.2: Photo of wall cloud (Fujita,1960a) at centre, and tail cloud (Fujita,1960a) at left, associated with mesocyclone of Leandra supercell 8 October 2007, looking west at 16h27SAST (14h27UTC), with clockwise rotation observed. From Rae (2007b), photo by this author.

In Table 4.3 a listing of primary observed thunderstorm parameters associated with the 15 supercell cases is provided. The distribution pattern of each of these 8 parameters was briefly assessed by means of box and whisker plots (Tukey, 1977). The nature of said distributions will however be reported in greater detail in Chapter 6, especially from a statistical perspective.

TABLE 4.3: Supercell thunderstorm parameters for the SUP sample. Units of measurement for SBCAPE and MUCAPE in J kg^{-1}, NCAPE in J kg^{-1} m^{-1} while SRH is m^2 s^{-2}. Corresponding unit of measurement for BRNshear is m^2 s^{-2}. BRN (also known as R) is dimensionless.

No.	Date YYYYMMDD	Location	SBCAPE	NCAPE	MUCAPE	SRH 1km	SRH 2km	SRH 3km	BRN	BRN shear
1	19851101	Pretoria	1131	0.2	1705	0	-30	-80	20	83.6
2	19991021	Heidelberg	313	0.18	1794	-124	-433	-459	11	163.4
3	20001205	Vereeniging	1354	0.18	1935	-38	-51	-55	41	46.9
4	20041027	Potchefstroom	444	0.13	1176	-73	-279	-338	9	126.4
5	20071006	Westonaria	202	0.12	1254	-64	-142	-214	11	110
6	20071007	Groblersdal	1223	0.26	2826	-49	-132	-142	18	152.8
7	20071008	Leandra (20km south of)	1962	0.27	2761	-167	-195	-226	20	140.8
8	20071019	Fochville	971	0.27	2556	-53	-92	-119	59	43.4
9	20071106	Vaalwater	715	0.21	2056	-74	-96	-110	88	23.4
10	20071116	Ermelo	1507	0.14	1071	-35	-72	-106	23	46.6
11	20081105	Parys/Potchefstroom	272	0.12	1270	-124	-158	-168	26	48.4
12	20091107	Meyerton	816	0.31	3463	-72	-263	-266	80	43.2
13	20101024	Marble Hall	393	0.13	1162	-215	-297	-374	12	97.1
14	20101105	Ermelo (2 cells)	1001	0.28	2736	-103	-184	-204	22	122.4
15	20111002	Brits	1103	0.08	800	-218	-385	-488	5	168

For reference purposes a table of the various sources consulted in relation to the SUP supercell sample is provided in Table 4.4. Of interest, the 2 November 2011 Brits case occurred on the same date as a tornadic, non-supercell thunderstorm which devastated parts of Duduza, south of Johannesburg. By contrast, the Brits storm, although clearly severe, is not known to have been associated with any reported tornadoes.

TABLE 4.4: Sources and references associated with each of the 15 SUP supercell cases.

No.	Date YYYYMMDD	Location	Province	Reference
1	19851101	Pretoria	Gauteng	Terblanche (1985)
2	19991021	Heidelberg	Gauteng	de Coning et al. (2000b)
3	20001205	Vereeniging	Gauteng	Rae (2000), The Citizen (2000)
4	20041027	Potchefstroom	NorthWest	Brimelow (2004), Clark (2004)
5	20071006	Westonaria	Gauteng	Brouwers & Todd (2007), SAWS (2007), Beeld (2007)
6	20071007	Groblersdal	Limpopo	Brouwers & Todd (2007), Rae (2007), SAWS (2007)
7	20071008	Leandra (20km south of)	Mpumalanga	Rae (2007a;2007b), SAWS (2007)
8	20071019	Fochville	NorthWest	Todd (2007), SAWS (2007)
9	20071106	Vaalwater	Limpopo	Todd (2009)
10	20071116	Ermelo	Mpumalanga	SAWS (2007), Rae (2007)
11	20081105	Parys/Potchefstroom	Free State	Rae (2008), SAWS (2008), Todd (2009)
12	20091107	Meyerton	Gauteng	Loots (2009)
13	20101024	Marble Hall	Limpopo	Powell et al. (2010), Powell (2011a; 2011b)
14	20101105	Ermelo (2 cells)	Mpumalanga	Powell (2011a; 2011b)
15	20111002	Brits	NorthWest	Todd (2011)

4.3 Box and whisker analysis: supercell sample

As can be seen in Fig. 4.3 as well as Table 4.3, the selected supercell cases were all associated with storm-relative helicity (SRH) ≤ 0 $m^2 s^{-2}$. Furthermore, with reference to Fig. 4.3, the smallest SRH median was encountered in the 0-1 km AGL layer whilst the largest SRH median was associated with the 0-3km AGL layer. Whilst each distribution, particularly in terms of interquartile range (IQR), appeared to show fairly marked differences, this aspect was investigated in greater depth through the use of "notched" MATLAB boxplots in Chapter 6. With reference to Table 4.3, all but the first supercell event returned non-zero values of 0-1 km SRH, hence it was considered useful and potentially informative to include 0-1 km SRH in the study design. The decision to utilise 0-1km SRH was also guided by the opinion of Rasmussen (2003) who discussed the selection of optimum SRH layers, other than 0-3km AGL. Whilst Rasmussen's particular focus was tornadic supercells, this author considered the possibility that 0-1km SRH may well have predictive utility with respect to supercells in general.

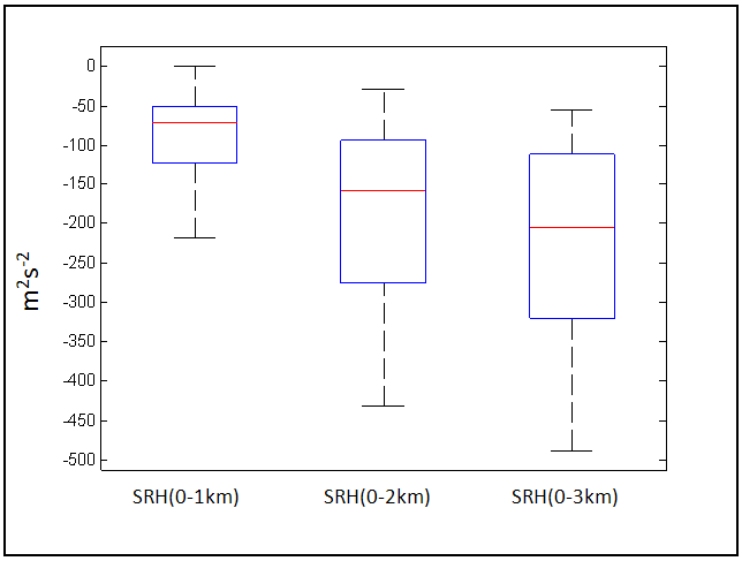

FIGURE 4.3: Box and whisker ('boxplot') representation of storm-relative helicity (through varying layers AGL), based on the SUP supercell dataset. Note that in all selected cases, SRH was negative, which is typical for EMM left movers in the southern hemisphere.

In Fig. 4.4 the distribution of Normalised CAPE (Blanchard, 1998) is indicated. Blanchard designed Normalised CAPE (hereafter NCAPE) in an effort to allow easier intercomparisons of upper air sounding profiles. NCAPE is simply CAPE divided by the total altitude, in metres, through which CAPE integration has taken place. Typically, for southern African conditions, this altitude is often of the order of 8000 to 12000m. Another alternative regarding NCAPE formulation is to divide CAPE by the pressure difference in hPa through which CAPE integration was performed. The latter formulation however was not utilised for this research work. In Fig. 4.4 it can be noted that NCAPE responded over a fairly compressed IQR with only a small magnitude of variation, making this parameter potentially an appealing candidate to consider for inclusion in MSCP. The question of whether NCAPE would indeed be normally distributed was further explored in Chapter 6.

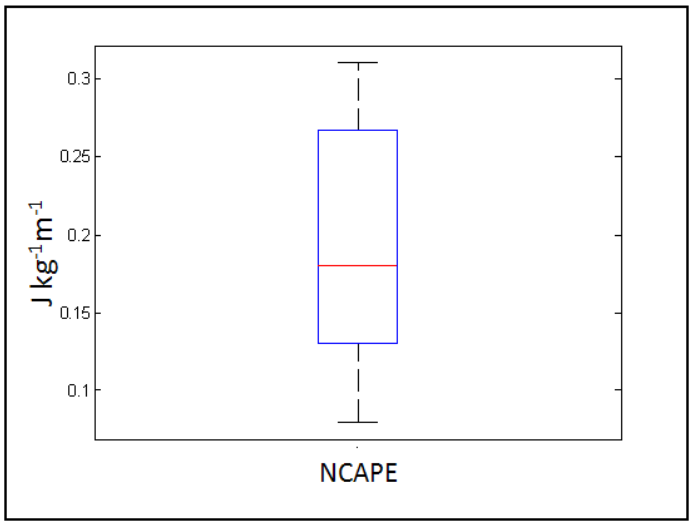

FIGURE 4.4: Normalised CAPE (Blanchard, 1998), based on the SUP supercell dataset.

The other two variants of CAPE considered in this study were Most Unstable Cape (MUCAPE) and Surface-based CAPE (SBCAPE) respectively. As each of these CAPE variants are expressed in units typical of CAPE calculations, namely J kg^{-1}, both were plotted side by side in Fig. 4.5. As would be expected, MUCAPE suggested a significantly wider IQR than SBCAPE. Furthermore there appeared to be an absence of overlap of the MUCAPE IQR with its SBCAPE counterpart, strongly suggesting the two distributions were likely to be markedly different. This aspect was also further investigated in Chapter 6.

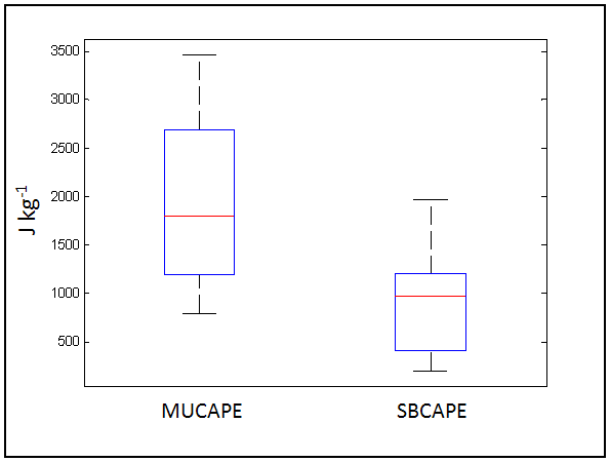

FIGURE 4.5: MUCAPE compared with SBCAPE for the SUP sample of 15 supercells.

The distribution of BRN in the SUP sample, as seen in Fig. 4.6, returned acceptable results, bearing in mind that all 15 cases were confirmed supercells and that Weisman & Klemp (1982, 1984) determined that the optimum range of BRN for supercell conditions was BRN Є [10; 40]. In Fig. 4.6 the value BRN = 10 and BRN = 40 were added as dashed lines to aid interpretation of Fig 4.6. The IQR of BRN conveniently fell within these two bounds, graphically supporting the position of Weisman and Klemp in this regard.

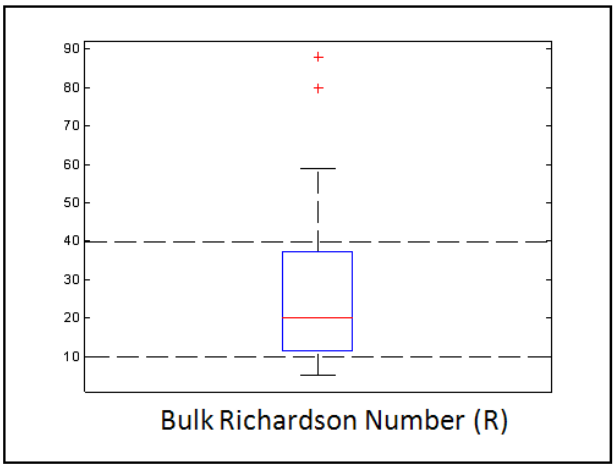

FIGURE 4.6: Bulk Richardson Number (R, also known as BRN). Work by Weisman & Klemp (1982, 1984) suggests that values of R between 10 and 40 (indicated by dashed lines in this figure) are optimal for supercell development.

A box and whisker plot of the shear term (denominator) of the Bulk Richardson Number, also known as Bulk Richardson shear, which quantifies the degree of west to east orientated (*i.e*. the 'x' component) wind shear is shown in Fig. 4.7. Larger values of BRN shear are proportional to increasing shear aloft. A fairly wide IQR was in evidence, indicative of large variability between cases. The median was approximately 100 $m^2 s^{-2}$.

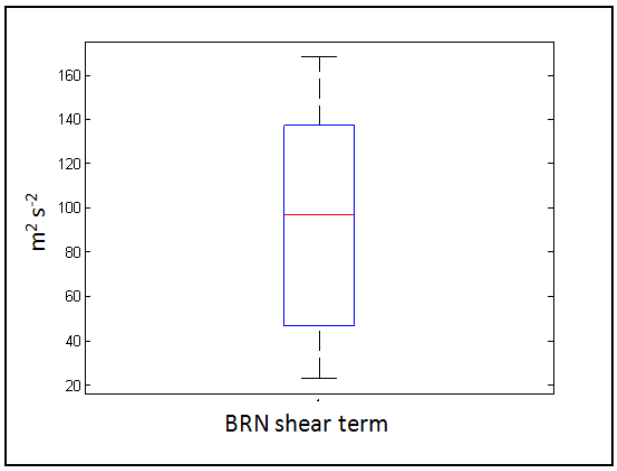

FIGURE 4.7: The shear term (denominator) of the Bulk Richardson Number for the 15 supercell cases in the SUP sample.

4.4 Other thunderstorms considered

Two significant historic thunderstorm cases considered for inclusion in this study but not appearing in the SUP supercell sample require at least a brief mention. The first was the long-track tornadic thunderstorm which devastated large parts of Roodepoort, Gauteng on 26 November 1948 (Goliger *et al*., 1997). Eye-witnessess reported that the tornado traversed from Roodepoort, east north-eastwards towards Irene, with the tornado damage swath recorded as being 64 km long (Goliger *et al*., 1997). Unfortunately this storm pre-dated the advent of instrument-enabled balloon soundings in South Africa and could not be further investigated for this study. It would seem unlikely that such a long-track tornado would not have been spawned by a supercell, however in the absence of additional supporting

evidence, the classification of particular case, in terms of storm type, remains at best one of speculative reflection.

The second storm, somewhat more recent in the historic record, was that of the very large-sized hail event which struck the Kempton Park area, resulting in extensive and extremely costly damage to commercial airliners at Jan Smuts Airport, now known as Oliver Tambo International Airport (ORTIA). This case was examined by Borstlap (1980). Irene radiosonde data as well as basic RADAR analyses were available during compilation of the original 1980 storm report. Whilst preliminary analysis of said upper air data (not shown) was not typically supportive of supercells, it remained intriguing that the storm was particularly long-lived, persisting from 12h00UTC to 15h20UTC, a matter of more than three hours according to Borstlap. Such longevity is suggestive that the storm in question was either a multicell- or supercell-type storm. Another intriguing aspect reported by Borstlap was the apparent absence of lightning at the airfield at the height of the hailstorm even though lightning both preceded and followed this period. He states "*...maar vanaf die haelaanslag (teen) 15h07* (SAST) *was die eienaardige afwyking dat weerligflitse ontbreek het.*" (Borstlap, 1980) or equivalently "…however, from the first onset of hail at 15h07 (SAST), it was an unusual departure (from typical storm behaviour?) that lightning discharges were absent…", leading to the possible interpretation that this could well have been an *in situ* observation of a "lightning hole" in association with a supercell mesocyclone. Such "lightning holes"; characterised by the supercell mesocyclone being almost totally devoid of lightning, have only in recent years been confirmed and documented in the literature via the superposition of high-resolution total lightning and RADAR data relating to supercells (MacGorman, 2002; Lang *et al.,* 2004; Calhoun *et al.*, 2013). These aspects are discussed in some detail in Chapter 2.

4.5 Summary

The SUP supercell sample was described, firstly in terms of geographic location of the 15 events within the Gauteng domain. Secondly, the particular supercell identification criteria for the supercell cases were listed in logframe format, along with corresponding references for each supercell storm case. Furthermore, box and whisker plots of such parameters as SRH, BRN, BRN shear and MUCAPE associated with the SUP supercell dataset were presented and discussed. Statistical aspects of this dataset were further investigated in Chapter 6, when quartiles of distribution for this data sample were established for use as threshold values in the definition of MSCP. Another component of general interest in this chapter was the brief discussion of two historic and significantly severe storms which were considered for inclusion in this study but which were omitted due to incomplete and/or inconclusive information.

CHAPTER V : THE NON-SUPERCELL SAMPLE DEFINED

Observational results relating to (1) SAWS LDN lightning data for Gauteng, (2) 2007-2011 upper air sounding data for Irene, Gauteng comprising 664 soundings as well as (3) the non-supercell sounding dataset of 2007-2011 austral summers, comprising 510 soundings (hereafter NON-SUP) are presented within this chapter. All three sets of data cover the period 2007-2011. Descriptive information is provided as to how each dataset was compiled and which data, if any, was discarded. Furthermore, intra-seasonal, graphic charts of selected Irene sounding-derived parameters for the period 2007-2011 are also presented, with the intention of gaining a deeper understanding of intra-seasonal variability of these parameters and how such variation could potentially influence the formulation of the Modified Supercell Composite Parameter.

It is important to mention that these three datasets had to be processed in sequential order and are thus presented in the chronological sequence in which they were created. In order to generate a master list of all Gauteng “thunderstorm days” for the period in question, the LDN data was processed first. This list of thunderstorm days was subsequently compared against available Irene 12h00UTC soundings in order to match each thunderstorm day with a corresponding sounding, resulting in 664 such soundings. This dataset of 664 soundings is representative of a storm climatology for Gauteng for the 2007 to 2011 period and is therefore presented and discussed in fair detail in order to better understand intra-seasonal nuances of thunderstorm parameters to be utilised in the design of the MSCP. The final activity relating to this chapter concerns the further truncation of the 664 sounding dataset to reflect only 510 austral summer cases. This was done in an effort to allow the distribution of storm parameters within the final non-supercell dataset to be more characteristic of the Gauteng thunderstorm season on the southern African Highveld, which is predominantly limited to the summer months (Tyson, 1997).

5.1 Lightning data (LDN), 2007-2011

Cloud-to-ground (CG) lightning stroke data for the entire Republic of South Africa (RSA) for the period 2007 to 2011, was obtained from the Vaisala Lightning Detection Network (LDN) of SAWS. There were no missing days of data from the dataset hence there were 1826 possible storm days to consider. The data was further filtered to include daily data only for the latitude and longitude coordinate box domain described in Chapter 3. This process produced a first cut of 989 storm days occurring within the period 00h00SAST to 24h00SAST daily. A further 61 storm days were precluded from the study, due to an absence of corresponding 12h00UTC Irene upper air data, resulting in (989 – 61) = 928 days. This preliminary dataset was trimmed once more, this time to include only lightning strokes for the daily 6 hour period, 11h00 to 17h00 to correspond with proximity sounding guidelines, where a six hour time-window was specified. A threshold criterion of two or more CG lightning strokes within the 6 hour window period was applied, in line with the approach adopted by Reap (1986). This process resulted in a further 171 of the 928 days being precluded from the pool of storm days, thus reducing the potential dataset to 757 days. However, once comprehensive QC of upper air data was applied as described in Chapter 3, a total of 664 days ultimately remained in the dataset.

5.2 Irene upper air soundings, 2007-2011

All available soundings for the period 2007-2011 for the Irene site were retrieved from the online archive of the University of Wyoming USA (UWYO, 2014) in text format, as per the data processing strategy outlined in Chapter 3. Only data pertaining to 12h00UTC soundings were utilised and analysed with the use of RAOB 6.3 software. Furthermore, all QC checks formulated and discussed in Chapter 3 were rigorously applied. Table 5.1 is a record of the relative tally of soundings used or not used as the case may be, for each respective year 2007 to 2011.

TABLE 5.1: Quality-control records of all upper air soundings considered for the study.

Irene (WMO station number 68263) upper air sounding data, 2007-2011						
Year	total possible soundings (2 per day)	number of soundings downloaded	number of midday soundings	storm days of interest	missing soundings on storm days	quality control , soundings of low quality, precluded from study
2007	730	531	298	126	28	5
2008	731	712	358	162	5	5
2009	730	694	347	168	3	13
2010	730	432	222	149	7	26
2011	730	510	258	126	14	18
Total	3651	2879	1483	731	57	67

In order to gain additional insight into the variation of certain thunderstorm parameters, particularly those of storm-relative helicity (SRH), CAPE, Bulk Richardson shear as well as the Bulk Richardson Number (BRN or R) which are all components in one form or another of the SCP (Thompson *et al*., 2002; 2003) it was considered relevant in the context of this study to graphically explore the 664 selected thunderstorm days across the full 2007 to 2011 period, particularly the intra-seasonal variation thereof. This prompted the inclusion of aspects of intra-seasonal variation in thunderstorm parameters over Gauteng as one of the stated Objectives of this study. It should be mentioned that, unlike a regular climatological record of all days within a defined chronological period, this particular dataset of N = 664 was unique in that it was a record that had been filtered, not only to represent "thunderstorm days" within the domain, but in particular (a) those days where thunderstorm activity was confirmed by SAWS LDN analysis to have been within a six hour window of the midday ascent and (b) where the parcel method of simulated convection could confidently be applied to the corresponding upper air sounding profile. Hence, the following series of MATLAB-generated box and whisker plots for N = 664 thunderstorm days offer a unique perspective into the monthly and seasonal variation in selected storm parameters for the 2007 to 2011 period in the Gauteng province, as represented by the Irene upper air data. RAOB 6.3 was utilised to process said sounding data, whilst MATLAB was utilised for visualisation thereof.

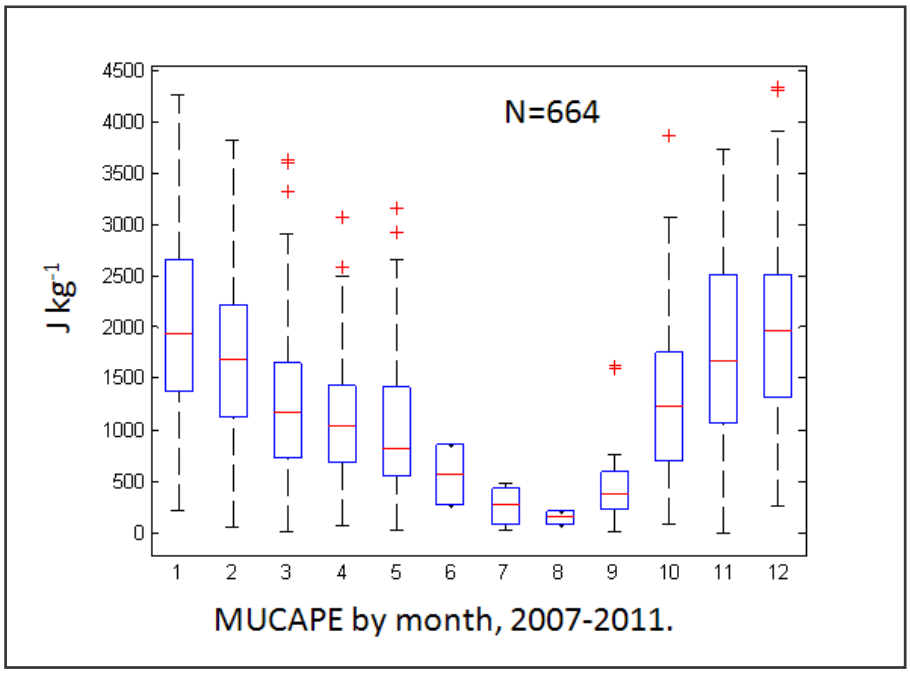

FIGURE 5.1: MUCAPE by month, 2007-2011 for all N = 664 soundings on storm days as defined for this study. In this Figure and in all subsequent box and whisker 'boxplots', the median (Me = Q2) is indicated as a red horizontal line segment within each box, while the lower and upper limits of the solid blue box are the first quartile (Q1) and third quartile (Q3) respectively. The lower and upper whisker limits respectively indicate the location of the 10th and 90th percentile of each distribution. Outlier or extreme values, exceeding the 10th and/or 90th percentile limits are indicated in the form of red crosses. It can be noted that in this plot and all subsequent box and whisker plots that no naturally-occurring outlier values were omitted or otherwise screened from any distribution.

As could be expected for the summer rainfall Highveld region, Most Unstable CAPE (hereafter MUCAPE) in Fig. 5.1 was highest in the summer months and dropped off to almost negligible values to well below 500 J kg^{-1}, especially in the winter months of July and August. It was notable that there was a pronounced "jump" or discontinuity, starting from the month of September and continuing into October, where a sharp rising trend was observed. It was also noted that the upper outliers (indicated henceforth in this and all subsequent MATLAB box and whisker plots with a red cross and defined in the caption of Fig. 5.1) were particularly prevalent in spring and autumn.

Bearing in mind that storm-relative helicity (SRH) is typically negative in the southern hemisphere, a few instances of positive SRH outliers were noted, indicating days where anticyclonic or atypical supercell development may have been favourable, given additional supporting factors.

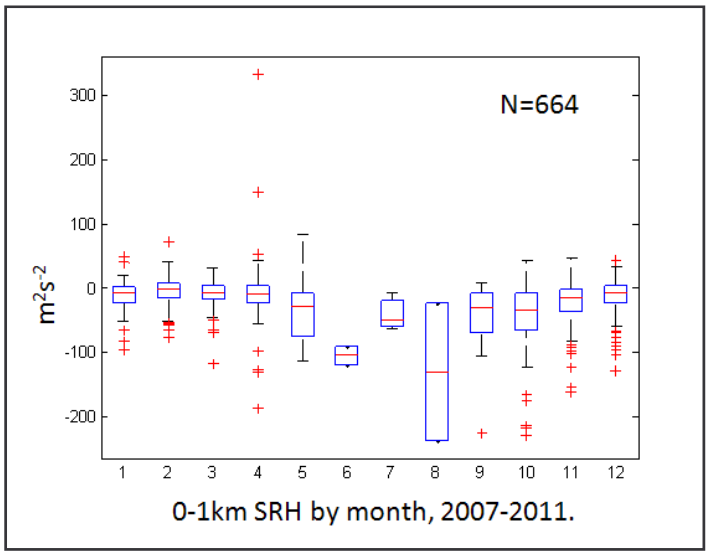

FIGURE 5.2: Storm-relative helicity (SRH), (0-1 km) by month, 2007-2011 for all N = 664 soundings on storm days as defined for this study.

This tendency was identified in the plots for SRH 0-1 km (Fig. 5.2), SRH 0-2 km (Fig. 5.3) and SRH 0-3 km (Fig. 5.4), with two outlier cases which occurred in the month of April. It was furthermore noteworthy that 0-1 km SRH (Fig. 5.2) indicated a high proportion of outliers, mostly in the summer months, at the negative-oriented, extreme end of the distribution.

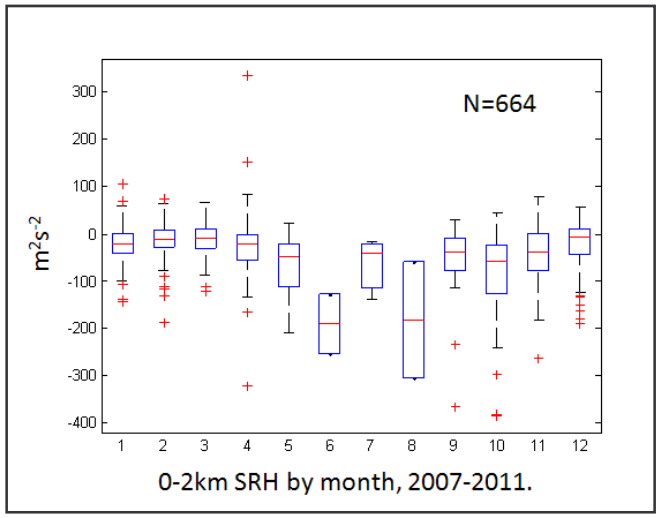

FIGURE 5.3: Storm-relative helicity (SRH), (0-2 km) by month, 2007-2011 for all N = 664 soundings on storm days.

Another interesting aspect was that in Fig. 5.2, 0-1 km SRH showed very little spread or variability in the interquartile range (IQR), compared with 0-2 km SRH and 0-3 km SRH. For 0-2 km SRH (Fig. 5.3) and 0-3 km SRH (Fig. 5.4), it could be concluded that

the SRH values in the first half of summer *i.e.* early summer were markedly greater than those of the months occupying late summer. It was thus inferred that general shearing, in a speed and directional shearing context (Markowski & Richardson, 2006), was markedly greater in the early months of summer as opposed to the latter. In general it was also noted that SRH values attained extremely large negative values at the height of winter. Hence thunderstorms in this season, albeit typically represented only by one or two such events per month, should be closely monitored as potential supercell candidates with a high likelihood of severity. The supercell storm outbreak of 23 June 2012 (Loots, 2012) is an excellent case in point. A final comment regarding SRH, for all three layer variants, is that whilst high magnitude, negative outliers were encountered across all summer months, the outliers with the greatest magnitude were clustered around the early summer months.

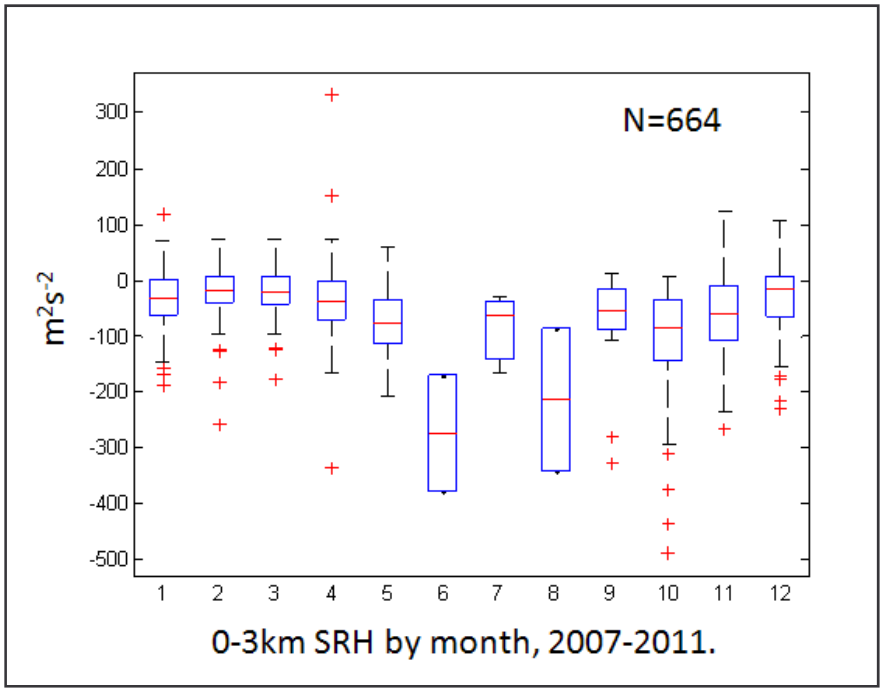

FIGURE 5.4: Storm-relative helicity (SRH), (0-3) by month, 2007-2011 for all N = 664 soundings on storm days.

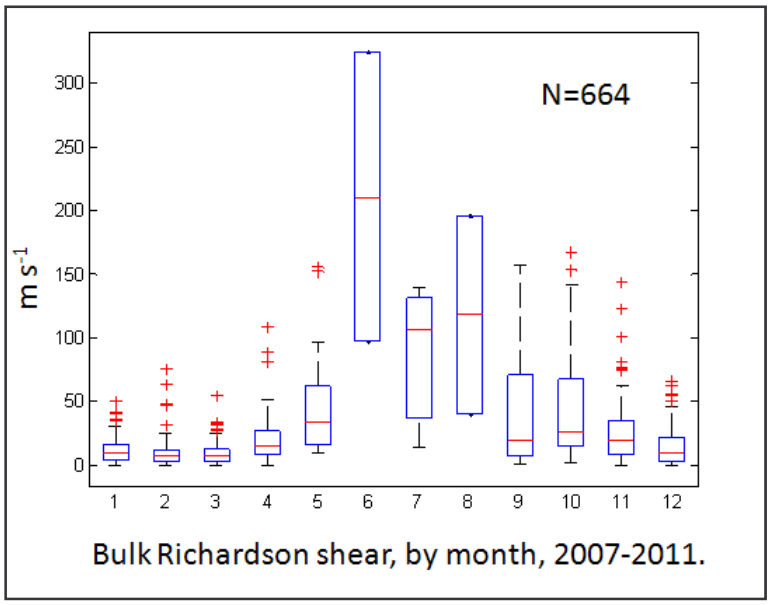

FIGURE 5.5: Bulk Richardson shear term, by month, 2007-2011 for all N = 664 soundings on storm days.

In Fig. 5.5, a box and whisker plot of Bulk Richardson shear (being the west-east speed shearing term of BRN), it was interesting to note that there was some evidence of a bi-modal monthly distribution as well as a distinct dichotomy between late summer months, characterised by low shearing and small variability in the IQR, as opposed to the early summer months, especially the period August to October, where high variability (as evidenced by the broad IQR spread) and high quantitative values were typically encountered. Extreme, positive outliers were strongly in evidence in numerous summer months.

5.3 The sample of 510 austral summer soundings, 2007-2011

In order to generate the non-supercell data sample which was to be further analysed and also statistically compared against the supercell sample in Chapter 6, the dataset of 664 soundings discussed in the preceding chapter section 5.2 required further adaptation. As mentioned in the introduction to this chapter, one of the objectives of this study was to conduct a comparison of a supercell sample contrasted against a sample of summer season, non-supercell thunderstorms within the same proximity

sounding domain. Whilst the mini-climatology of 664 thunderstorms of 2007 to 2011 fulfilled a key role in terms of allowing this author to better visualise intra-seasonal changes in said thunderstorm parameters, there was simultaneously also a concern that the winter months, dominated by low CAPE, high magnitudes of deep layer speed shear as well as very low monthly frequencies of thunderstorms, would unduly bias the distributions of thunderstorm parameters being investigated. This concern chiefly surrounded the quantification of the first quartile (Q1) of such distributions, some of which, according to this study design, would potentially be harnessed to provide threshold normalisation values for the three MSCP factors.

To address the above concern, it was decided to follow the approach of Dyson *et al.* (2014) and to focus attention on the six austral summer months of October to March in the compilation of the non-supercell sounding dataset. The SUP supercell sample dates all fell within this six month period, especially the months of October and November. Whilst is is not completely unprecedented to experience winter supercells in Gauteng (Loots, 2012), this could be considered to be a rare event. This study relied strongly on the quantification of typical Gauteng supercells, with such quantitative information utilised to modify and fine-tune the MSCP for typical Gauteng supercell conditions. As elaborated in Chapter 1, it is known and accepted that Gauteng thunderstorms are almost exclusively limited to the summer months, with only isolated individual records occurring in the winter months. Henceforth, it was thus both logical and justifiable to preclude the winter months from further study in relation to quantifying inputs into MSCP.

Consequently, to create the NON-SUP sample, the dataset of 664 Irene soundings described in the preceding section was trimmed of all thunderstorm cases occurring in the period 1 April to 30 September. In order to ensure that the NON-SUP dataset was as statistically independent as possible from the SUP dataset, any known supercell cases within the 2007-2011 period occurring within the NON-SUP dataset were also precluded from the NON-SUP dataset. This aspect was very important in relation to discussion and statistical assessment conducted in Chapter 6 surrounding the independence of the SUP versus NON-SUP samples. The prototype NON-SUP

dataset numbered 535 soundings, following deletions of winter storms as well as supercell dates common to the SUP dataset. Furthermore, an additional 25 soundings required removal, due to missing values of SBCAPE when processed by the RAOB program. The resulting sample of non-supercell soundings ultimately numbered n_2 = 510 soundings and was henceforth designated as the NON-SUP sample.

A selection of box and whisker plots of storm parameters for 510 thunderstorm days in austral months, 2007-2011 at Irene are provided in Fig. 5.6 to Fig 5.8. For brevity, only three such representative parameters were selected for display, as the full month by month climatology was presented and discussed detail in the preceding chapter subsection. In Fig.5.6, the pattern of MUCAPE was relatively symmetric, when the latter part of summer was compared against the early summer months. The months of January and December were characterised by the greatest median values. The IQR for November month was fairly large, suggestive of wide variation in values, in comparison with other austral summer months where more conservative IQR values were in evidence.

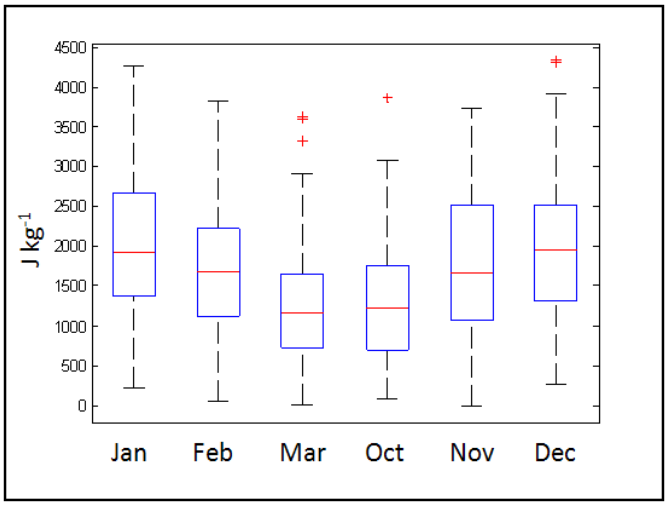

FIGURE 5.6: MUCAPE for austral months, 2007-2011 for all N = 510 soundings.

In terms of storm-relative helicity, the layer from the surface up to 3 km AGL was arbitrarily selected to be a representative plot for discussion and is shown in Fig 5.7. As expected, the monthly distributions are strongly biased towards negative values of SRH, although the upper extremes of each monthly distribution extended into

positive SRH values. There was also a strong indication of many outliers in most months, however the most extreme negative outliers, indicative of the presence of strong low-level helicity were clearly associated with the month of October. The month of October was also the summer month associated with the largest, negative-orientated, median value.

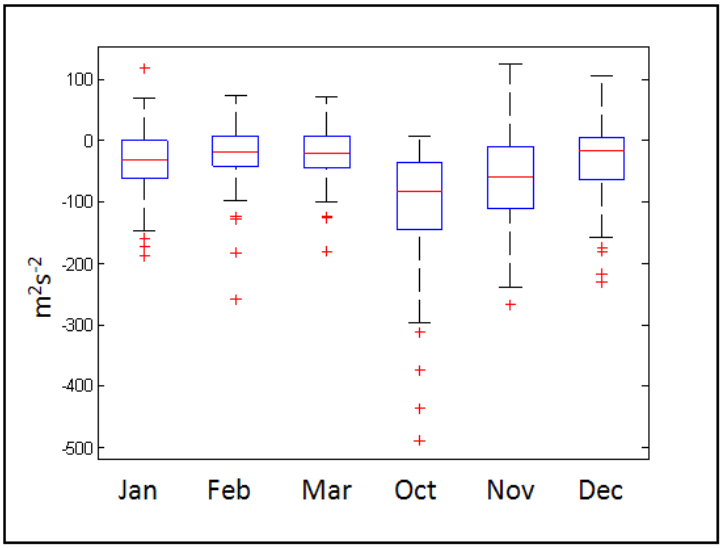

FIGURE 5.7: Storm-relative helicity, 0-3 km AGL (SRH3) for austral months, 2007-2011 for all N = 510 soundings.

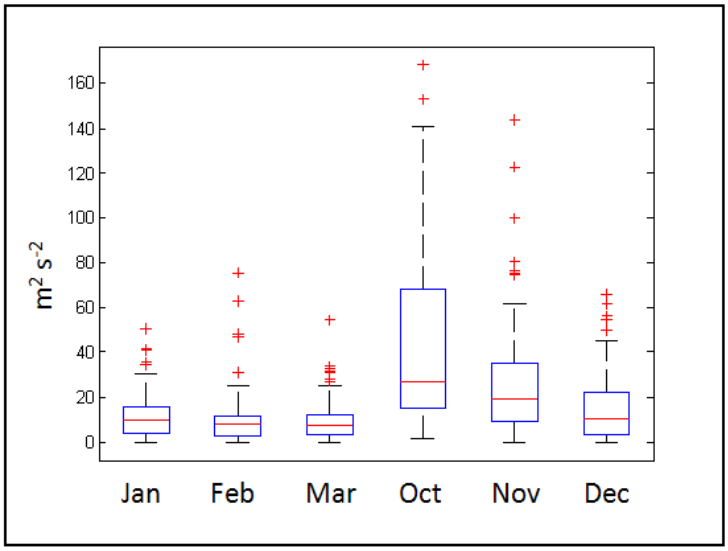

FIGURE 5.8: Bulk Richardson shear term (BRN shear) for austral months, 2007-2011 for all N = 510 soundings.

Quite a number of interesting features were noted in Fig 5.8. Firstly what was quite apparent was the sharp contrast in BRN shear values between the early and later

summer months. In the case of the former, the medians and well as IQR were significantly inflated, whereas by contrast, in the latter case, both the IQR range as well as medians were markedly suppressed. The month associated with the most extreme shearing within the fist 6 km AGL was the month of October, closely followed by November.

The introduction of a brief caveat is appropriate at this time; in order to serve as a reminder that, whilst the overwhelming majority of storms in the NON-SUP sample where characteristic of ordinary, non-severe airmass thunderstorms, there were certainly numerous cases of severe, albeit non-supercell thunderstorms within the NON-SUP sample, so the term NON-SUP does not automatically imply non-severe.

5.4 Summary

This chapter firstly introduced the SAWS LDN lightning data and put into context the key role this high-quality data played in terms of explicitly identifying days associated with thunderstorm activity in the Gauteng domain. Thunderstorm days were then compared against available upper air sounding data to ultimately establish a dataset of 664 proximity sounding thunderstorm days in Gauteng when storms were confidently known to have occurred within the temporal period 09h00UTC to 15h00UTC. In accordance with the study Objectives declared in Chapter 1, this dataset was graphically explored in detail with the aid of box and whisker plots with the intention of examining aspects of intra-seasonal variation in the behaviour of thunderstorm-related parameters such as CAPE, SRH and Bulk Richardson shear. Following this exercise, it was realised that whilst thunderstorms occurring over Gauteng during the winter months were relatively uncommon events, they were nevertheless often associated with extremely high shear through the lowest 6 km AGL. As a consequence, in order to suppress this and other effects which had the potential to introduce undesirable bias into the non-supercell sample, it was decided to focus the study exclusively on the austral summer season, when Highveld

thunderstorms were most prevalent. In this fashion, the truncation of the dataset of 664 thunderstorm days to filter out the winter months, April to September from the 2007-2011 sample, resulted in a final sample of 510 austral summer thunderstorm days, henceforth termed the NON-SUP, non-supercell thunderstorm sample. This concluded Chapter 5 with the intent that the NON-SUP sample, now clearly quantified, was to be further scrutinised and compared against the SUP supercell sample in Chapter 6 to follow.

CHAPTER VI : Sample comparison and MSCP formulation

In this chapter, the SUP and NON-SUP samples declared and presented in Chapters 4 and 5 were further analysed with a view to statistical intercomparison between said datasets. The aim of this activity was to gain further insight into of the nature and extent of the contrast between these datasets. Furthermore, as stated in the study Objectives in Chapter 1, to exploit these contrasts in order to redefine and fine-tune the SCP, thence to arrive at a Modified SCP (MSCP).

6.1 The supercell sample

As a precursor activity to the comparison between the SUP and NON-SUP samples, standard measures of location and dispersion were calculated for each sample. Eight RAOB-based thunderstorm parameters were generated for the SUP sample as per Table 6.1, resulting in a 15 x 8 matrix of 8 column vectors. Measures of distribution and location were calculated as per Table 6.2, including minimum, maximum, sample mean, sample median, sample variance, first quartile (Q1 = 25th percentile) and third quartile (Q3 = 75th percentile). MUCAPE was calculated using the virtual temperature (T_v) correction (Doswell & Rasmussen, 1994) and the level of free convection (LFC) whilst SBCAPE was calculated using surface temperature and dewpoint (T and T_d respectively), no T_v correction and parcel ascent up to the convective condensation level (CCL). By convention, the shearing term of the Bulk Richardson Number, referred to throughout as BRN shear, was calculated though a layer extending from the surface, up to 6 km AGL. Note that in Table 6.1, and in accordance with the approach followed by Thompson *et al*. (2002) the SUP sample exclusively comprised typical supercells which moved in an EMM fashion, in other words, equatorwards of mean storm motion, *i.e.* austral “left-movers”. This tendency could also be inferred from the distribution of SRH values, being exclusively negatively distributed. PMM

supercell movement, as discussed in depth within Chapter 2, is also possible but is encountered less frequently than the EMM left-movers. Austral PMM right-movers, if one ignores the contribution of splitting storms, can be generated by a speed and directional shear regime that exhibits a clockwise tendency with increasing altitude, hence resulting in atypical supercell movement. Under such austral conditions, SRH will typically be > 0 $m^2 s^{-2}$ for the majority of the first 3 km AGL. In the context of this study, it should thus be noted that, whilst MSCP was calibrated with 'typical' austral EMM supercells in mind, the final mathematical formulation of MSCP appearing later in this chapter nevertheless also accommodated the possibility of atypical supercell development.

TABLE 6.1: Supercell thunderstorm parameters for the SUP sample. Units of measurement as per Table 4.3.

No.	Date YYYYMMDD	Location	SBCAPE	NCAPE	MUCAPE	SRH 1km	SRH 2km	SRH 3km	BRN	BRN shear
1	19851101	Pretoria	1131	0.2	1705	0	-30	-80	20	83.6
2	19991021	Heidelberg	313	0.18	1794	-124	-433	-459	11	163.4
3	20001205	Vereeniging	1354	0.18	1935	-38	-51	-55	41	46.9
4	20041027	Potchefstroom	444	0.13	1176	-73	-279	-338	9	126.4
5	20071006	Westonaria	202	0.12	1254	-64	-142	-214	11	110
6	20071007	Groblersdal	1223	0.26	2826	-49	-132	-142	18	152.8
7	20071008	Leandra (20km south of)	1962	0.27	2761	-167	-195	-226	20	140.8
8	20071019	Fochville	971	0.27	2556	-53	-92	-119	59	43.4
9	20071106	Vaalwater	715	0.21	2056	-74	-96	-110	88	23.4
10	20071116	Ermelo	1507	0.14	1071	-35	-72	-106	23	46.6
11	20081105	Parys/Potchefstroom	272	0.12	1270	-124	-158	-168	26	48.4
12	20091107	Meyerton	816	0.31	3463	-72	-263	-266	80	43.2
13	20101024	Marble Hall	393	0.13	1162	-215	-297	-374	12	97.1
14	20101105	Ermelo (2 cells)	1001	0.28	2736	-103	-184	-204	22	122.4
15	20111002	Brits	1103	0.08	800	-218	-385	-488	5	168

It will be recalled from Chapter 3 that selected quartiles from this sample were to be identified as threshold normalisation values for MSCP. For clarification, the first quartile (Q1), or equivalently the 25th percentile of the distribution, was typically used as a potential threshold value for a particular parameter, given a positively distributed variable. Conversely however, for distributions displaying predominantly negative values, as in SRH (0-1 km), SRH (0-2 km) and SRH (0-3 km), in absolute terms, the smallest values correspond to Q3, being closest to the origin. Hence the latter quartile was utilised for SRH-related normalisation factors.

TABLE 6.2: Measures of location and dispersion associated with the SUP supercell sample (n_1 = 15). Units of measurement as per Table 4.3.

sample = SUP	SBCAPE	NCAPE	MUCAPE	SRH 1km	SRH 2km	SRH 3km	BRN	BRN shear
Mean:	894	0.19	1904	-94	-187	-223	30	94.4
Min value*:	202	0.08	800	-218	-433	-488	5	23.4
Max value*:	1962	0.31	3463	0	-30	-55	88	168.0
Quartile Q1 (P25):	406	0.10	1195	-124	-275	-320	11	46.7
Quartile Q2 (Me):	971	0.20	1794	-73	-158	-204	20	97.1
Quartile Q3 (P75):	1200	0.30	2691	-50	-93	-112	37	137.2
Skewness:	0.34	0.16	0.39	-0.73	-0.63	-0.70	1.29	0.08
Kurtosis:	2.36	1.70	1.97	2.57	2.38	2.32	3.33	1.53
Variance:	260600	0.0051	644701	4186	14693	18556	672	2488.4
n =15								

Another preparatory activity in terms of comparing the SUP and NON-SUP samples was to visually investigate and to note qualitative differences between the samples when plotted on a standard skew *T* / log p aerological diagram as in the RAOB-generated Fig. 6.1 for the SUP sample. In this Fig. the upper air data for the 15 supercell proximity sounding cases were averaged using an inbuilt RAOB function. With reference to Fig. 6.1, five main features, labelled “A” to “E” respectively were flagged for further discussion, especially in relation to how markedly the SUP supercell sample differed from its non-supercell counterpart, presented in Fig. 6.2. Firstly, at bottom right of Fig. 6.1, for the supercell case, the readily apparent presence of low-level north-easterly flow, backing anticlockwise with increasing altitude to a north-westerly flow within the first two kilometres AGL was noted. This type of directional shearing is the classic default shear profile for southern hemisphere supercells and is associated with large negative SRH values within the first three kilometres AGL. By contrast, this feature was entirely absent in the corresponding skew *T* / log p for the NON-SUP sample in Fig. 6.2. Additional, speed-related shearing features on the SUP averaged profile were also identified at “B” and “C” respectively, where wind speed values were on average, significantly stronger than for the NON-SUP counterpart at comparative altitudes. Furthermore, for the supercell sample, the upper winds in the free atmosphere exhibited a more north-westerly tendency than the NON-SUP sample, whereas the latter suggested a predominantly unidirectional, westerly flow at all levels.

At this point, particular note should be made that in Fig. 6.1 and in all subsequent RAOB-based skew *T* / log p plots; wind speed is expressed in knots, a non-S.I. unit of measurement. Whilst metres per second, the unit of measure for velocity in the S.I. system of measurement, is the preferred default scientific unit of measure, winds measured in knots are in routine and everyday operational use by forecasters and aviators alike and enjoy widespread use in the literature. As this research work has a strongly operational perspective, a conscious decision was made to adopt knots as the unit of measurement for wind speed, particularly with respect to graphs of aerological soundings as well as hodographs. Within the case studies presented and discussed in Chapter 7, frequent reference is made to the WINDEX (McCann, 1994) which is expressed in knots. The convenience of this choice is also highlighted in RAOB plots in Chapters 6 and 7, where wind strength is graphically coded according to long-established international convention for plotted aerological diagrams. Ten knots is represented as a full barb, five knots by a half-sized barb and fifty (50) knots by a triangular feather. To convert knots to metres per second ($m.s^{-1}$), use can be made of the relationship: 1 knot = 0.5144 m s^{-1}. The author however wishes to emphasise that this limited departure from the use of S.I. units of measure was informed by a desire to maintain ease of understanding for the reader, though the use of familiar wind barb graphical representation. However, notwithstanding the above, the author also wishes to make specific mention that for all calculations and formulas incorporating wind velocity, such as storm-relative helicity, Bulk Richardson Number and Bulk Richardson shear, the prescribed S.I. wind velocity unit of m s^{-1} was applied uniformly throughout this work.

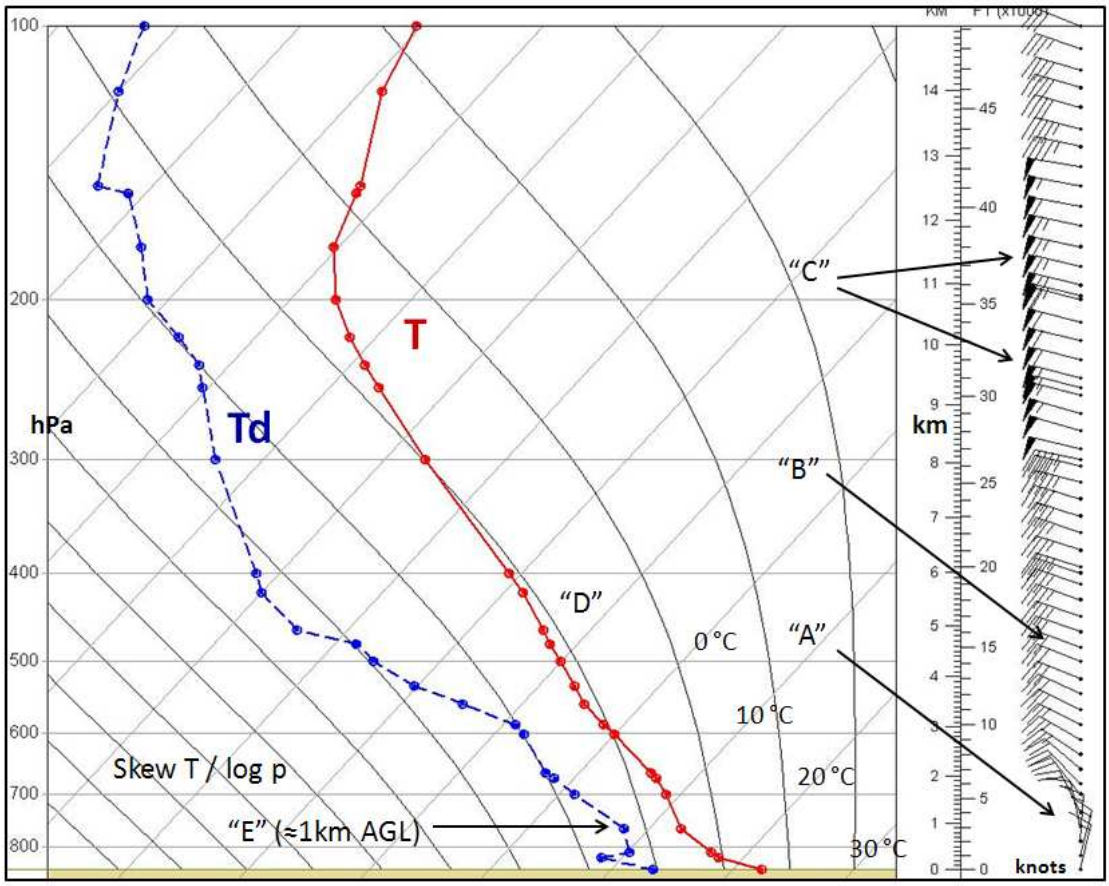

FIGURE 6.1: Averaged Irene midday soundings for 15 SUP supercell cases in skew *T*/ log p format. The red "*T*" trace represents observed environmental air temperature whilst the blue "T_d" trace correspondingly indicates environmental dewpoint. Units of *T* and T_d in °C. Logarithmic isobaric lines are drawn horizontally, while isotherms (°C) are angled at 45° from the horizontal plane, decreasing from bottom right to top left. Curved lines are saturated adiabats (°C) following the saturated adiabatic lapse rate. For improved clarity, neither dry adiabats nor mixing ratio lines are shown. The vertical scale at right represents altitude AGL, in km. Sounding diagram generated using RAOB 6.3, as in all subsequent skew *T* / log p diagrams.

Whilst both the SUP and the NON-SUP sample hinted at moderate levels of elevated instability, as indicated by the *T* trace at "D" associated with a more pronounced concave curvature away (to the left of the graph) from the closest saturated wetbulb curve, the SUP sample appeared slightly more unstable than the NON-SUP counterpart. Finally, with respect to "E", at approximately 1 km AGL, the SUP sample, on average, appeared to show a local maxima in available moisture, in the dewpoint (T_d) trace, corresponding to a value of about 8 °C. By contrast, whilst the NON-SUP sample was undoubtedly relatively moist in the near-surface layer, bearing in mind that the NON-SUP sample was for 510 known summer thunderstorm proximity sounding days, the NON-SUP sample exhibited a slightly less saturated near-surface layer than seen in the SUP sample. However, in mitigation of this observation; due to the large size (n_2 = 510 soundings) of the NON-SUP sample, the

RAOB program averaged and plotted the standard, mandatory WMO pressure levels (WMO, 1996), whereas in the SUP sample, additional 'significant' levels were averaged and plotted to augment the standard WMO levels. In other words, while the SUP and NON-SUP samples had comparable data density in the vertical, the RAOB algorithm automatically thinned the density of the data in the case of the large NON-SUP sample.

6.2 The non-supercell sample

The NON-SUP sample represented a sample of n_2 = 510 non-supercell Irene proximity sounding cases for 2007 to 2011 austral summers associated with diurnal thunderstorm activity on "thunderstorm days", 09h00 UTC to 15h00 UTC. The NON-SUP dataset was selected such that no known supercell cases and/or cases from the SUP sample occur therein. Whilst it was conceded that there may have been a few hitherto unidentified supercells within the NON-SUP sample, it was reasoned that, given the comparatively large size of the NON-SUP dataset, the presence of isolated unidentified supercells would not be sufficiently great as to significantly alter the likelihood of a Type I error during hypothesis testing. The validity of this assumtion was also revisited at the end of this chapter. By means of a hypothetical example to illustrate this; 10 supercells within a set of 510 thunderstorm days would only constitute approximately 2% of the overall sample. A Type 1 statistical error is defined as the incorrect rejection of the null hypothesis, while a Type II error is committed if one accepts the null hypothesis, when it is in fact false. Whilst the NON-SUP sample comprised non-supercell days, this did not preclude the fact that some storm-days in NON-SUP were associated with severe storms. In a similar fashion to the manner in which the SUP sample was expanded in Chapter 6.1, eight RAOB-based thunderstorm parameters were generated, resulting in a 510 x 8 matrix containing 8 column vectors. Measures of location and dispersion were calculated and presented as per Table 6.3, including minimum, maximum, sample mean, sample median, sample variance, first quartile (Q1 = 25^{th} percentile)) and third quartile (Q3 = 75^{th} percentile).

TABLE 6.3: Measures of location and dispersion associated with the NON-SUP non-supercell sample (n_2 = 510). Units of measurement as per Table 4.3.

sample : NON-SUP	SBCAPE	NCAPE	MUCAPE	SRH 1km	SRH 2km	SRH 3km	BRN	BRN shear
Mean:	603	0.17	1716	-18	-32	-45	307	18.7
Min value*:	0	0.00	8	-230	-385	-488	0	1.0
Max value*:	3003	0.40	4334	74	106	124	3166	168.0
Quartile Q1 (P25):	195	0.12	1077	-30	-56	-77	60	4.7
Quartile Q2 (Me):	482	0.16	1623	-10	-20	-33	135	11.6
Skewness:	1.16	0.30	0.42	-1.92	-1.63	-1.54	2.88	2.71
Kurtosis:	4.35	2.86	2.69	9.86	8.94	8.80	12.84	12.98
Quartile Q3 (P75):	868	0.22	2289	1	5	-2	325	24.5
Variance:	260841	0.0047	777895	1154	3174	4708	208689	467.0
n = 510								

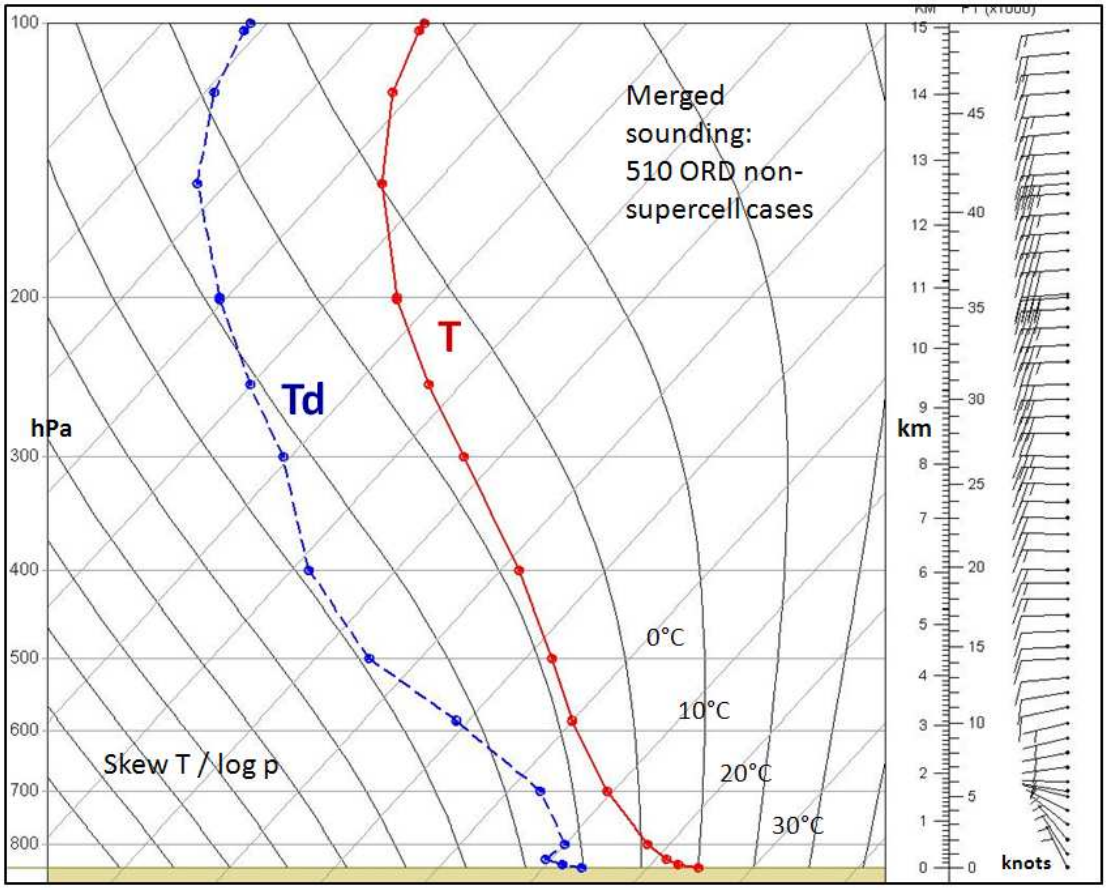

FIGURE 6.2: Averaged Irene midday soundings for 510 NON-SUP non-supercell soundings for austral summers, 2007-2011, in skew *T* / log p format. The red "*T*" trace represents observed environmental air temperature whilst the blue "T_d" trace correspondingly indicates environmental dewpoint. Units of *T* and T_d in °C. Additional reference lines and units as per Fig 6.1.

6.3 Statistical intercomparison of supercell and non-supercell samples

Before further analysis of the SUP versus NON-SUP samples could be contemplated, some basic assumptions requiring the nature of the samples had to be established (Wilks, 2011). These assumptions related to

(1) independence of said samples.
(2) the assumption that the samples were drawn from a Gaussian normal distribution.
(3) that the variance of each column vector of the samples was equal, or alternatively that the variance values did not differ too markedly from each other.

Following discussion presented in Chapter 5.3, it was established for the purposes of this study that assumption (1) was sufficiently met. Hence a like-for-like comparison of column vector components of SUP versus NON-SUP could similarly be considered to be independent. As each of SUP and NON-SUP contained eight column vectors, grouped by (a) CAPE-based parameters (b) helicity-based parameters and (c) shear-based parameters which corresponded broadly with the three components of the Supercell Composite Parameter, the column vector components of SUP and NON-SUP were similarly investigated in natural sub-groupings in terms of their normality and variance, being assumptions (2) and (3) respectively.

6.3.1 CAPE-based parameters

As per Fig. 6.3 MATLAB 'normplot', a plot of the cumulative probability distribution was applied to the first three column vectors of the SUP dataset. These three components were SBCAPE (surface-based CAPE), NCAPE (normalised CAPE) as well as MUCAPE (most unstable CAPE). In Fig.6.3, the plotted values of each parameter were considered to correspond closely to the normal distribution if they followed the solid linear line joining Q1 to Q3 of the respective distribution. The dotted line extending above and below the solid line represents whiskers and outliers that

extrapolate beyond the interquartile range (IQR). On preliminary visual inspection of this Fig. it was inferred that there was a fair degree of linearity exhibited by NCAPE, SBCAPE and MUCAPE respectively. Also notable were the outliers at either extreme of each distribution. While the outliers could conceivably result in challenges related to further parametric analysis, these extremes were judged to be important in the context of the SUP supercell sample, especially given the small sample size (n_1 = 15) of the dataset and were therefore not screened or filtered in any way. While these initial results were encouraging, further quantitative analysis was required to investigate the question of normality in greater detail.

In terms of kurtosis, in Fig. 6.4 one can graphically infer that the three CAPE variants of the SUP dataset exhibited markedly kurtotic features located around the peak of each distribution. The apparent bimodality of the NCAPE dataset was judged to probably relate to the small sample size and was not investigated further. In other words, in general, there was evidence of 'bunching' or 'peakedness' around the median. Quantitatively this was confirmed by the positive kurtosis values reflected in Table 6.2. Again, with reference to the MATLAB histfit plots in Fig. 6.4, not much skewness was in evidence across the three datasets in question, supported by small, positive calculated values of skewness in Table 6.2. Parametric and non-parametric tests of normality were then performed. At the alpha = 0.05 (95%) level, the standard one-sample Kolmogorov-Smirnov (K-S) test rejected the null hypothesis that each of the three distributions were normally distributed. Whilst being non-parametric, the K-S test is nevertheless considered to be a fairly stringent test and it was surmised that the markedly kurtotic tendencies of the distributions could well have been a contributory factor towards rejection of the null hypothesis. Consequently the D'Agostino test of normality (D'Agostino, 1970; Trujillo-Ortiz & Hernandez-Walls, 2003) which includes a scheme to compensate for skewness and/or kurtosis, was applied at the alpha = 0.05 level, accepting the null hypothesis for all three distributions. Similarly, the Jarque-Bera 'jbtest' (Bera & Jarque, 1982) as well as the Lilliefors 'lillietest' test (Lilliefors, 1967; 1969) also provided acceptance of the null hypothesis, again at the alpha = 0.05 level, further supporting the D'Agostino

result. It was therefore concluded that for the purposes of this research that the three CAPE variant samples emanating from the SUP supercell sample were judged to be approximately normally distributed, thus satisfying requirement (2).

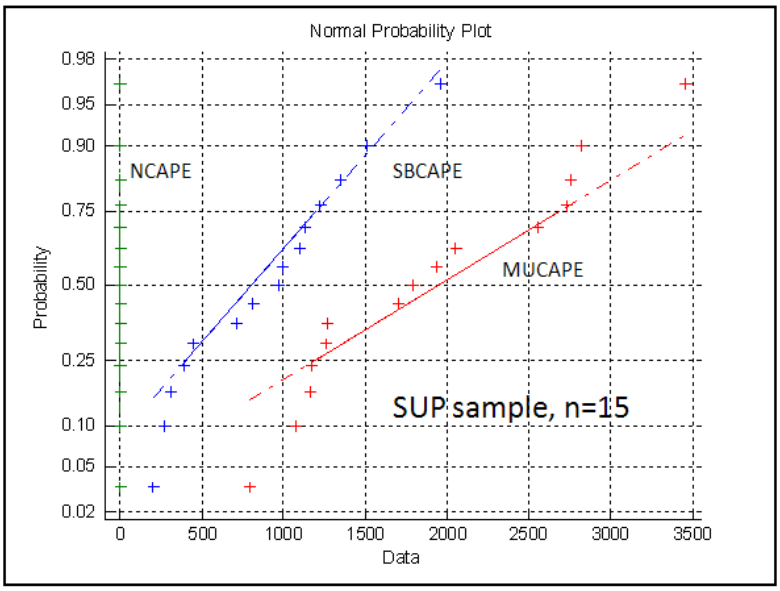

FIGURE 6.3: MATLAB-generated 'normplot' of CAPE sub-types for the SUP sample. The cumulative normal distribution values lie along the Y-axis while CAPE values in J kg^{-1} are ranged along the X-axis.

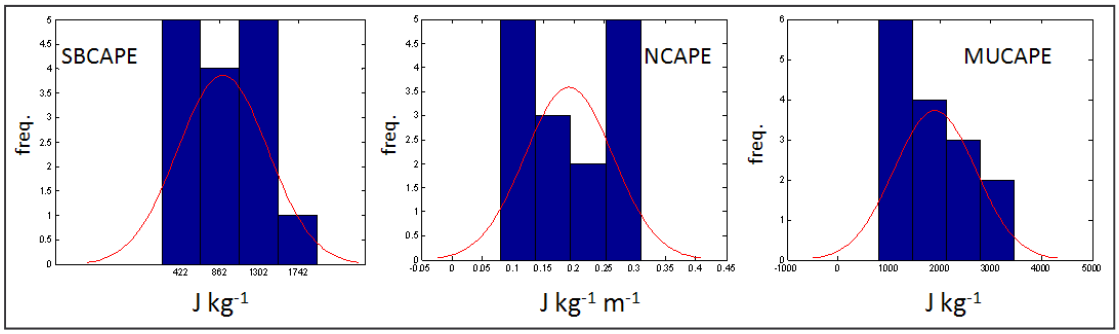

FIGURE 6.4: MATLAB-generated 'histfit' thumbnail images of CAPE sub-types for the SUP sample (n = 15), illustrating a basic histogram with a standard normal distribution superimposed.

TABLE 6.4: Sample variance for the SUP and NON-SUP samples, for CAPE-based thunderstorm parameters.

sample : SUP vs NON-SUP	SBCAPE	NCAPE	MUCAPE
Var (SUP) sample:	260600	0.0051	644701
Var (NON-SUP) sample:	260841	0.0047	777895

In terms of variance of SBCAPE, NCAPE and MUCAPE, when comparing SUP and NON-SUP samples, the sample variance was calculated as per Table 6.4. Upon visual inspection there did not seem to be much difference between the variance pairs, thus it was accepted that for the purposes of hypothesis testing that the sample variances were equal.

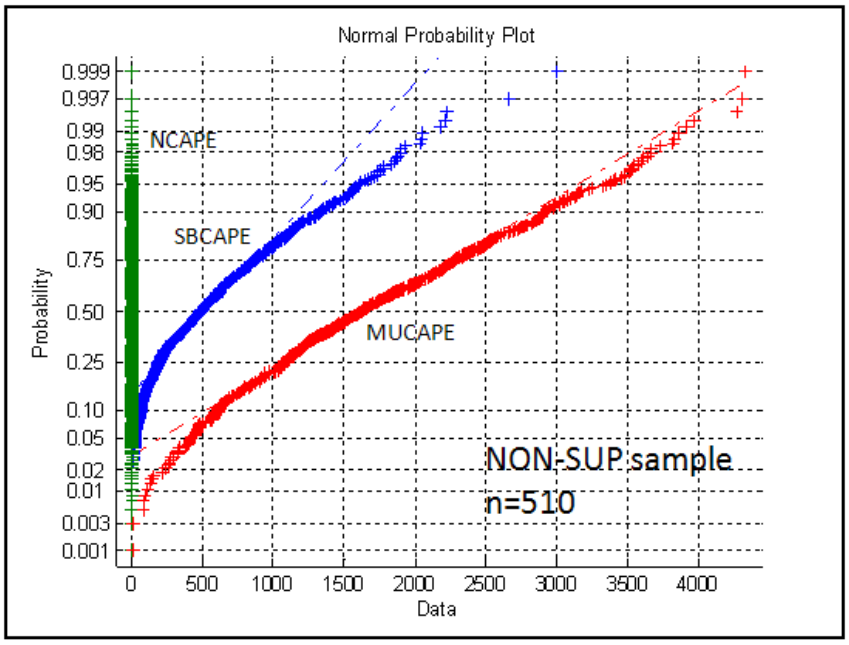

FIGURE 6.5: 'Normplot' of CAPE sub-types for the NON-SUP sample. The cumulative normal distribution values lie along the Y-axis while CAPE values in J kg^{-1} are ranged along the X-axis.

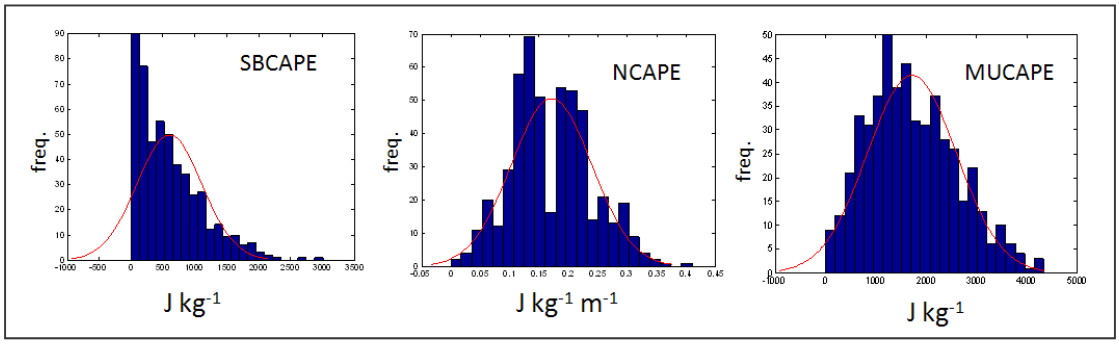

FIGURE 6.6: 'Histfit' thumbnail images of CAPE sub-types for the NON-SUP sample (n = 510), illustrating a basic histogram with a standard normal distribution superimposed.

With reference to the normal probability plot of CAPE variants for the NON-SUP sample of n_2 = 510 in Fig. 6.5, the initial visual impression appeared to be one of linearity when considering NCAPE and MUCAPE respectively. However it needed to be kept in mind that NCAPE was typically distributed over a very small range, in

comparison to either SBCAPE or MUCAPE. The MUCAPE plot (in red) appeared fairly straight but deviated quite markedly beyond the interquartile range, with curvature being introduced at either extreme end of the distribution. SBCAPE displayed even more curvature. These observed trends did not bode well regarding the proposed assumption of normality and, as in the SUP supercell sample discussed above, further quantitative analysis was required.

In Fig. 6.6 a visual overview of 'histfit' histograms, superimposed over a standard normal distribution revealed some interesting features. On first impression, MUCAPE for the NON-SUP sample appeared to fit a standard normal distribution fairly well. NCAPE again displayed evidence of bimodality which was commented upon earlier when the SUP sample NCAPE was discussed. SBCAPE in Fig. 6.6 showed both marked kurtosis (4.35) as well as slight skewness (1.16) in Table 6.3. As in the SUP sample, further testing was required. A range of parametric and non-parametric tests, including Kolmogorov-Smirnov, D'Agostino, Lilliefors, Jarque-Bera and Shapiro-Wilk (Shapiro & Wilk, 1965) were all attempted at the alpha = 0.05 level. However, all such tests returned a rejection of the null hypothesis at a 95% confidence level. A Box-Cox transformation (Box & Cox, 1964; Leontitsis, 2001; Dror, 2006) was also performed, producing visually appealing, corrected and normalised distributions (not shown), which still disappointingly failed the K-S test for normality (alpha = 0.05). It was therefore concluded that the three CAPE variant vectors of n = 510, representing NON-SUP days were not normally distributed.

So, while earlier results confirmed the assumption of normality for SUP vectors of CAPE, allowing their inter-comparison by parametric means, the same could not be said for CAPE variants from the NON-SUP sample. It was thus an appropriate time to turn to additional non-parametric methods in order to make comparisons between the SUP and NON-SUP samples respectively.

In order to investigate hypotheses surrounding the nature of CAPE variants, when contrasting SUP and NON-SUP datasets in a non-parametric manner, the Mann-Whitney rank-sum U test (Mann & Whitney, 1947) was utilised. The null hypothesis

for this test was that, for each CAPE variant pair in turn, the median of the SUP sample did not differ markedly from the corresponding median of the NON-SUP sample. The alternative, hypothesis was that the medians did indeed differ markedly and with statistical significance at the $\alpha = 0.05$ level. With this test, contrary to many other hypothesis tests, the p value that is returned will be very small or tend towards zero when medians differ markedly, while larger p values indicate that medians are equal or that there is not any significant difference between the two medians. The $\alpha = 0.05$ level was chosen as a baseline level of significance and the SBCAPE, MUCAPE and NCAPE datasets were each tested in turn, contrasting the SUP samples with the NON-SUP samples. MUCAPE returned a non-zero p value of $p = 0.3855$, resulting in the null hypothesis being accepted, implying that the medians were not significantly different. Similarly NCAPE returned a p value of 0.3236, also implying that there was negligible difference in NCAPE medians, for SUP versus NON-SUP datasets. The only dataset to return a result other than that discussed above was the SBCAPE dataset, where, at the $\alpha = 0.05$ level, the alternative hypothesis was accepted, due to a very small calculated p value ($p = 0.0183$). An identical outcome was upheld even at more conservative alpha thresholds of 0.025 (two-tailed, 97.5% confidence) and 0.01 (two-tailed, 99.0% confidence) respectively. Consequently the inference was that, of the SBCAPE, MUCAPE and NCAPE datasets, it was only the SBCAPE dataset where the median of the SUP sample could be judged to differ significantly from that of the NON-SUP sample. In other words, in the context of this research, the SBCAPE dataset for the SUP and NON-SUP samples respectively would form an ideal basis to utilise within the MSCP formulation. In particular, the measures of distribution and dispersion of SBCAPE for the SUP sample would be interrogated further.

While the Mann-Whitney test did not provide an opinion as to whether the SBCAPE median of the SUP sample was greater or smaller than the corresponding median for the NON-SUP sample, the notched boxplot in Fig. 6.7 clearly indicated that the median for the SUP sample was significantly larger than it's NON-SUP counterpart, with an absence of overlap of the notched region straddling each respective median.

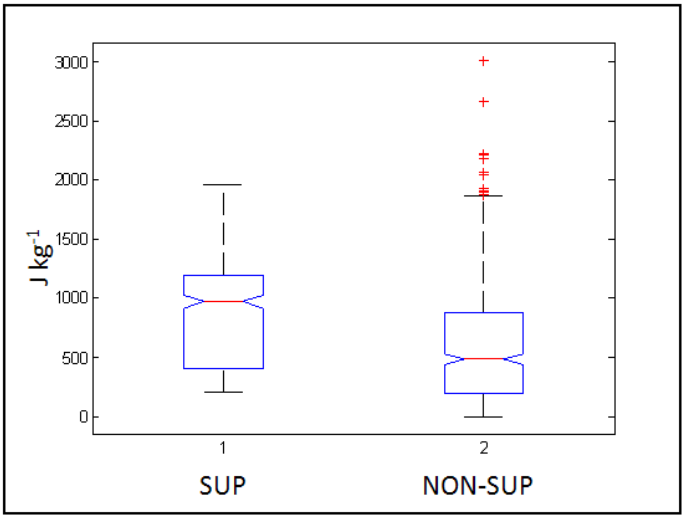

FIGURE 6.7: Notched 'boxplot' of SBCAPE for the SUP and NON-SUP datasets respectively.

Consequently it was concluded that for the purposes of this study, SBCAPE was an appropriate parcel 'instability' parameter to utilise in the formulation of MSCP. Furthermore, for the denominator of the first term of MSCP, a suitable threshold normalisation factor was sought. In keeping with the approach of T(2003), the first quartile (Q1) of SBCAPE = 406 J kg^{-1} from the SUP sample of 15 supercells in Table 6.2 was selected to be used in the MSCP formulation. The 'instability' term for MSCP was therefore defined as:

MSCP parcel instability factor = [SBCAPE] / 406 (1)

Note:- as the units of both the numerator and the denominator in (1) are J kg^{-1} the resultant for the instability factor is thus a dimensionless number.

6.3.2 Helicity-based parameters

For helicity-based parameters in the SUP versus NON-SUP samples, namely SRH1, SRH2 and SRH3 being storm-relative helicity at 0-1 km, 0-2 km and 0-3 km respectively, a similar investigative strategy to that followed for the CAPE-based parameters was adopted. The statistical results were, however markedly different in a number of respects.

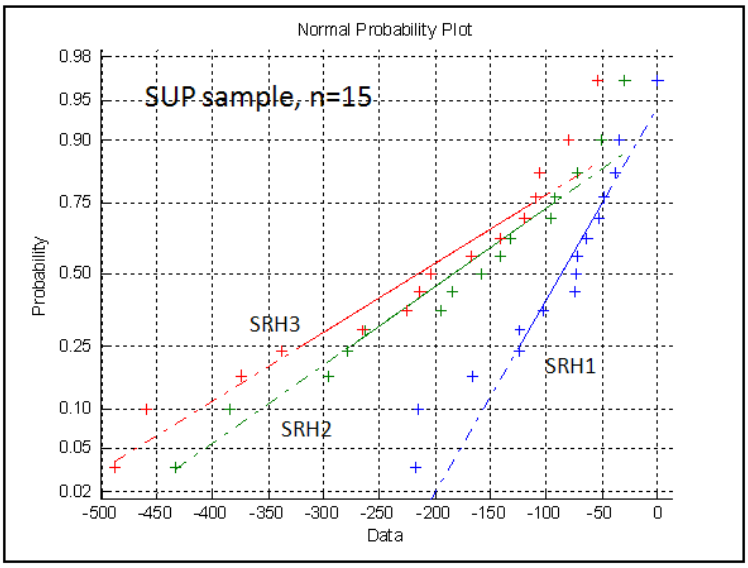

FIGURE 6.8: 'Normplot' of SRH (storm-relative helicity) sub-types for the SUP sample. The cumulative normal distribution values lie along the Y-axis while negatively distributed SRH values are ranged along the X-axis.

Preliminary inspection of the cumulative normal probability plot for SRH sub-types relating to the SUP sample were plotted in Fig. 6.8 and revealed that there was a fair degree of linearity associated with each of SRH1, SRH2 and SRH3 in turn. Again, as mentioned in the preceding discussion section for CAPE variants, the presence of outliers was somewhat of a concern. Inspection of basic histograms for each of SRH1, SRH2 and SRH3 of the SUP sample, when compared against standard normal bell curves in Fig. 6.9 indicated slight skewness towards the upper end of the range. There was also an indication of all three distributions being markedly kurtotic. Quantitatively, this was confirmed by inspection of Table 6.2 where mildly negative skewness was indicated, combined with small kurtosis values. By contrast, the NON-SUP sample, in Fig 6.11, while also showing slight negative skewness, showed sharp kurtosis, with markedly larger calculated kurtosis values. The cumulative normplot in Fig. 6.10 for the NON-SUP SRH variants also showed marked deviation away from linearity of response, suggesting that the assumption of normality for (at least) the NON-SUP samples would be doubtful.

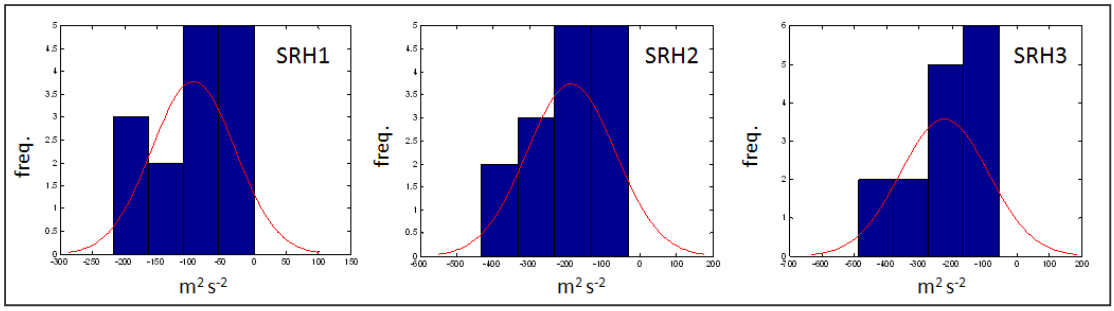

FIGURE 6.9: 'Histfit' thumbnail images of SRH sub-types for the SUP sample (n = 15), illustrating a basic histogram with a standard normal distribution superimposed.

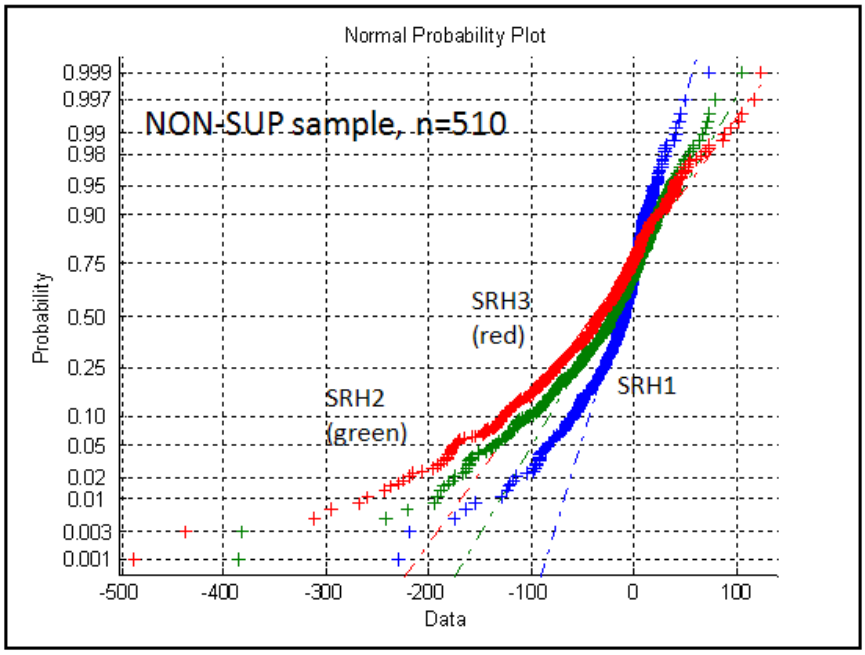

FIGURE 6.10: 'Normplot' of SRH (storm-relative helicity) sub-types for the NON-SUP sample. The cumulative normal distribution values lie along the Y-axis while (predominantly negatively distributed) SRH values are ranged along the X-axis.

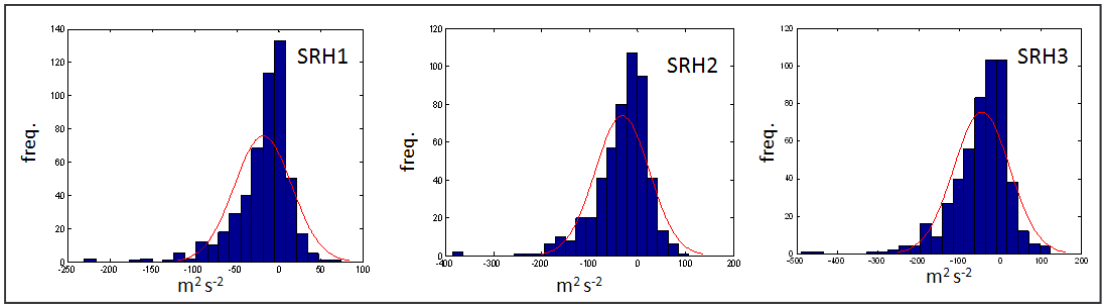

FIGURE 6.11: 'Histfit' thumbnail images of SRH sub-types for the NON-SUP sample (n = 510), illustrating a basic histogram with a standard normal distribution superimposed.

In order to objectively establish whether the assumption of normality would be appropriate for the SUP and NON-SUP samples with respect to SRH variants, a range of normality tests were performed at the $\alpha = 0.05$ level. The SUP samples were tested first, followed by the NON-SUP samples. While the SUP samples of SRH1, SRH2 and SRH3 were not able to pass the Kolmogorov-Smirnov test, application of additional tests, including D'Agostino, Jarque-Bera and Shapiro-Wilk suggested that there was scope to consider the SUP sample (for SRH variants) as being 'near-normal' as all three such tests affirmed normality at the $\alpha = 0.05$ level. Again, as mentioned previously, D'Agostino's approach attempts to compensate for the presence of skewness as well as kurtosis; both of which were acknowledged to be present in varying degrees. The SUP samples were thus, for the purposes of this research, considered to be 'near-normal', thus allowing the assumption of normality.

In the case of the NON-SUP samples of SRH1, SRH2 and SRH3, application of all four previously mentioned tests for normality (at the accustomed $\alpha = 0.05$ level) disappointingly returned results strongly indicative of non-normality. Consequent to this result, and acknowledging the known markedly dissimilar variance between SUP and NON-SUP pairs in Table 6.5, use was again made of the non-parametric Mann-Whitney ranked-sum U test, in a two-tailed, non-directional form. Preliminary visual 'eyeballing' of the corresponding boxplot for SRH variants for the SUP and NON-SUP samples in Fig 6.12 suggested that there would indeed be a consistent indication of markedly different medians, for each of SRH1, SRH2 and SRH3 respectively. Quantitative Mann-Whitney testing upheld this initial impression, indicating at the customary 0.05 level as well as at a more conservative 0.025 level, a statistically significant difference of medians for each of SRH1 ($p \approx 0$) , SRH2 ($p \approx 0$), as well as SRH3 ($p \approx 0$). It will be recalled from prior discussion regarding CAPE variants that the Mann-Whitney test did not provide inference regarding the size of the medians, relative to each other but merely that the difference in medians was judged to be statistically significant at the chosen alpha level.

TABLE 6.5: Sample variance for the SUP and NON-SUP samples, relating to storm-relative helicity (SRH), indicating markedly dissimilar values between SUP and corresponding NON-SUP values.

sample : SUP vs NON-SUP	SRH 1km	SRH 2km	SRH 3km
Var (SUP) sample:	4186	14693	18556
Var (NON-SUP) sample:	1154	3174	4708

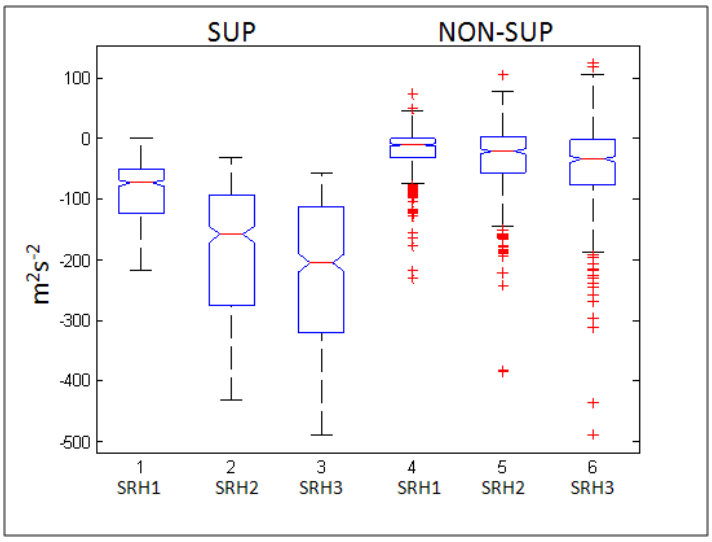

FIGURE 6.12: Notched 'boxplot' of SRH1,SRH2 and SRH3 for the SUP and NON-SUP datasets respectively.

TABLE 6.6: Sample median (Me) values for the SUP and NON-SUP samples, relating to storm-relative helicity (SRH). The greatest algebraic difference between the respective sample medians was found in the SRH (0-3 km) parameter in the rightmost column. Units of measurement for SRH in $m^2 s^{-2}$.

sample : SUP vs NON-SUP	SRH 1km	SRH 2km	SRH 3km
Me (SUP) sample:	-73	-158	-204
Me (NON-SUP) sample:	-10	-20	-33
Me(SUP) - Me(NON-SUP):	-63	-138	-171

Furthermore, when the respective medians of each distribution were compared in Table 6.6, the greatest difference between medians occurred when comparing SRH3 (SUP) with SRH3 (NON-SUP). Hence on the basis of this significant contrast between distributions, it was decided that whilst each SRH component showed much merit for inclusion in the MSCP formulation, in terms of significant dissimilarity between SUP and NON-SUP, it was SRH3 (*i.e.* SRH 0-3 km) that returned the greatest spatial

difference in distribution. At this point, the author also allowed himself to be guided by prior knowledge that the T(2002) and T(2003) iterations of SCP had both justified the preferable utilisation of 0-3km SRH over and above the alternatives of 0-1km SRH or 0-2km SRH. As the title of this work deals explicitly with the design of a modified SCP, it could justifiably be argued that, in the absence of any strong argument and/or mathematical results to the contrary, it would be logical to elect to use SRH3, with due consideration to an appropriate, locally determined choice of scaling threshold. It can therefore be noted for the benefit of later possible research subsequent to this work, that either SRH1 or SRH2 may well have a degree of merit in the context of MSCP.

In a similar fashion to the methodology used for the CAPE-based component, the corresponding quartile of the SRH3 distribution was selected as the threshold normalisation factor. In the case of southern hemisphere SRH which is most frequently negatively distributed, the particular quartile closest to the origin, in other words -112 $m^2 s^{-2}$ in Table 6.2, represented an appropriate threshold value, which according to MATLAB convention is named Q3. Hence the helicity-based factor for MSCP was declared thus:

MSCP helicity factor = [SRH (0-3 km)] / (-112) (2)

note:- as the units of both the numerator and the denominator in (2) are $m^2 s^{-2}$ the resultant is a dimensionless number for the helicity factor.

6.3.3 Shear-based parameters

Cumulative probability plots of BRN and BRN shear were generated for the SUP sample and the NON-SUP sample in Fig. 6.13 and 6.15 respectively. Firstly, for the SUP sample, it was seen that for BRN shear, the values were fairly large and occured to the right of the graph in green. As the SUP sample was a dataset composed of supercells, one would have expectd the shear values to be significantly elevated, in

comparison with those of the NON-SUP sample. Furthermore, in Fig. 6.13 the SUP sample BRN shear was near-normally distributed, with the data points not deviating much from the straight line as indicated. Conversely, for the Bulk Richardson Number (BRN), the values were relatively small, as expected for supercells, although the distribution, as seen in the blue values in Fig. 6.13, was quite clearly curved and thus deviated from a normal distribution. Once again, as noted in earlier analysis, the presence of outliers was considered to be a potential confounding factor.

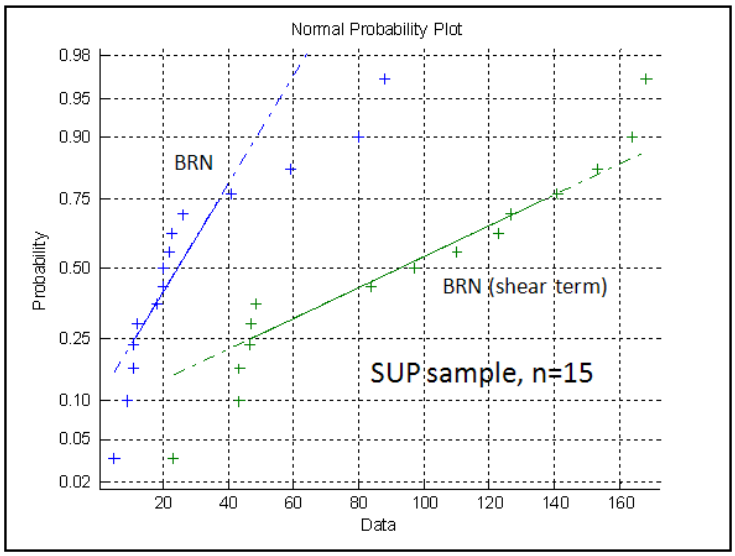

FIGURE 6.13: 'Normplot' of BRN and BRN shear for the SUP sample. The cumulative normal distribution values lie along the Y-axis.

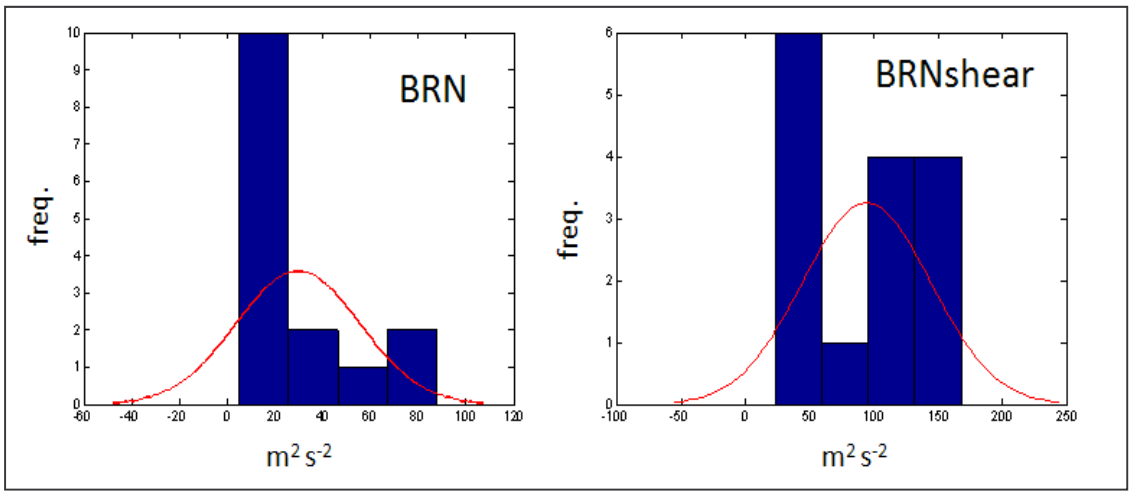

FIGURE 6.14: 'Histfit' thumbnail images of BRN and BRN (shear term) sub-types for the SUP sample (n = 15), illustrating a basic histogram with a standard normal distribution superimposed.

In Fig. 6.15 similar results for BRN and BRN shear are shown but for the NON-SUP non-supercell sample. For this sample one would have expected low shear values (green trace) as well as large BRN values (blue trace) associated with this large, albeit non-supercell sample. Again, as with the SUP sample in Fig. 6.13, it was notable that BRN deviated markedly from a linear response, indicating non-normality of the distribution, whilst conversely, BRN shear was considered to be "near normal" as inferred from the linear response of the green trace.

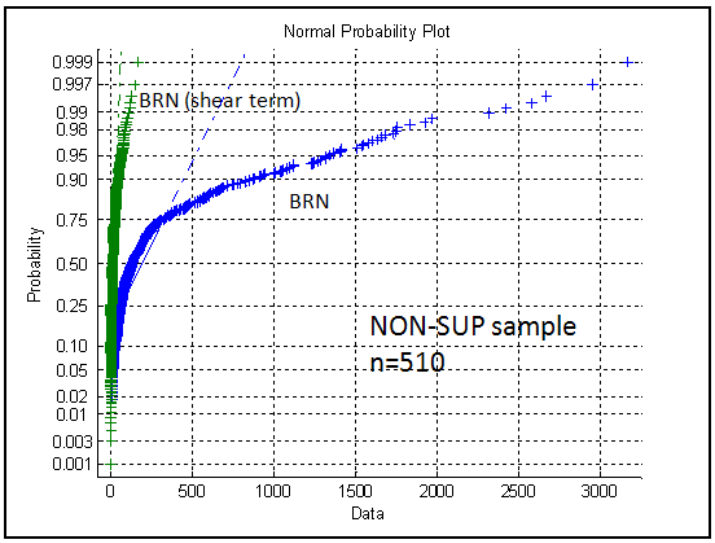

FIGURE 6.15: 'Normplot' of BRN and BRN shear for the NON-SUP sample. The cumulative normal distribution values lie along the Y-axis.

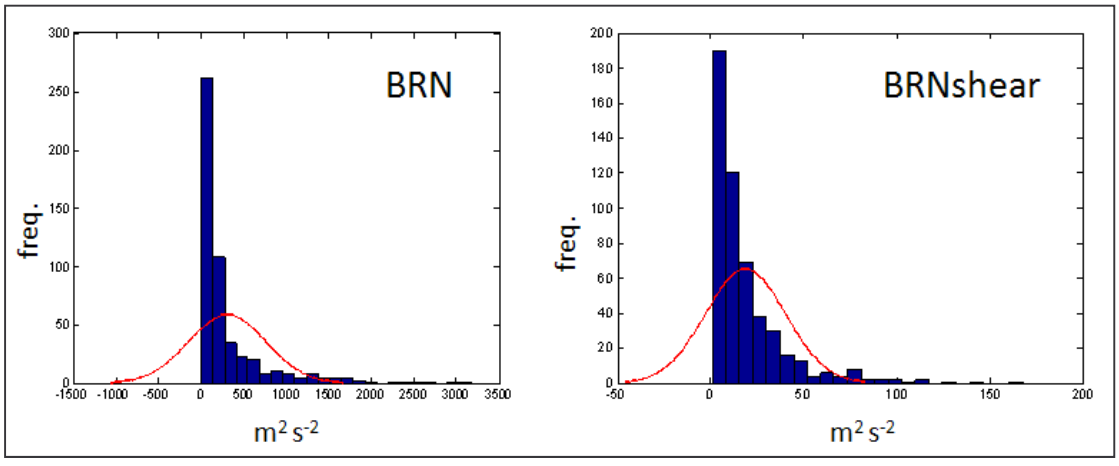

FIGURE 6.16: 'Histfit' thumbnail images of BRN and BRN (shear term) sub-types for the NON-SUP sample, (n = 510), illustrating a basic histogram with a standard normal distribution superimposed.

In order to objectively assess the question of normality of the SUP and NON-SUP samples of BRN and BRN shear respectively, the relative skewness and kurtosis of each distribution were considered in turn. For the SUP sample, BRN showed slight positive skewness (1.29) while BRN shear returned hardly any indication of skewness (0.08), correspondingly confirmed graphically in the histograms in Fig 6.14 and Fig. 6.15 respectively. Kurtosis, while present was fairly conservative, at 3.33 and 1.53 for BRN and BRN shear respectively. By contrast, for the NON-SUP sample, there was evidence of strongly kurtotic distributions, with BRN and BRN shear both returning values exceeding 12. Strong indication of positive skewness could also be inferred from skewness values; only fractionally less than +3 in both cases. In Fig 6.16 for the NON-SUP sample, the sharp peak to the left of centre of the normal bell curve could clearly be seen, coupled with a long, 'skinny' tail of extreme values extending to the upper, rightmost side of the distribution. While the SUP and NON-SUP samples of BRN and BRN shear all displayed commonality in terms of an absence of non-positive values, the SUP sample clearly showed more focussed 'bunching' around the IQR. In both the BRN and BRN shear case from the SUP set, while there was some evidence of bimodality, this could perhaps have been an artefact of the small sample size? In other words, the true overall, as yet unknown distribution, of BRN and BRN shear for supercells might well deviate from these initial impressions.

Upon application of parametric and non-parametric tests of normality for the SUP and NON-SUP samples, with relation to BRN and BRN shear, it was perhaps unsurprising, given the strong indications of both skewness and kurtosis, especially so in the case of the NON-SUP sample, that without exception, Kolmogorov-Smirnov failed to indicate normality associated with any of the datasets. Supplemental application of D'Agostino, Jarque-Bera and Shapiro-Wilk delivered similar results, however in this case it was judged to be significant in that, of all three mentioned schemes, the sole dataset that passed the normality test was that of BRN shear for the SUP supercell dataset.

TABLE 6.7: Sample variance for the SUP and NON-SUP samples, relating to BRN as well as BRN shear, indicating markedly dissimilar values between SUP and corresponding NON-SUP values.

sample : SUP vs NON-SUP	BRN	BRN shear
Var (SUP) sample:	672	2488.4
Var (NON-SUP) sample:	208689	467.0

Given the marked lack of normality in the NON-SUP data, any comparisons between the SUP and NON-SUP data, especially given the acknowledged dissimilarity of variance displayed in Table 6.7, would need to rely on non-parametric methods. As before, the Mann-Whitney U test was performed at the $\alpha = 0.05$ level and returned a high confidence result ($p \approx 0$ in both cases) that the median of the SUP dataset differed markedly from that of the NON-SUP dataset, applicable both in the case of BRN as well as BRN shear.

At face value, such results as presented above might seem to suggest that either BRN or BRN shear could be equally considered as likely candidates to use as a factor within a modified formulation of SCP. However it will be recalled from Chapter 2 that the formula for the Bulk Richardson Number is classically presented as a quotient of CAPE divided by BRN shear. Inclusion of BRN in a formulaic expression of MSCP would therefore imply covariance between the first (CAPE) term and third (shear) term of MSCP, which in general would be an undesirable quality within a composite index. Additionally it was encouraging that T(2002) and T(2003) consistently made use of BRN shear as opposed to BRN, thus further endorsing the use of BRN shear as the third, deep layer shearing, term for MSCP.

In the light of the favourable results pertaining to BRN shear, particularly that the medians of the SUP and NON-SUP datasets were judged to be significantly dissimilar, with respect to BRN shear, at the alpha = 0.01 level of significance, it was considered appropriate to similarly utilise BRN shear as the shearing term of MSCP.

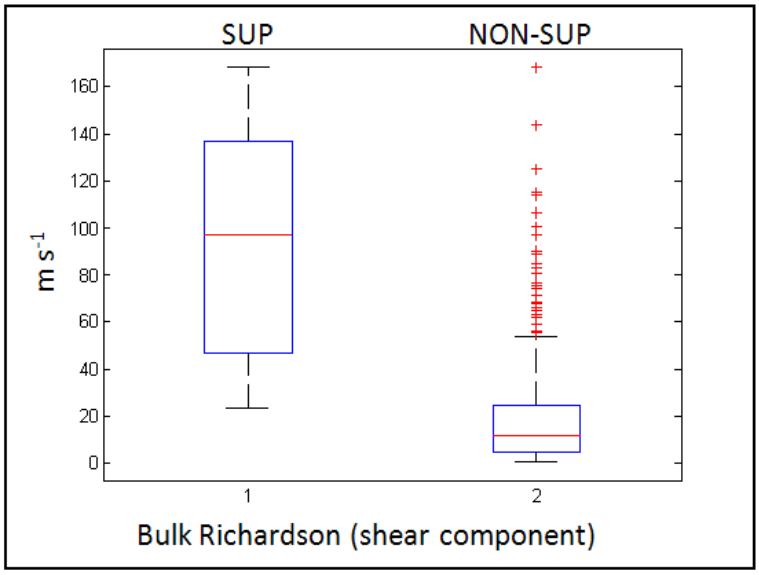

FIGURE 6.17: 'Boxplot' of BRN shear for the SUP and NON-SUP datasets respectively.

This decision was further corroborated in Fig. 6.17 by the box and whisker plot of BRN shear, in relation to the SUP and NON-SUP samples, where a marked spatial separation of IQR of each of the two sets was clearly noted. If one considers that the IQR of the NON-SUP set is extremely compressed, with a range of Q1 = 4.7 to Q3 = 24.5 (implying an IQR of 19.8), while by comparison the corresponding IQR for supercells is a staggering 90.5; based on Q1 = 46.7 and Q3 = 137.2 respectively. BRN shear was therefore judged to be a powerful discriminatory factor for MSCP, when attempting to distinguish between supercell and non-supercell pre-storm environmental conditions.

BRN shear was thus selected to be the final factor of MSCP, closely in line with the existing formulation of SCP in T(2002) and its T(2003) iterative counterpart. From the SUP sample in Table 6.2, the corresponding Q1 first quartile for BRN shear was 46.7 $\approx$ 47 $m^2 s^{-2}$. Hence the third and final factor for MSCP was formulated as

MSCP deep layer shear factor = [BRN shear] / 47 (3)

Note:- as the units of both the numerator and the denominator in (3) are $m^2 s^{-2}$ the resultant is a dimensionless number for the deep layer shear factor.

6.4 The complete MSCP formula

It will be recalled from Chapter 2 that the formula for the T(2002) iteration of SCP is given by equation (4) below:

$$\textbf{SCP} = [\ (\text{MUCAPE}/1000) * (\text{SRH}_{0\text{-}3\text{km}}\ /150) * (\ (½U^2)\ /40\ )\ ] \qquad (4)$$

Similarly, it will be recalled from Chapter 2 that the updated formulation of SCP as given by T(2003) is:

$$\textbf{SCP} = [\ (\text{MUCAPE}/1000) * (\text{SRH}_{0\text{-}3\text{km}}\ /100) * (\ (½U^2)\ /20\ )\ ] \qquad (5)$$

where, in both (4) and (5), ½ U^2 represents the Bulk Richardson shear term.

In (1), (2) and (3) earlier in this chapter it was established that the three separate dimensionless factors of MSCP would be quantified as follows:

MSCP parcel instability factor = [SBCAPE] / 406 (1)

MSCP helicity factor = [SRH (0-3km)] / (-112) (2)

MSCP deep layer shear factor = [BRN shear] / 47 (3)

Hence it follows that:

$$\textbf{MSCP} = [\ (\text{SBCAPE}/406) * (\text{SRH}_{0\text{-}3\text{km}}\ /(-112)) * (\ (½U^2)\ /47\ )\ ] \qquad (6)$$

note:- As MSCP is the product of three dimensionless factors, it follows that MSCP is similarly not associated with any units of measurement and could be termed a composite index.

An additional note was required at this point, in relation to equation (6). In line with the approach used in T(2002), which used a sample of typical northern hemisphere

EMM "right-movers", delivering a threshold value of +150 (typically SRH > 0 $m^2 s^{-2}$ for northern hemisphere), which would result in T(2002) SCP > 0 for typical EMM storms. Equivalently, the present study made use of a sample of typical southern hemisphere EMM "left-movers" delivering a threshold value < 0. Therefore for typical southern hemisphere supercell storms, MSCP > 0. However, in the special, less frequent case of shearing orientation which favours atypical supercells as discussed at length in Chapter 2.5.3.5, SRH will be > 0 $m^2 s^{-2}$, thus leading to a helicity term < 0 and hence MSCP < 0. Therefore MSCP may indeed assume a real value which is either positive or negative or zero, but which would most frequently be expected to be > 0. A similar argument holds for atypical northern hemisphere supercells, which could be expected to display SCP < 0, given SRH < 0 $m^2 s^{-2}$.

A comparison of MSCP versus the SCP schemes of T(2002) and T(2003) was subsequently conducted with application to the SUP supercell dataset of 15 cases, the results of which appear in Fig. 6.18. It was noted that whilst T(2002) provided comparable results to that of MSCP, by contrast the T(2003) results responded with markedly higher values in the interquartile range, far more so than the IQR of either MSCP or T(2002). The relevance and possible impact of this aspect is explored and discussed further in Chapters 7 and 8.

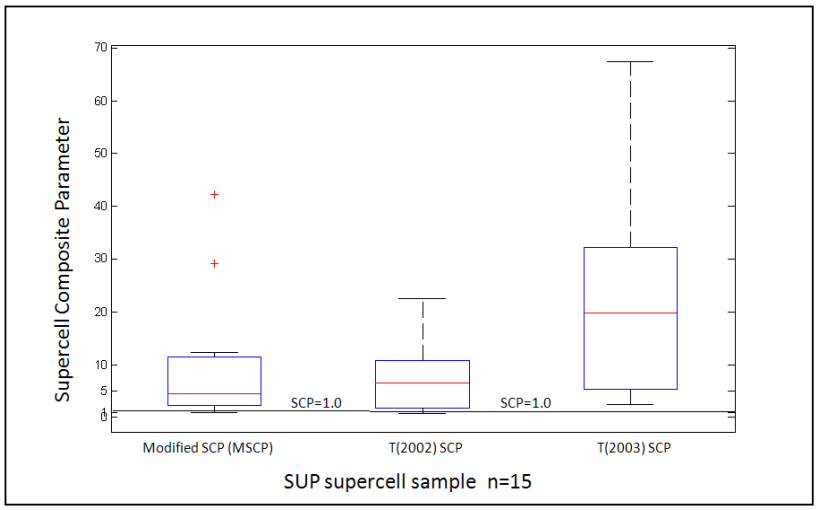

FIGURE 6.18: 'Boxplot' of MSCP, SCP T(2002) and SCP T(2003) for the SUP and NON-SUP datasets respectively, indicating the similarity of response for MSCP and T(2002) SCP, contrasted against T(2003) SCP at far right. All distributions calculated using the 15 SUP supercell sample. The threshold significant value of SCP ≥ 1.0 is indicated by the solid line as a convenient reference.

6.5 Summary

The purpose of this chapter was to perform statistical comparisons between the SUP sample of 15 supercells and the NON-SUP sample of 510 non-supercells with the intention of highlighting or contrasting such differences between these sets. These differences, when carefully quantified would better define and calibrate the MSCP, as the essential function of MSCP is to provide a means of discrimination between supercell and non-supercell type soundings.

At the beginning of the chapter, the SUP and NON-SUP samples were first compared on a largely qualitative basis, where the graphic differences between the two datasets were discussed by means of a a skew *T* / log p aerological plot, averaged for each of the SUP sample and the NON-SUP sample respectively. In this way, five major features of the SUP average profile were identified and their significance discussed, while by contrast, for the NON-SUP sample these particular discriminatory features were found to be absent.

Such qualitative differences between supercell soundings and non-supercell soundings as discussed in the preceding paragraph are without doubt very useful in an operational context, when a single, current sounding diagram is typically available for scrutiny. The thrust of the remainder of the chapter was to translate such qualitative, graphic insight into numerically quantifiable terms, hence to be applied to the final formulation and calibration of the MSCP. In order to structure this process, each of the three factors of SCP were discussed in turn and the merit (or otherwise) of each candidate component discussed in detail, especially with respect to (1) statistical independence (2) (in)equality of variance between SUP and NON-SUP parameters as well as whether particular SUP and NON-SUP parameters could be considered to be normally distributed. Due to the finding that the SUP samples were generally normally distributed, while the NON-SUP samples were not normally distributed, traditional parametric inter-comparisons between the SUP and NON-

SUP datasets were not appropriate. Use was therefore made of non-parametric techniques to conduct such comparisons.

Within the SUP sample, the smallest quartile of storm parameters so chosen to represent MSCP was then selected as the threshold scaling values for each of the three factors in MSCP, thus explicitly defining MSCP. In addition, environmental conditions which might favour an MSCP delivering either a positive or negative resultant were also noted and discussed in the context of appropriate and robust mathematical formulation of MSCP.

The chapter concluded with a box and whisker comparison of the relative spread of SCP values in relation to the 15 supercell SUP sample, using MSCP, SCP T(2002) as well as SCP T(2003). Such graphically presented insights were deemed useful, ahead of the case-studies to be explored in the forthcoming chapter, where the response of each of the aforementioned three SCP schemes were quantified and discussed on a case by case basis, in relation to historic storm events within the study domain.

CHAPTER XII : MSCP AND SCP APPLIED TO CASE-STUDIES

This is the penultimate chapter and offers a selection of mini case-studies of thunderstorm events in and adjacent to Gauteng province, spanning the two month period October to November 2013. The rationale in so doing was to illustrate that the Modified Supercell Composite Parameter (MSCP) was viable and robust in an operational context, given varying pre-storm environmental conditions, as inferred from the MSCP derived from the corresponding Irene proximity sounding for each respective case.

Furthermore, the T(2002) and T(2003) iterations of SCP were concurrently calculated for each of the five cases, in order to establish a means of measuring the response of MSCP, relative to alternative formulations of SCP. Five cases were considered; three being supercell thunderstorms and two being non-supercell storms. Of the three supercell cases presented, the first stemmed from a weak or borderline supercell scenario while the second was a well-defined, classic supercell case. The third supercell case was illustrative of a particularly long-lived, long-track, severe supercell that traversed 3 provinces.

Two non-supercell storms complete this chapter, the first of these being the Rust de Winter storm which was non-severe and of a non-supercell type. The Benoni / ORTIA storm, being the second member of the two non-supercell cases, was a good example of a particularly severe, but non-supercell storm occurring within a slightly sheared environment.

At some stage in their respective lifetimes, all five storms were within 200km from the Irene weather office, hence Irene midday 12h00UTC ascents, as previously defined in Chapter 3, were utilised as proximity soundings to quantify and assess the corresponding pre-storm environment. In all five cases, thunderstorm development occurred in the afternoon and early evening hours, within a temporal period of only

a matter of hours following the ascents being performed. There was thus a high degree of confidence that the sounding data, and by implication the sounding-derived SCP and MSCP parameters, were duly representative of the prevailing pre-storm environments for the cases in question. The results from each of the five cases were arranged in chronological order and are presented below. A short summary concludes the chapter.

7.1 Villiers, Free State, 7 October 2013

Case 1 : Analysis and comment:

This case presented a weak or borderline scenario for supercell development. The storm was noted to be active in the period from approximately 12h50UTC to 13h45UTC, exhibited a BWER, showed rotation in the RADAR radial velocity data and was also a deviant left-mover, with storm motion being oriented equatorwards of mean storm motion (EMM).

In Fig. 7.1 at top right, the RAOB determination of Bulk Richardson Number (BRN) at 54 seemed somewhat high for supercells, given the optimum range of BRN suggested to be between 10 and 40 (Weisman & Klemp, 1986). A BRN of 54 was thus highly suggestive of the presence of large values of speed shear aloft. In Table 7.1, note that T(2002) and T(2003) reflected an SCP well above 1.0, whilst MSCP = 2.3.

The Lifted index was calculated at -9, indicative of extreme instability, while there was calculated to be abundant CAPE at 2300 J kg^{-1}. The WINDEX (McCann, 1994) was calculated to be 48 kts, indicative of a potential for severe, dry downburst events.

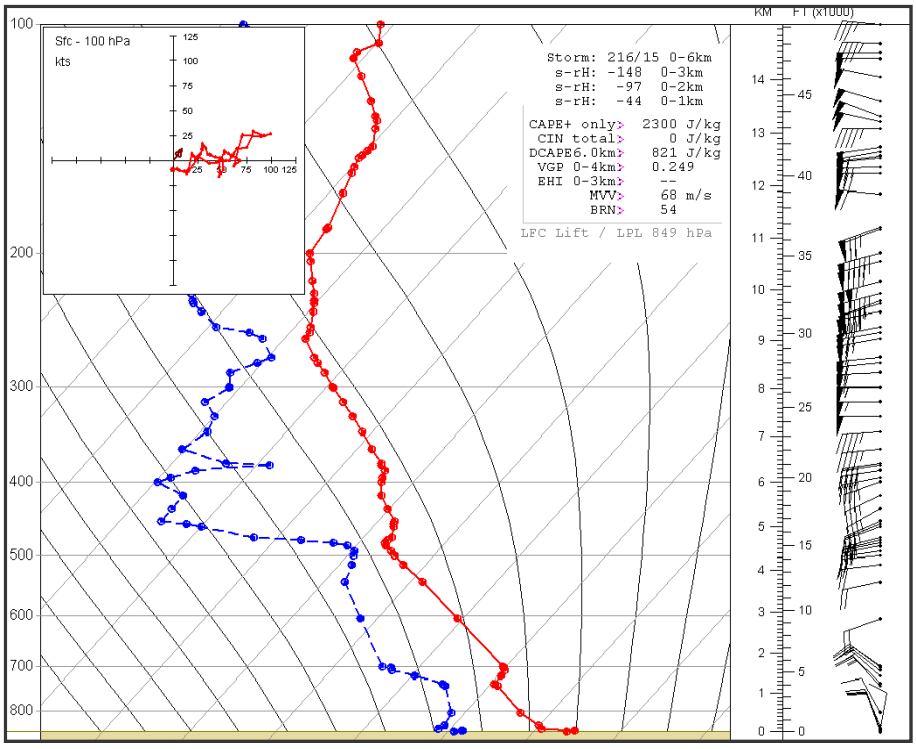

FIGURE 7.1: Irene midday sounding (skew *T* / log p plot) for 07 October 2013. Axes and measurement units as per skew *T* / log p plot in Fig. 6.1 . The red trace represents observed environmental air temperature whilst the blue trace correspondingly indicates environmental dewpoint. Units of *T* and T_d in °C.

TABLE 7.1: MSCP, T(2002) and T(2003) SCP, together with sounding-derived parameters for the 7 October 2013 case. Units of measurement for SBCAPE and MUCAPE in J kg^{-1}, NCAPE in J kg^{-1} m^{-1} while SRH is m^2 s^{-2}. Corresponding unit of measurement for BRNshear is m^2 s^{-2}. BRN is dimensionless.

Supercell Composite Parameter

7 October 2013

INPUT:

SBCAPE:	800	SRH(0-1km):	-44
MUCAPE:	2300	SRH(0-2km):	-97
NCAPE:	0.26	SRH(0-3km):	-149
BRNshear:	42.4		

OUTPUT:

SCP Thompson et al (2002) :	2.422
SCP Thompson et al (2003) :	7.265
Modified Supercell Composite Parameter (MSCP) :	2.365

7.2 Bapsfontein, Gauteng, 19 October 2013

Case 2 : Analysis and comment:

This particular case was associated with a well-defined, classic supercell, which displayed a BWER, hook echo (Fig. 7.3) and deviant left movement (EMM). Bulk Richardson Number was rated by RAOB to be 25 (Fig. 7.2), thus falling well between 10 and 40 (Weisman & Klemp, 1986). Modest, but not extreme, storm-relative helicity (SRH) was notable in the sounding throughout the first three kilometres AGL as indicated in Fig. 7.2 at top right. MSCP returned a value of 4.2, while T(2002) and T(2003) returned SCP values of SCP = 1.8 and SCP = 5.4 respectively (Table 7.2). Thus MSCP as well as the two variants of SCP correctly signalled “supercells likely” on the day in question.

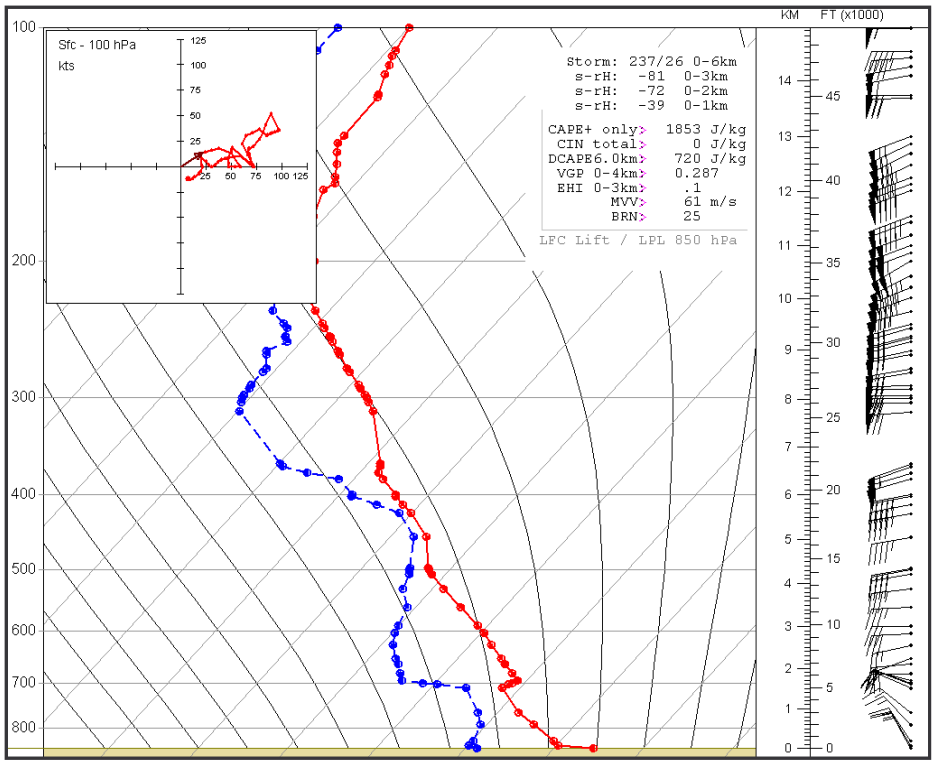

FIGURE 7.2: Irene midday sounding (skew *T* / log p plot) for 19 October 2013. Axes and measurement units as per skew *T* / log p plot in Fig. 6.1. The red trace represents observed environmental air temperature whilst the blue trace correspondingly indicates environmental dewpoint. Units of *T* and T_d in °C.

TABLE 7.2: MSCP, T(2002) and T(2003) SCP, together with sounding-derived parameters for the 19 October 2013 case. Units of measurement as per Table 7.1.

Supercell Composite Parameter

19 October 2013

INPUT:

SBCAPE:	1544	SRH(0-1km):	-39
MUCAPE:	1853	SRH(0-2km):	-72
NCAPE:	0.21	SRH(0-3km):	-81
BRNshear:	73		

OUTPUT:

SCP Thompson et al (2002) :	1.826
SCP Thompson et al (2003) :	5.478
Modified Supercell Composite Parameter (MSCP) :	4.272

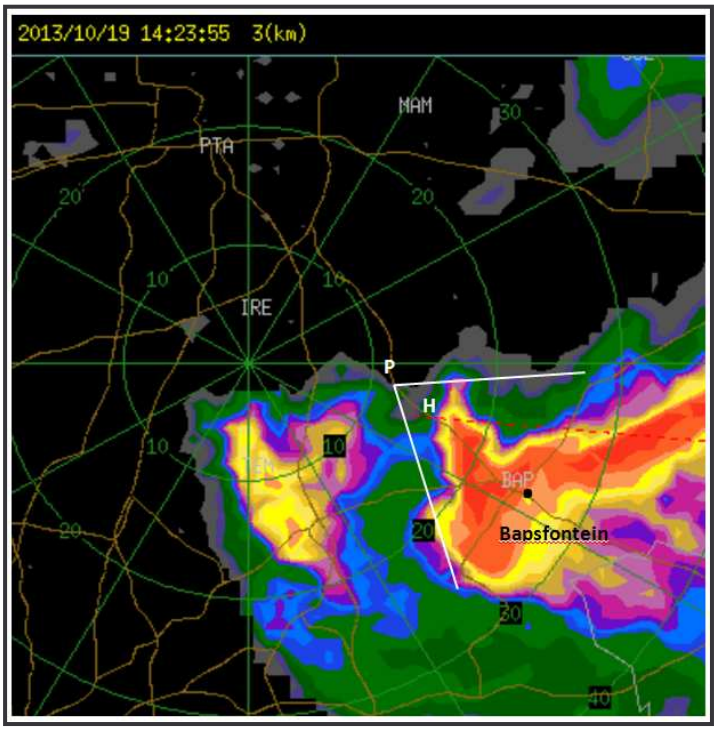

FIGURE 7.3: Irene S-band RADAR 3 km CAPPI reflectivity scan of the supercell thunderstorm near Bapsfontein, Gauteng, Saturday 19 October 2013 @ 16h23SAST (14h23UTC), Image provided by C. Powell, SAWS. RADAR visualisation: TITAN software (Dixon & Weiner, 1993).

The image in Fig. 7.3 indicates an Irene S-band RADAR 3 km CAPPI reflectivity scan of the supercell thunderstorm near Bapsfontein, Gauteng, Saturday 19 October 2013 at 16h23SAST (14h23UTC). The photo perspective was towards the south-east, from a point approximately 12 km ESE of the Irene RADAR, as indicated by "P". A prominent hook echo ("H") dominated the thunderstorm structure, with a BWER on the northern, equatorward side of the storm.

7.3 Benoni, Gauteng, 11 November 2013

Case 3 : Analysis and comment:

An example of a severe, but non-supercell thunderstorm storm which delivered large, damaging hail in the Kempton Park, Benoni and Oliver Tambo International Airport (ORTIA) areas. Bulk Richardson Number was assessed by RAOB to be excessively strong for supercell development (BRN = 74), indicative of a strongly speed-sheared environment aloft, as confirmed by the RAOB skew *T* / log p plot in Fig. 7.4. The value of the Modified Supercell Composite Parameter (MSCP) was calculated to be 2.5 while by comparison, T(2002) and T(2003) suggested 1.8 and 5.4 respectively as seen in Table 7.3. These particular T(2002, 2003) values of SCP were co-incidentally very similar to the preceding case-study.

Whilst this author was initially disappointed that MSCP and SCP appeared to "overwarn" and consequently did not signal "supercell unlikely", a plausible alternative hypothesis was that supercells were indeed possible on the given day but that none actually developed. On the basis of MSCP and SCP results one could justifiably have classified this case as a borderline supercell scenario, as the strongly speed-sheared environment could still have supported supercells though the storm-splitting process described in Chapter 2.

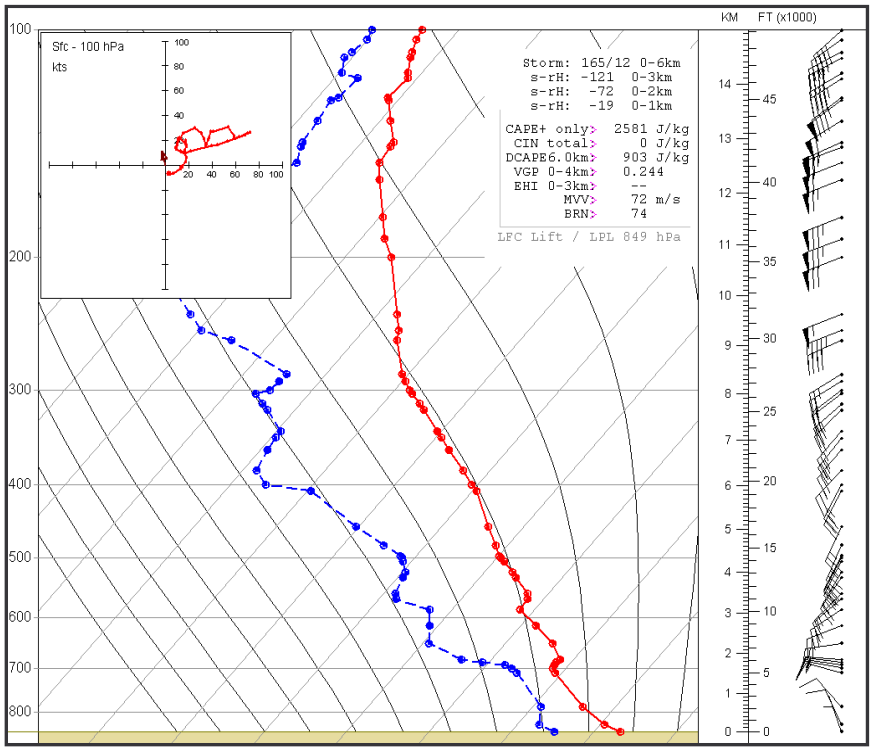

FIGURE 7.4: Irene midday sounding (skew *T*/ log p plot) for 11 November 2013. Axes and measurement units as per skew *T* / log p plot in Fig. 6.1. The red trace represents observed environmental air temperature whilst the blue trace correspondingly indicates environmental dewpoint. Units of *T* and T_d in °C.

TABLE 7.3: MSCP, T(2002) and T(2003) SCP, together with sounding-derived parameters for the 11 November 2013 case. Units of measurement as per Table 7.1.

Supercell Composite Parameter
11 November 2013

INPUT:

SBCAPE:	1287	SRH(0-1km):	-19
MUCAPE:	2581	SRH(0-2km):	-72
NCAPE:	0.26	SRH(0-3km):	-121
BRNshear:	35		

OUTPUT:

SCP Thompson et al (2002) :	1.822
SCP Thompson et al (2003) :	5.465
Modified Supercell Composite Parameter (MSCP) :	2.550

7.4 Rust de Winter, Limpopo, 17 November 2013

Case 4 : Analysis and comment:

An example of a case of isolated, non-severe thunderstorms occurring north-east of a well-defined dryline (Schaefer, 1986). The dryline bisected Gauteng, resulting in thunderstorms being limited to the north-eastern part of Gauteng as well as adjacent provinces such as Limpopo and Mpumalanga as seen in the accompanying satellite image in Fig. 7.6. In Table 7.4, the SCP based on T(2002) correctly suggested 0.52 although T(2003) still suggested 1.55, in other words, an SCP > 1.0.

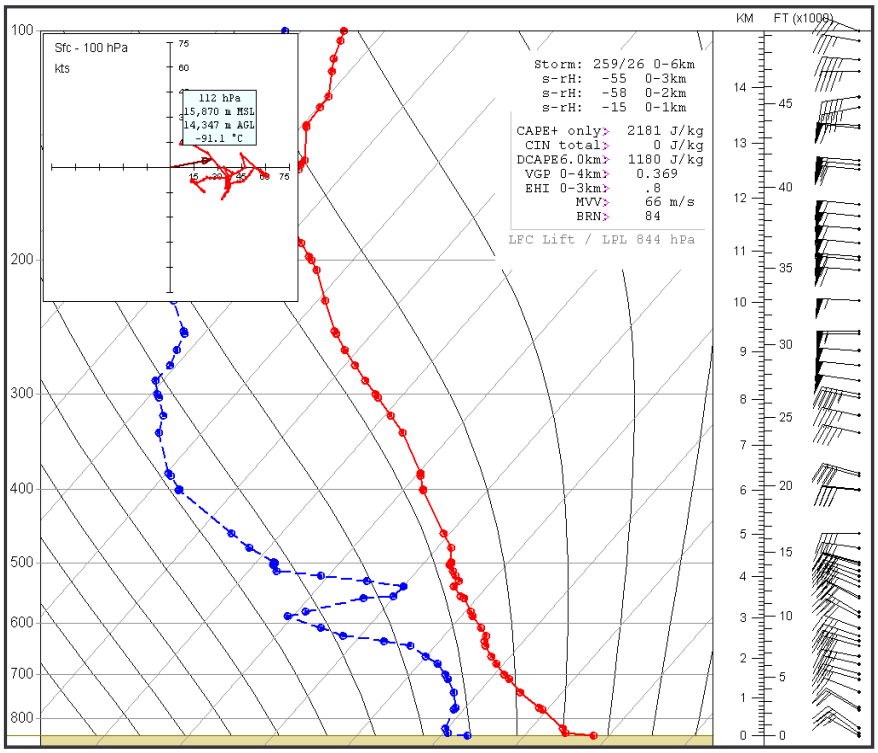

FIGURE 7.5: Irene midday sounding (skew *T*/ log p plot) for 17 November 2013. Axes and measurement units as per skew *T* / log p plot in Fig 6.1. The red trace represents observed environmental air temperature whilst the blue trace correspondingly indicates environmental dewpoint. Units of *T* and T_d in °C.

Encouragingly, MSCP returned a predicted value of 0.45, well below the 1.0 threshold and thus a correct prediction for "no supercell". There was still however the potential for aspects of incipient severity in this storm scenario with the

convective cloudbase located well above the surface, suggestive of an "inverted-vee" type convective profile of the type envisaged by Johns & Doswell (1992) as could be inferred visually from the corresponding sounding diagram in Fig. 7.5. The likelihood of a dry downburst scenario was further corroborated by the WINDEX (McCann, 1994) which was calculated as 57 kts, suggesting that surface gusts initiated by dry downbursts had the potential to be fairly severe, a scenario often, but not exclusively, encountered along the dryline (Schaefer, 1986).

TABLE 7.4: MSCP, T(2002) and T(2003) SCP, together with sounding-derived parameters for the 17 November 2013 case. Units of measurement as per Table 7.1.

Supercell Composite Parameter

17 November 2013

INPUT:

SBCAPE:	682	SRH(0-1km):	-15
MUCAPE:	2181	SRH(0-2km):	-58
NCAPE:	0.21	SRH(0-3km):	-55
BRNshear:	25.9		

OUTPUT:

SCP Thompson et al (2002) :	0.518
SCP Thompson et al (2003) :	1.553
Modified Supercell Composite Parameter (MSCP) :	0.455

Furthermore in Fig. 7.5, RAOB estimated the Bulk Richardson Number to be 84, which was also generally too high for supercells. It will be recalled that BRN between 10 and 40 were considered by Weisman & Klemp (1986) to be optimal for supercell genesis, as mentioned previously. This augmented the notion that supercells were unlikely and that multicells would more likely have been favoured in this particular case, where strong, predominantly unidirectional shear was abundant.

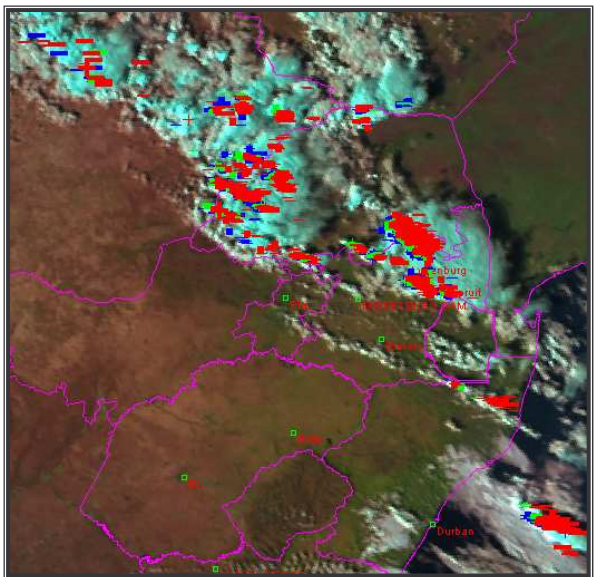

FIGURE 7.6: Meteosat 9 Day-Natural RGB image on 17 November 2013 at 15h00UTC, with LDN lightning detections (14h00 to 15h00UTC) overlaid. A pronounced surface dryline was located over Gauteng province at the time, bisecting the province along an axis from the north-west to south-east, limiting storms to the north-eastern part of Gauteng. Image © EUMETSAT 2013.

7.5 Viljoenskroon, Free State, 28 November 2013

Case 5 : Synoptic and upper air situation

The prevailing circulation pattern at the time of this event was characterised by a surface thermal trough over the central and western interior of southern Africa, as shown in the accompanying Mean Sea Level Pressure (MSLP) analysis for 12h00UTC in Fig. 7.7. A weak surface anticyclone was also in evidence, immediately south of the country, promoting south-easterly airflow along the southern coast. Over the north-eastern interior, including Gauteng, the surface airflow was predominantly a moisture-laden north-easterly, with a surface dewpoint of 14 °C at Pretoria and 12 °C reported at Welkom. A surface dryline was, however immediately west of the initial storm development, with Potchefstroom reporting a fairly dry surface dewpoint of only 4 °C, associated with a significantly drier north-westerly flow in opposition to the otherwise dominant north-easterly flow.

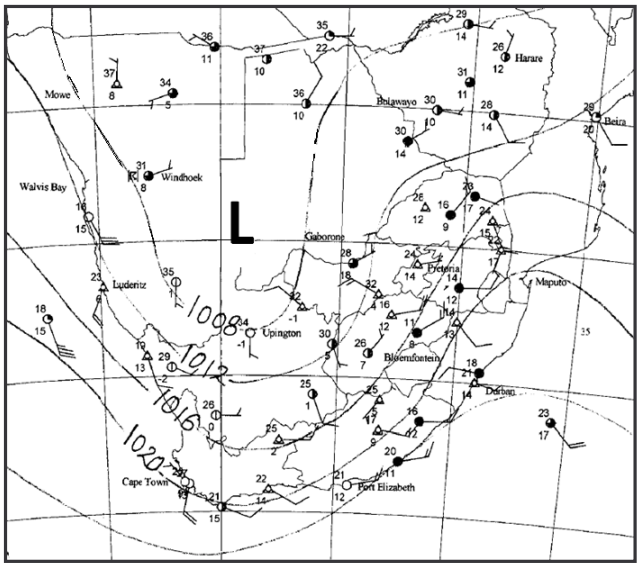

FIGURE 7.7: Synoptic MSLP analysis valid for 12h00UTC 28 November 2013, indicating a surface thermal trough over central and western parts of the interior. Isoline contour interval = 4 hPa. Source: SAWS.

With reference to Fig. 7.8 and 7.9 respectively, the corresponding upper air pattern at 700hPa and 500hPa valid for 12h00UTC included a number of circulatory components requiring discussion. An upper air anticyclone was in place over the Atlantic ocean, seawards of Namibia, whilst over the southern parts of South Africa, a low pressure system was evident, with a fairly extensive upper trough feature over the Northern Cape province. Over the Gauteng province however, there was an interesting setup of upper air flow. At 700hPa, corresponding to approximately 3300m MSL, or about 1800m AGL, a shortwave trough can be identified in Fig. 7.8, with fresh north-westerlies over Mpumalanga and Gauteng, becoming more west north-westerly in the west. Whilst this shortwave trough was also identifiable at 600hPa (not shown), by contrast, at 500hPa there was little evidence of this feature on the morning of 28 November 2013, with fairly brisk south-westerly, 40 to 50 kt winds suggested. This particular juxtaposition of upper air winds at 700 hPa and 500 hPa as suggested by the UM NWP is judged to be an accurate representation of the prevailing airflow at the time, as confirmed in Fig. 7.10 by the measured values returned by the 12h00UTC upper air sounding performed at Irene, Gauteng. Furthermore, in Fig. 7.10 one can identify clear evidence of a marked zone of predominant upper air dryness as revealed by the dewpoint profile at altitudes exceeding the 600 hPa isobaric level.

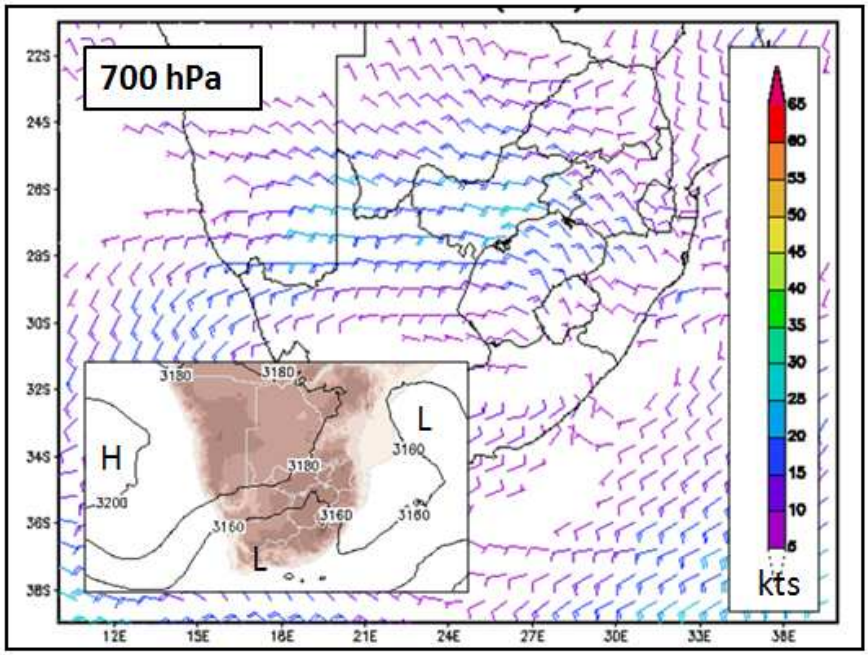

FIGURE 7.8 Upper air circulation at 700hPa (corresponding to 3300m MSL) for 12h00UTC 28 November 2013, based on the Unified Model xaant run of 201311280000UTC. Modelled wind barbs (knots) in colour, while the inset at bottom left indicates the corresponding contours of geopotential height (metres) at the 700hPa isobaric level. Source: SAWS.

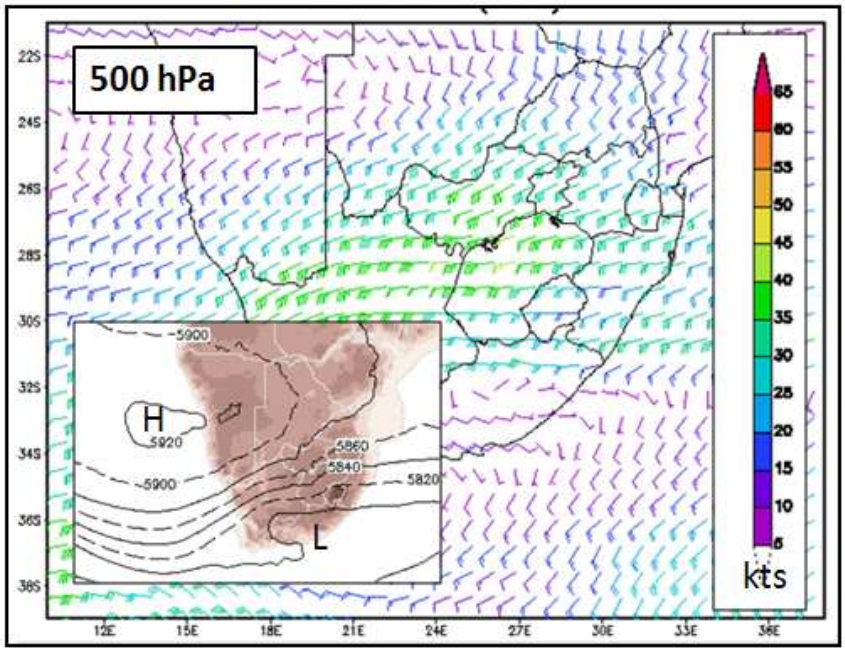

FIGURE 7.9 Upper air circulation at 500hPa (corresponding to 6000m MSL) for 12h00UTC 28 November 2013, based on the Unified Model xaant run of 201311280000UTC. Modelled wind barbs (knots) in colour, while the inset at bottom left indicates the corresponding contours of geopotential height (metres) at the 500HPa isobaric level. Source: SAWS.

Extreme dryness in the upper air profile is a known ingredient which promotes hail growth in thunderstorms. Mid-tropospheric dry, stable air has the opportunity to be ingested into the lee (*i.e.* the rear) of said storms, leading to rapid 'flushing' of thunderstorm ice products towards the ground, often resulting in hailfall at the surface.

With further reference to the skew *T* / log p aerological diagram in Fig. 7.10, a typical southern hemisphere supercell-type sounding profile is self-evident, especially in the light of earlier discussion presented in Chapter 6.1 regarding the typical supercell features revealed by averaging of the 15 supercell SUP sample. One of the typical supercell features associated with Fig. 7.10 include the marked anticyclonic tendency of wind direction with increasing altitude, with fresh north-easterlies at the surface, progressing rapidly to northerly to north-westerly flow at successive levels within the first 3000 m aloft, thus supporting negatively-oriented SRH of a significantly high magnitude as confirmed in Table 7.5.

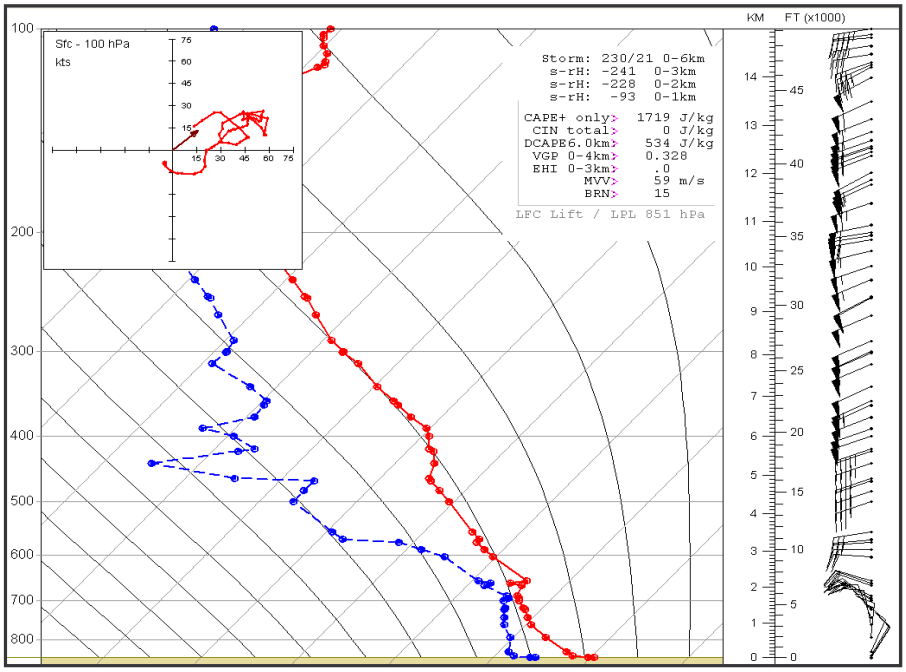

FIGURE 7.10: Irene midday sounding (skew *T*/ log p plot) for 28 November 2013. Axes and measurement units as per skew *T* / log p plot in Fig 6.1. The red trace represents observed environmental air temperature whilst the blue trace correspondingly indicates environmental dewpoint. Units of *T* and T_d in °C.

TABLE 7.5: MSCP, T(2002) and T(2003) SCP, together with sounding-derived parameters for the 28 November 2013 case. Units of measurement as per Table 7.1.

Supercell Composite Parameter

28 November 2013

INPUT:

SBCAPE:	432	SRH(0-1km):	-93
MUCAPE:	1719	SRH(0-2km):	-228
NCAPE:	0.16	SRH(0-3km):	-241
BRNshear:	117		

OUTPUT:

SCP Thompson et al (2002) :	8.078
SCP Thompson et al (2003) :	24.235
Modified Supercell Composite Parameter (MSCP) :	5.700

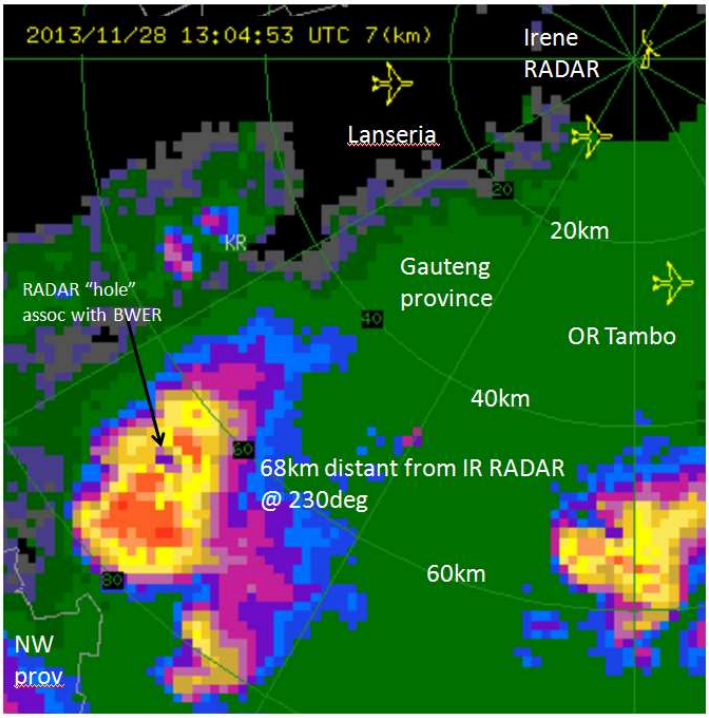

FIGURE 7.11: The position of Viljoenskroon supercell storm at 13h04UTC, as shown by Irene S-band RADAR. This dBZ (reflectivity) CAPPI scan at 7 km level reveals a clearly defined reflectivity "hole", or "echo doughnut", in association with the BWER. At this time the storm was somewhat beyond 60 km distant from the Irene RADAR, having traversed a section of NorthWest province, at extreme bottom-left of image. RADAR visualisation: TITAN software (Dixon & Weiner, 1993). Source: SAWS.

Case 5 : Storm analysis and comment:

The IR satellite image in Fig. 7.12 gives some indication of the spatial extent and position of the storm at 13h15UTC. This was a long-lived supercell, which traversed no less than three provinces (namely Free State, North West and thence into Gauteng). It was first noted near Viljoenskroon, north-west Free State, corresponding to the bottom left extreme trackpoint in Fig. 7.13, at approximately 09h10UTC and continued to be a major storm feature on the Irene RADAR, weakening and strengthening at intervals. It was subsequently observed to collapse rapidly at about 13h34UTC at a location south-east of Klerksdorp, near Soweto. The longevity of this particular storm was at least 4.5 hours and in addition it was associated with a sustained, well-defined BWER. Also in evidence was an "echo doughnut" or reflectivity hole associated with the BWER in a cross-section revealed by the 7 km PPI reflectivity image in Fig. 7.11. It was stated in Chapter 3.5.2 that not all supercells display deviant motion, hence it is noteworthy to observe in Fig. 7.10 that the Hail Mass Aloft (HMA) composite track (Dixon & Weiner, 1993 ; Powell, 2012) strongly indicated that the long track was not truly "deviant"; being neither significantly left (EMM) nor right (PMM) of the predicted Bunkers storm movement of 230 degrees at 21 kt, thus an excellent example of a long-lived, severe supercell that did not exhibit deviant motion.

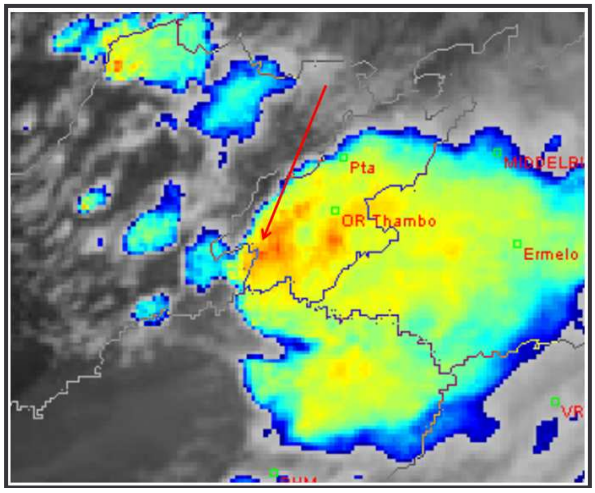

FIGURE 7.12: Meteosat 9 enhanced-IR satellite image, indicating the storm position at 13h15UTC, shortly after the time of the RADAR image discussed in Fig. 7.11. The supercell storm lay just beyond, to the south and south-east of the red arrow tip as indicated on the image. Source: EUMETSAT 2013.

From Table 7.5, NCAPE = 0.16, MUCAPE = 1719 J kg^{-1}, while in terms of Bulk Richardson Number, Fig. 7.9 shows the corresponding RAOB analysis, with a calculated BRN = 15 which fitted well with the findings of Weisman & Klemp (1986) who stated that BRN should ideally lie between 10 and 40 for supercells.

SRH(0-3 km) = -241 $m^2 s^{-2}$, SRH(0-2 km) = -228 $m^2 s^{-2}$ and SRH(0-1 km) = -93 $m^2 s^{-2}$, which suggested a very strong shear pattern through the entire layer, from the surface up to 3 km AGL. This strong, low-level shearing pattern could also be visually confirmed in the RAOB skew *T* / log p plot in Fig. 7.10, where the anticlockwise "twisting" tendency of the low-level wind vectors, with increasing altitude, was self-evident.

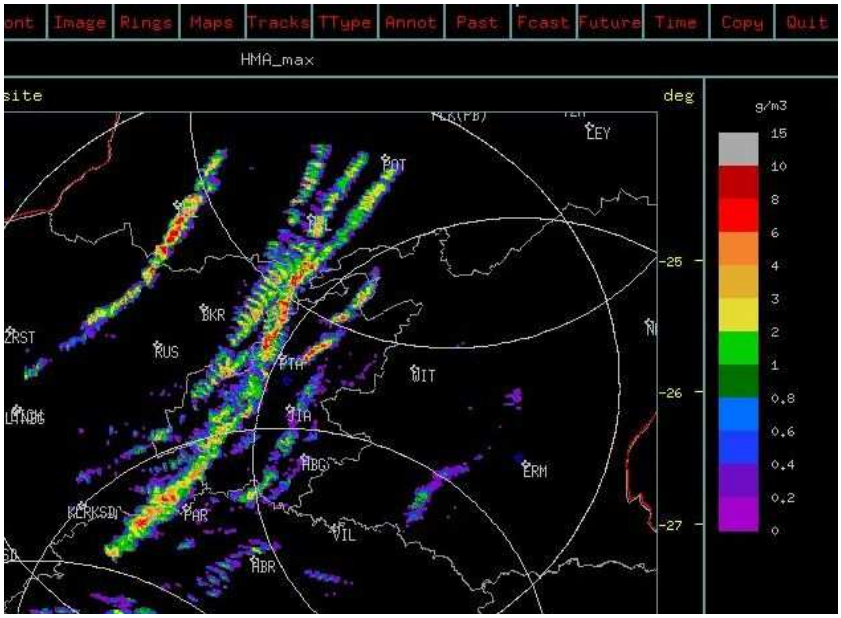

FIGURE 7.13: Composite tracks of RADAR-detections of Hailmass Aloft (HMA) (Dixon & Weiner, 1993; Powell, 2012) in g m^{-3} for 28 November 2013 storms. The track of the Viljoenskroon storm begins at bottom left of the image and proceeds north-east towards Johannesburg. Other long-lived and/or severe storms were similarly captured on the same day as the Viljoenskroon storm. RADAR visualisation: TITAN software (Dixon & Weiner, 1993). Image provided by C. Powell (SAWS).

In Table 7.5, MSCP = 5.7 while T(2002) and T(2003) suggested SCP = 8.0 and SCP = 24.2 respectively. The occurrence of a numerically large value of MSCP = 5.7 in this particular case leads this author to consider the possibility that MSCP and/or SCP may well be directly proportional to supercell severity, at least with respect to the

upper end of an SCP distribution. The suggestion of such a relationship is purely speculative at this stage and falls beyond the scope of the current study. Notwithstanding this, the notion of utilising SCP to predict supercell severity remains an intriguing concept and possibly merits further study. Consequently, this aspect is briefly discussed in the closing arguments in Chapter 8 to follow.

7.6 Summary

As seen in Table 7.6 (A) and 7.6 (B), MSCP successfully identified the 3 supercell cases at the upper end of the spectrum of cases assessed, while the weakest event was also correctly identified as being a non-supercell candidate. By comparison, the SCP of T(2002) returned a performance in a very similar vein to that of MSCP, providing further endorsement that MSCP had been formulated acceptably.

TABLE 7.6(A): The five case studies in chronological order indicating Modified SCP (MSCP), T(2002) and T(2003) in the same order as presented above.

TABLE A

Case	Date YYYYMMDD	Location	Type	MSCP	SCP T(2002)	SCP T(2003)
7.1	20131007	Villiers	weak, borderline supercell	2.36	2.42	7.26
7.2	20131019	Bapsfontein	classic supercell	4.27	1.83	5.48
7.3	20131111	Benoni	severe, non-supercell	2.55	1.82	5.46
7.4	20131117	Rust de Winter	isolated, non-severe, non-supercell on dryline	0.45	0.52	1.55
7.5	20131128	Viljoenskroon	very long-lived, very severe supercell, non-deviant track	5.70	8.08	24.23

By contrast, the SCP of T(2003) returned an SCP well in excess of the SCP = 1.0 discriminarory threshold for all five cases. It could justifiably be argued on the basis of these results that T(2003) appeared to over-warn for Gauteng Highveld thunderstorm scenarios. This statement provides an additional, independant corroboration of the notion first raised in the summary of Chapter 6, where the significantly elevated box and whisker distribution of T(2003) SCP clearly stood out in marked contrast to the distributions of MSCP and T(2002) SCP for the SUP 15

Gauteng supercell sample. Generally speaking; the phenomenon of overwarning in an operational forecasting and risk mitigation context is not a desirable attribute in a predictive index.

TABLE 7.6(B): As in (A) above, indicating Modified SCP (MSCP), T(2002) and T(2003) but ranked from highest MSCP to lowest MSCP.

TABLE B

Case	Date YYYYMMDD	Location	Type	MSCP	SCP T(2002)	SCP T(2003)
7.5	20131128	Viljoenskroon	very long-lived, very severe supercell, non-deviant track	5.70	8.08	24.23
7.2	20131019	Bapsfontein	classic supercell	4.27	1.83	5.48
7.3	20131111	Benoni	severe, non-supercell	2.55	1.82	5.46
7.1	20131007	Villiers	weak, borderline supercell	2.36	2.42	7.26
7.4	20131117	Rust de Winter	isolated, non-severe, non-supercell on dryline	0.38	0.52	1.55

CHAPTER XIII : CONCLUSION

8.1 Summary of main findings

Chiefly by means of upper air sounding analysis, this research work set out to investigate the nature and extent of any contrasts between supercell and non-supercell storms on the Gauteng Highveld of South Africa. Once quantified, such constrasts were utilised in the design of a Supercell Composite Parameter (SCP), modified and tuned to typical Gauteng conditions, henceforth to be termed the modified Supercell Composite Parameter (MSCP). This was accomplished through the compilation and intercomparison of two distinct and independant datasets, namely the SUP (supercell) and NON-SUP (non-supercell) samples respectively. Broadly, it was found that there were indeed numerous qualitative and quantitative differences in the SUP and NON-SUP datasets as revealed and discussed in Chapter 6. In the case of qualitative differences, these were presented and analysed though the use of merged or averaged soundings applied to each of the two respective datasets and visualised by means of RAOB-generated aerological diagrams. Furthermore, the quantitative differences between said samples were explored through the use of box and whisker plots as well as statistical hypothesis testing, utilising parametric as well as non-parametric tests. These investigations revealed (a) which thunderstorm parameters would be best suited to be utilised in MSCP and (b) an explicit quantification of threshold normalisation factors to apply to MSCP.

In relation to the six main study Objectives associated with this research work, it can be reported that all the Objectives were completed in the manner envisaged in Chapter 1. In particular, Objective 1 required 2007-2011 SAWS LDN data to be analysed in order to identify thunderstorm days within the Gauteng domain. This activity was described in detail in Chapter 3.4 as well as Chapter 5.1. The explicit identification of thunderstorm days was critical as this information was required to accomplish Objective 2, which dealt with the construction of a proximity sounding

dataset of radiosonde data from the Irene site as well as investigation regarding the intraseasonal variation thereof. Furthermore, Objective 2 required the initial dataset to be further filtered to reflect only thunderstorm days occurring during the austral summer months. This filtered dataset, deemed the NON-SUP dataset was essential in order to provide a baseline reference group of non-supercell soundings to compare with the SUP sample of supercell events. Incidentally, the SUP sample was also successfully compiled as per the requirements set out in Objective 3 and described in detail in Chapter subsections 4.1 to 4.3. Subsequent to the creation of the NON-SUP and SUP datasets respectively, the next logical step which was accomplished in terms of Objective 5 was to compare and discuss differences in these sets from a statistical perspective. In so doing, candidate storm parameters for utilisation in the formulation of MSCP were so identified, as well as measures associated with the location and dispersion of said parameters. Objective 5 was fulfilled by the compilation of the final mathematical formula for MSCP, as shown in Chapter 6.4. The final Objective required that the performance of MSCP as well as the T(2002) and T(2003) variants of SCP be tested in a semi-operational manner, with the application thereof to a range of case-studies within the Gauteng domain. This activity was indeed performed in relation to five such case-studies, the results of which appear in Chapter 7, thus concluding the Objectives of this research work.

Following the definition of MSCP in Chapter 6, some research highlights, chiefly determined by Chapter 7 case-study results were as follows:

1. Gauteng supercells typically form in association with near-storm environmental conditions having much in common with conditions quantified in the USA-based SCP study of Thompson *et al*. (2002). This is attested to by MSCP and the SCP of T(2002) possessing similar formulation and normalisation factors, particularly in terms of 0-3 km SRH as well as BRN shear. A comparison of the distribution of MSCP as well as the T(2002) SCP applied to the 15 SUP supercell cases, revealed that both MSCP and T(2002) SCP operate within a similar interquartile range (IQR).

2. Based on the five case studies discussed in Chapter 7, preliminary assessment suggests that MSCP delivers meaningful, useful and relatively accurate guidance in terms of the binary, "yes/no" short-term forecast question of "Given that thunderstorms are a certainty in Gauteng, are supercell storms reasonably likely?" thus fulfilling the final Objective of this work, declared in Chapter 1.
3. Furthermore, the SCP as defined by T(2002) could possibly be applied in an operational context in a Gauteng domain, as a second-choice alternative to MSCP.
4. However, notwithstanding relatively favourable performance of T(2002) SCP alluded to in points (1) and (3) above, the author is of the opinion that in an operational context, the MSCP is likely to be the SCP scheme least susceptible to overwarning, given that in Fig. 6.18 MSCP displayed the lowest median of the three schemes.
5. By contrast to the above, the formulation of SCP in T(2003), whilst displaying at least equal discriminatory power to that of MSCP and T(2002) SCP formulations, in terms of correctly identifying incipient supercell environments as provisionally established in Chapter 7, nevertheless appears to display marked positive bias, potentially favouring overwarning. This attribute was also independently illustrated in Fig. 6.18 where the relative IQR distributions of each of MSCP, SCP T(2002) and SCP T(2003) were displayed for the SUP sample of 15 supercell cases.

8.2 Conclusions

In a logical distillation of the five main findings listed and discussed in the preceding chapter section, the following primary conclusions may be drawn. The overarching objective of this study was to design and implement a range of modifications to the Supercell Composite Parameter (SCP) originally designed by Thompson *et al*. (2002, 2003) in such a way that the resulting Modified Supercell Composite Parameter (MSCP) would be fine-tuned to Gauteng Highveld conditions and could confidently

be applied as a short-term predictive tool to identify atmospheric conditions which could support supercell-type thunderstorm development, as opposed to alternative thunderstorm types, such as multicells or airmass thunderstorms.

In accordance with the research Objectives defined for this study, the MSCP was duly formulated with the aid of a representative sample of 15 supercell proximity soundings. In order to establish an objective, albeit provisional assessment of MSCP operational performance, the MSCP was tested against five Gauteng case-studies. These case-studies, drawn from the summer months of the 2013 calendar year were a mixture of supercell and non-supercell events, some of which were severe and some non-severe. Subsequent case by case analysis of MSCP performance in Chapter 7 demonstrated that MSCP appears to have tangible, quantifiable discriminatory ability to effectively perform the function for which it was designed. Furthermore, intercomparison of MSCP with T(2003) SCP in relation to the same case-studies, strongly suggests that T(2003) would have a marked tendency to overwarn. In an operational context, overwarning is not generally a desirable feature. Consequently MSCP is judged to be the preferred SCP scheme as it appears to function within a conservative interquartile range (IQR) as well as possessing a desirably low median value as opposed to the corresponding IQR and median of the T(2003) scheme, despite the latter being a refined and updated iteration of T(2002).

These results are deemed to be significant and unique in that, prior to this research, the use and application of any form of SCP in a southern African domain had hitherto not been formally tested. Furthermore, the results of this Highveld-based study have additional significance, due to the unique elevated terrain of the Gauteng region, characterised by an atmosphere that is markedly less dense than is typical of other localities closer to mean sea level.

In the light of the above, it is advised unreservedly that MSCP be implemented operationally within a Gauteng domain. It is further advised that, should the use of T(2003) SCP be considered at any time in a Gauteng domain, that this form of SCP only be utilised with due consideration to the possible risk of undesirable positive bias in the SCP response (*i.e.* overwarning or false positives).

8.3 Discussion of challenges

A CLIMATOLOGY OF HIGHVELD SUPERCELLS

A constraint of this research was the absence of a pre-existing southern African, or Highveld, climatology of supercells, which prompted the allocation of a significant period of time to assemble a supercell database suitable for use in the study. In mitigation thereof, a sizable sample of southern African Highveld supercell storms were identified in the course of this research, not all of which were suited for use in this study. A listing of 29 such storms is provided in the Appendix. It is hoped that this embryonic database may serve as a useful catalyst to initiate further development of a supercell climatology for the Highveld region.

QUALITY AND CONSISTENCY OF UPPER AIR SOUNDINGS

Of the 2879 Irene soundings initially utilised out of a possible total of 3651 soundings, there was found to be significant variability in the quality of Irene radiosonde soundings throughout the 2007-2011 period, particularly from 2010 onwards. The prototype dataset of close to 1000 preferred soundings of interest required meticulous scrutiny, following quality control procedures similar to those of Durre *et al*. (2006). There were even periods where no soundings were performed at the Irene facility. Regretfully, a number of otherwise excellent, “textbook” supercell cases had to be precluded from the study due to absence of a corresponding upper air ascent in close temporal proximity to the event. Such preclusions included, but were not limited to, the 23 June 2013 winter supercell outbreak as well as the 20 October 2012 Midrand supercell event, both of which were significant severe storm cases in their own right.

8.4 Implications for existing theory

Prior to this research and in the absence of similar such studies, it was largely unknown whether the Supercell Composite Parameter (SCP) could be applied successfully in a southern African Highveld context, despite the SCP being composed of robust thunderstorm parameters in common usage. Before embarking on this study, the author was acutely aware of other predominantly USA-based thunderstorm indices that, for a variety of reasons, including the unusually high altitude of the southern African Highveld domain, have been found to have only limited applicability to a Highveld domain. The Showalter Index (Showalter, 1953) and the K Index (George, 1960) are two such examples which are illustrative of the potential limitations and pitfalls surrounding the applicability of thunderstorm parameters or indices sourced internationally.

Firstly, through the formulation of MSCP, this research has provided a new composite index that has ability to identify pre-storm conditions which may favour the development of supercell-type thunderstorms in Gauteng province, on the southern African Highveld, where previously there was no such methodology available. Secondly, an unexpected, co-incidental result revealed by this research was that, in a Gauteng domain, there is apparently preferable utility of T(2002), the first iteration of the Supercell Composite Parameter as originally formulated by Thompson *et al*. (2002), over and above that of T(2003) the later, refined iteration of SCP. Acknowledging the theoretical and practical cautions expressed by Doswell & Schultz (2006), when considering the merits and limitations of composite thunderstorm indices in general, the MSCP and case-study results presented herein are a further testament that the three factor, composite index formulation of SCP first envisaged by Thompson *et al.* (2002, 2003) to represent instability, helicity and deep shear contributions towards supercell development, represents a realistic and robust approach to a complex problem.

8.5 Recommendations relating to implementation

A SINGLE GRIDPOINT APPROACH TO MSCP

A single-point based implementation, based on an upper air profile derived from real (radiosonde) or synthetic (NWP) data would be straightforward to apply. A number of commercial sounding display and analysis tools such as RAOB (Shewchuck, 2013) could be customised to display MSCP and/or SCP. This approach would typically be appropriate for a single station, such as a major airport or to quantify the prevailing SCP for a small province such as Gauteng. A limitation to this approach is that no information regarding spatio-temporal changes, within a mesoscale region surrounding said gridpoint, would be available to the end user. Despite this drawback, this approach does have merit in that the MSCP and/or SCP results would be based on actual sounding observations, as opposed to synthetic NWP values.

GRIDDED 2-D NWP OUTPUT

A more holistic approach which could enjoy wider use and operational applicability would be to utilise NWP post-processing and to generate 2-D spatial fields of MSCP and/or SCP. A forecaster tasked with nowcasting analysis of the near real-time thunderstorm environment could then gain more insight into the spatial distribution of MSCP at a particular point in time, relative to his or her location as well as the temporal evolution thereof. As with all NWP, It could justifiably be argued however that the spatial resolution and accuracy of NWP, particularly within the Planetary Boundary Layer (PBL), may not always be a realistic and faithful interpretation of the current state of the atmosphere.

A TWO-TIERED, PARALLEL APPROACH

There is no strong argument to preclude either of the two preceding recommendations. Each approach has merit in an operational context, as well as unavoidable limitations. A pragmatic solution to effectively reconcile these two widely contrasting concepts, would be to adopt and implement both solutions in

parallel. From a forecaster perspective, it is undeniable that benefit could potentially be derived from routine access to 'ground truth' sounding-derived observations to quantify the current state of the atmosphere and thence MSCP. Concurrent to this, the application of NWP-based MSCP would typically provide useful insight into upcoming spatio-temporal changes in MSCP at, as well as in close proximity to, the sounding location.

8.6 Suggestions for further research

DISCRIMINATION BETWEEN TORNADIC VS NON-TORNADIC SUPERCELLS

Notwithstanding the fact that the SCP was designed by Thompson *et al*. (2002; 2003) exclusively to provide discrimination between supercell and non-supercell thunderstorm events in a binary yes/no sense, there is scope to investigate the possible degree of correlation between large SCP values at the upper end of the distribution of SCP and the phenomenon of tornadic supercell thunderstorms. In other words, to explore the viability of determining an additional threshold, other than the existing, current threshold of SCP = 1, which may provide discriminatory power in terms of identifying a distinction between tornadic and non-tornadic supercell storms. A recent study by Parker (2014), utilising 134 near-storm soundings relating to 12 supercell storms from the VORTEX2 dataset presented striking evidence (refer Parker's Table 17) to support the hypothesis that both the STP (Thompson *et al*., 2003) and SCP (Thompson *et al*. 2003, 2007) show a markedly different quantitative response to tornadic supercells as opposed to non-tornadic supercells, with SCP apparently registering significantly higher values for tornadic supercells.

Whilst tornadic storms in general and tornadic supercells in particular have been indeed been documented within this study domain, these cases are currently not numerous and any fresh studies would benefit greatly, at least from a statistical viewpoint, from analysis of a larger population of realisations of such events drawn from a longer temporal record. Notwithstanding the above, it is feasible that

additional valuable insight into the existing datasets discussed in this work could be gained through use of RAOB hodograph analysis. This approach would be especially useful in terms of identifying nuances in the low-level speed and directional shearing profile within the first 1000 m AGL, as proposed by Esterheld & Giuliano (2008) in relation to discrimination between tornadic and non-tornadic supercells as discussed earlier in the literature study of this work.

DAILY TEMPORAL TRENDS OF SCP

Acknowledging the ongoing mainstream use of traditional balloon-borne radiosonde ascent data, a notable and unavoidable restriction of such data however is obviously one of temporal resolution, with scheduled ascents at fixed gridpoint stations such as Irene, Gauteng, typically being performed only at 12-hourly intervals. Arguably there is much opportunity in the intervening hours between successive soundings for the local airmass to undergo significant changes in terms of a variety of meteorological parameters, especially within the planetary boundary layer (PBL). Markowski *et al*. (1998b) determined that storm-relative helicity is highly variable in space and time, as cited by Dupilka & Reuter (2006b) when referring to the limitations of proximity soundings. By contrast, readily available AMDAR data, emanating from commercial aircraft taking off (or respectively, landing) at ORTIA are a convenient source of high quality (Drüe *et al*., 2008) and high spatio-temporal atmospheric data. Typically such aircraft-borne instrumentation provides at least five to six individual soundings per hour, with ORTIA data being particularly numerous during the diurnal period. A novel and useful application of AMDAR data would be to investigate hourly as well as daily temporal trends in speed and directional shearing parameters such as storm-relative helicity (SRH) and Bulk Richardson shear through varying thicknesses of the lower atmosphere.

Acknowledging that both storm-relative helicity as well as Bulk Richardson shear are critical input components contributing towards quantification of SCP and MSCP, it would be an engaging research question to further explore the nature and extent of short-term temporal variability in SCP and/or MSCP at ORTIA. Furthermore, would such short-term variability in MSCP have measurable utility in terms of promoting

enhanced levels of safety for the aviation community at large, through a better understanding of the pre-storm environment at the airfield in question? The aforementioned aspect could be especially relevant in the context of early identification of pre-storm environmental conditions which could favour the development and onset of severe thunderstorms and particularly supercells. It could be envisaged that the MSCP, with fresh input based largely on AMDAR data and updated at 10 to 15 minute intervals, could ultimately become an additional nowcasting technique to effectively monitor the incipient threat of severe supercell thunderstorms developing in close proximity to large, busy airports.

ααΩΩΩΩΩαα

REFERENCES

Achtemeier, G.L. (1975). Doppler velocity and reflectivity morphology of a severe left-moving split thunderstorm. Preprints: 16th RADAR Meteorology Conference, Houston, Texas, 93-98.

Admirat, P., Goyer, G. G., Wojtiw, L., Carte, E. A. & Roos, D. (1985). A comparative study of hailstorms in Switzerland, Canada and South Africa. Journal of Climatology, **5(1)**, 35-51.

Allen, J. (2012). Supercell Storms: Melbourne's white Christmas 2011. Bulletin of the Australian Meteorological and Oceanographic Society, **25(3)**, 47-51.

Australian Bureau of Meteorology (BoM), severe storm definition (2013). Available at: http://www.bom.gov.au/vic/sevwx/about.shtml last accessed: 12 December 2013.

Barnes, G. (2001). Severe local storms in the Tropics. In Severe Convective Storms, Meteorological Monographs, No.28 (359-432). Boston, United States of America: American Meteorological Society.

Beeld newspaper (2007). *Dis die natuur wat terugslaan*. Monday 8 October 2007.

Beeld newspaper (2012). *Student (22) sterf by dam*. Monday 25 June 2012.

Bedka, K., Brunner, J., Dworak, R. & Feltz, W. (2011). Objective satellite-based overshooting top and enhanced-V / cold ring signature detection. 6th European Conference on Severe Storms, Palma, Mallorca.

Bera, A. K. & Jarque, C.M. (1982). Model specification tests: A simultaneous approach. Journal of Econometrics, **20**, 59-82.

Betchov, R. (1961). Semi-isotropic turbulence and helicoidal flows. Physics of Fluids, **4**, 925-926.

Blanchard, D. O. (1998). Assessing the vertical distribution of convective available potential energy. Weather and Forecasting, **13(3)**, 870-877.

Blanchard, D. O. (2011). Forecasters Forum: Supercells in environments with atypical hodographs. Weather and Forecasting, **26**, 1075-1083.

Bluestein, H. & Parks, C. (1983). A Synoptic and Photographic climatology of Low-precipitation Severe Thunderstorms in the Southern Plains. Monthly Weather Review, **111(10)**, 2034-2046.

Borstlap, G.P. (1980). *Kwarteeu Haelstorm : JanSmutsLughawe : 15 Januarie 1980*. South African Weather Bureau monthly newsletter, **370**, January 1980.

Box, G.E.P. & Cox, D.R. (1964). An Analysis of Transformation, Journal of the Royal Statistical Society. Series B (Methodological), **26 (2)**, 211-252.

Brimelow, J.C. (2004). Personal communication: Julian Brimelow (Dr.), meteorology lecturer, University of Alberta, Edmonton, Alberta, Canada, e-mail RE: Potchefstroom supercell, 28 October 2004. Current affiliation: Centre for Earth Observation Science, University of Manitoba, Canada. E-mail: umbrimel@cc.umanitoba.ca

Brimelow, J.C., Reuter, G.W. & Poolman, E.P. (2002). Modeling Maximum Hail Size in Alberta Thunderstorms. Weather and Forecasting, **17**, 1048-1062.

Brooks, E. (1949). The tornado cyclone. Weatherwise, **2**, 32-33.

Brooks, H., Doswell, C. A. III & Cooper, J. (1994). On the environments of tornadic and nontornadic mesocyclones. Weather and Forecasting, **9**, 606-618.

Brouwers, E. & Todd, M. (2007). A weekend of severe weather across parts of the country. South African Weather Service media release. Monday, 8 October 2007, Pretoria, Gauteng, South Africa.

Brown, R. & Meitlin, R. (1994). Evolution and morphology of two splitting thunderstorms with dominant left-moving members. Monthly Weather Review, **122**, 2052-2067.

Browning, K. (1962). Cellular structure of convective storms. The Meteorological Magazine, **91**, 341-350.

Browning, K. (1964). Airflow and precipitation trajectories within severe local storms which travel to the right of the winds. Journal of Atmospheric Science, **21**, 634-639.

Browning, K. & Ludlam, F. (1962). Airflow in convective storms. Quarterly Journal of the Royal Meteorological Society, **88**, 117-135.

Browning, K. A., Fankhauser, J.C., Chalon, J.P., Eccles, P.J., Strauch, R.G., Merrem, F.H., Musil, D.J., May, E.L. & Sand, W.R. (1976). Structure of an evolving hailstorm. Part V: Synthesis and implications for hail growth and hail suppression. Monthly Weather Review, **104**, 603-610.

Bunkers, M. (2002). Vertical wind shear associated with left-moving supercells. Weather and Forecasting, **17**, 845-855.

Bunkers, M., Klimowski, B., Zeitler, J., Thompson, R. & Weisman, M. (2000). Predicting supercell motion using a new hodograph technique. Weather and Forecasting, **15**, 61-79.

Bunkers, M., Hjelmfelt, M. & Smith, P. (2006a). An observational examination of long-lived Supercells, Part I: characteristics, evolution and demise. Weather and Forecasting, **21**, 673-688.

Bunkers, M., Johnson, J., Czepyha, L., Grzywacz, J.M., Klimowski, B.A. & Hjelmfelt, M.R. (2006b). An observational examination of long-lived supercells, Part II: environmental conditions and forecasting. Weather and Forecasting, **21**, 689-714.

Bunkers, M. & Stoppkotte, J. W. (2007). Documentation of a rare tornadic left-moving supercell. Electronic Journal of Severe Storms Meteorology, **2**, 1-22.
Available at: http://www.ejssm.org/ojs/index.php/ejssm/article/viewFile/14/16 last accessed: 28 January 2014.

Burgess, D. & Lemon, L. (1990). Severe thunderstorm detection by RADAR. In RADAR in Meteorology, Atlas, D. (ed.), American Meteorological Society, 619-656.

Burgess, D., Wood, V. & Brown, R. (1982). Mesocyclone evolution statistics. Preprints, 12th Conference on severe local storms, San Antonio, Texas, American Meteorological Society, 422-424.

Byers, H. (1942). Nonfrontal thunderstorms. Miscellaneous report No. 3, Chicago: University of Chicago Press.

Byers, H., & Braham, R. (1949). The Thunderstorm. Washington, D.C: U.S. Government Printing office. 287 pp.

Calhoun, K.M., MacGorman, D. R., Ziegler, C. L. & Biggerstaff, M. I. (2013). Evolution of Lightning Activity and Storm Charge relative to Dual-Doppler Analysis of a High-Precipitation Supercell Storm. Monthly Weather Review, **141**, 2199-2223.

Carte, A. & Basson, I. L. (1970). Hail in the Pretoria-Witwatersrand area 1962-1969 CSIR Report 293 (1-28). CSIR, Pretoria, South Africa.

Carte, A. & Held, G. (1972). Hailstorms in 1970/71, CSIR Report 312, 1-45. CSIR, Pretoria, South Africa.

Chisholm, A. & Renick, J. (1972). The kinematics of multicell and supercell Alberta hailstorms. Alberta Hail Studies, 1972. **72 (2)**, 24-31.

Clark, L. (2004). Extensive hail damage on the Highveld and surrounding areas on 27 October 2004. SAWS news article, Thursday 28 October 2004, Pretoria, Gauteng.

Clarke, T. (1979). Numerical simulations with a three-dimensional cloud model: Lateral boundary condition experiments and multicellular storm simulations. Journal of Atmospheric Science, **36**, 2191-2215.

Colquhoun, J. (1980). A method of estimating the velocity of a severe thunderstorm using the vertical wind profile in the storm environment. Preprints: 8th Conference on Weather Forecasting and Analysis (316-323). Denver, Colorado, American Meteorological Society.

Cotton, W. R. & Anthes, R. A. (eds.) (1989). Storm and Cloud Dynamics. San Diego, California, United States of America: Academic Press.

Craven, J. & Brooks, H. (2004). Baseline climatology of sounding derived parameters associated with deep, moist convection. National Weather Digest, **28**, 12-24.

D' Abreton. P. (1991). A synoptic characterization of some South African tornadoes. South African Journal of Science, **87(1)**, 56-61.

D'Agostino, R.B. (1970). Transformation to normality of the null distribution of g1. Biometrika, **57 (3),** 679–681. doi:10.1093/biomet/57.3.679

Dahl, J.M.L. (2006). *Superzellen – Dynamik und Vorhersage* (Supercells – Their Dynamics and Prediction). Unpublished MSc dissertation, Free University of Berlin, Berlin, Germany.

Darkow, G.L. (1968). The total energy environment of severe storms. Journal of Applied Meteorology. **7**, 199-205.

Darkow, G.L. (1969). An analysis of over 60 tornado proximity soundings. Preprints, 6th Conference on Severe Local Storms, Chicago, Illinois, American Meteorological Society, 218-221.

Davies, J. M. (1998). On supercell motion in weaker wind environments. 19th Conference on Severe Local Storms (685-688). Minneapolis, Minnesota, American Meteorological Society.

Davies, J.M. (2004). Estimations of CIN and LFC Associated with Tornadic and Non-tornadic Supercells. Weather and Forecasting, **19 (4),** 714-726.

Davies, J. & Johns, R. (1993). Some wind and instability parameters associated with strong or violent tornadoes. Part 1: wind shear and helicity. In Geophysical Monographs: 79. The Tornado: Its Structure, Dynamics, Prediction and Hazards (583-590). American Geophysical Union.

Davies-Jones, R. (1984). Streamwise vorticity: The Origin of Updraft Rotation in Supercell Storms. Journal of the Atmospheric Sciences, **41(20)**, 2991-3006.

Davies-Jones, R., Burgess, D. & Foster, M. (1990). Test of helicity as a tornado forecast parameter. Preprints, 16th Conference on Severe Local Storms, 588-592.

de Coning, E. & Adam, B. (2000). The tornadic thunderstorm events during the 1998-1999 South African summer. Water SA, **26(3),** 361-376.

de Coning, E., Adam, B., & Banitz, L. (2000a). A severe weather event on 29 December 1997; synoptic and mesoscale perspectives. Water SA, **26(2)**, 137-146.

de Coning, E., Adam, B.F., Goliger, A.M. & van Wyk, T. (2000b). An F3 tornado in Heidelberg, South Africa on 21 October 1999. National Weather Association e-journal.
Available at: http://www.nwas.org/ej/heidelberg last accessed: 28 January 2014.

Dessens, J. & Snow, J.T. (1993). Comparative description of tornadoes in France and the United States. In The Tornado: Its Structure, Dynamics, Prediction and Hazards. Geophysical Monographs, Vol 79, 110-132. American Geophysical Union.

Dixon, M. & Wiener, G. (1993). TITAN: Thunderstorm Identification, Tracking, Analysis and Nowcasting - A RADAR-based methodology. Journal of Atmospheric and Oceanic Technology, **10(6)**, 785-797.

Dostalek, J., Weaver, J. & Phillips, G. (2004). Aspects of a tornadic left-moving thunderstorm of 25 May 1999. Weather and Forecasting, **19(3)**, 614-626.

Doswell, C. A. III (1987). The distinction between large-scale and mesoscale contribution to severe convection: a case-study example. Weather and Forecasting, **2**, 4-16.

Doswell, C. A. III (1991). A review for forecasters on the application of hodographs to forecasting severe thunderstorms. National Weather Digest, **16(1)**,2-16.

Doswell, C. A. III (1995). Comments on 'Single Doppler RADAR observations of a mini-supercell tornadic thunderstorm'. Monthly Weather Review, **123**, 230-234.

Doswell, C. A. III & Burgess, D. (1993). Tornadoes and tornadic storms: A review of conceptual models. In Geophysical Monographs: 79. The Tornado: Its Structure, Dynamics, Prediction and Hazards (161-182). American Geophysical Union.

Doswell, C. A. III & Rasmussen, E. N. (1994). The effect of neglecting the virtual temperature correction on CAPE calculations. Weather and Forecasting, **9**, 619-623.

Doswell, C. A. III & Schultz, D. (2006). On the use of parameters and indices in forecasting severe storms. Electronic Journal of Severe Storms Meteorology, **1(3)**, 1-22. Available at: http://www.ejssm.org/ojs/index.php/ejssm/issue/view/3 last accesed: 20 January 2014.

Doviak, R. & Zrnic, D. (eds.) (2006). Doppler RADAR and Weather Observations. 2nd edition. Mineola, New York: Dover Publications Incorporated. ISBN: 0-486-45060-0.

Dror, H. (2001). Boxcoxlm: Calculation of suitable lamda values required for the Box-cox transformation. A Matlab file. Available at: http://www.mathworks.com/matlabcentral/fileexchange/10419-box-cox-power-transformation-for-linear-models/content/boxcoxlm.m last accessed: 19 October 2014

Drüe, C., Frey, W., Hoff, A. & Hauf, T. (2008). Aircraft type-specific errors in AMDAR reports from commercial aircraft. Quarterly Journal of the Royal Meteorological Society, **134**, 229-239.

Dupilka, M. & Reuter, G. (2006a). Forecasting tornadic thunderstorm potential in Alberta using environmental sounding data. Part I: Wind shear and bouyancy. Weather and Forecasting, **21**, 325-335.

Dupilka, M. & Reuter, G. (2006b). Forecasting tornadic thunderstorm potential in Alberta using environmental sounding data. Part II: Helicity, precipitable water and storm convergence.Weather and Forecasting, **21**, 336-346.

Durre I., Vose, R.S. & Wuertz, D.B. (2006). Overview of the Integrated Global radiosonde Archive. Journal of Climate, **19**, 53-68.

Dyson, L. L. (2009). Heavy daily-rainfall characteristics over the Gauteng province. Water SA, **35(5)**, 627-638.

Dyson, L. L., van Heerden, J. & Sumner, P.D. (2014). A baseline climatology of sounding-derived parameters associated with heavy rainfall over Gauteng, South Africa. International Journal of Climatology. doi: 10.1002/joc.3967.

Edwards, R. (2006). Supercells of the Serrianas del Burro, Mexico. Preprints, 23rd Conference on Severe Local Storms, St Louis, Missouri, P6.2.

Edwards, R. & Hodanish, S. (2004). Environmental analysis and photographic documentation of an intense left-moving supercell on the Colorado plains. Monthly Weather Review, **134 (12),** 3753-3763.

Edwards R., Thompson, R. L., Crosbie, K. C., Hart, J. A. & Doswell, C.A. III (2004a). Proposals for modernizing the definitions of tornado and severe storm outbreaks. Preprints: 22nd Conference on severe local storms. Hyannis, Massachusetts, USA.

Edwards, R. Thompson, R. & Mead, C. (2004b). Assessment of anticyclonic supercell environments using close proximity soundings from the RUC model.Preprints: 22nd Conference on severe local storms, Hyannis, Massachusetts, USA.

Esterheld, J. M. & Giuliano, D.J. (2008). Discriminating between tornadic and non-tornadic supercells: A new hodograph technique. Electronic Journal of Severe Storms Meteorology, **3(2),** 1-50.
Available at: http://www.ejssm.org/ojs/index.php/ejssm/issue/view/13 last accessed: 15 February 2014.

Fankhauser, J. (1971). Thunderstorm-environment interactions determined from aircraft and RADAR observations. Monthly Weather Review, **99**, 171-192.

Fawbush, E.J. & Miller, R.C. (1953). A Method of Forecasting Hail size at the Earth's Surface. Bulletin of the American Meteorological Society, June 1953.

Forbes, G. S. (1981). On the reliability of hook echoes as tornado indicators. Monthly Weather Review, **109**, 1457-1466.

Forbes, G.S. & Bluestein, H.B. (2001). Tornadoes, Tornadic thunderstorms and Photogrammetry: A Review of the Contributions by T.B. Fujita. Bulletin of the American Meteorological Society, **82(1)**, 73-96.

Fowler, H. & Fowler, F. G. (eds.) (1964). The Concise Oxford Dictionary of Current English. 5th edition. Oxford, United Kingdom: Clarendon Press.

Fujuta, T. (1960a). A detailed analysis of the Fargo tornadoes of June 20 1957. US Weather Bureau Research Paper No.42. US Weather Bureau. 67pp.

Galilei, G. (1632). *Dialogo sopra I due massimi sistemi del mondo* (Dialogue concerning the two chief world systems). Florence, Italy.

Galway, J. G. (1977). Some climatological aspects of tornado outbreaks. Monthly Weather Review, **105**, 477-484.

George, J. J. (1960). Weather Forecasting for Aeronautics. New York, Academic Press. 407-415.

Gijben, M. (2012). The lightning climatology of South Africa. South African Journal of Science, **108**, 1-10.

Gill, T. (2008). Initial Steps in the Development of a Comprehensive Lightning Climatology of South Africa. Unpublished MSc dissertation, University of Witwatersrand, Johannesburg, Gauteng, South Africa.

Glickman, T. S. (ed.) (2000). Glossary of Meteorology. 2nd edition. Boston, United States of America: American Meteorological Society.

Goliger, A. & Milford, R. (1998). A review of worldwide occurrence of tornadoes. Journal of Wind Engineering and Industrial Aerodynamics, **74**, 111-121.

Goliger, A., Milford, R., Adam, F. & Edwards, M. (1997). *Inkanyamba* - Tornadoes in South Africa. Pretoria, South Africa: United Litho. ISBN: 0-7988-5417-0.

Goliger, A. & Retief, J. V. (2007). Severe wind phenomena in South Africa and the related damage. Journal of Wind Engineering and Industrial Aerodynamics, **95**, 1065-1078.

Hart, J.A. & Korotky, W.R. (1991). The SHARP workstation Users Guide V1.50. (30 pp). National Weather Service, NOAA, US Dept of Commerce.

Held, G. (1973). Ten years of hail observations in the Pretoria-Witwatersrand area. *Journal de Recherches Atmospheriques*, **7**, 185-197.

Held, G. (1978). The probability of hail to RADAR echo heights on the South African Highveld. Journal of Meteorological Applications, **17**, 755-762.

Held, G. (1981). Comparison of RADAR observations of a devastating hailstorm and a cloudburst at Jan Smuts Airport. In Cloud Dynamics, Agee, E. M. & Asai, T. (eds.). Dordrecht, Netherlands. 273-284.

Held, G., Gomes, A.M., Naccarato, K.P., Pinto, O. Jr. & de Lima Nascimento, E. (2006). The structure of three tornado-generating storms based on Doppler RADAR and lightning observations in the State of Sao Paulo, Brazil. Proceedings of 8th ICSHMO, *Foz do Iguacu*, Brazil, April 24-28. 1787-1797.

Held, G., Gomes, A. & Naccarato, K.P. (2010). The structure and behaviour of supercell storms in the State of Sao Paolo, Brazil. Proceedings, ERAD2010, The 6th European Conference on RADAR in Meteorology and Hydrology.

Houston, A.L., Thompson, R.L. & Edwards, R. (2008). The Optimal Bulk Wind Differential Depth and the Utility of the Upper Tropospheric Storm-Relative Flow for Forecasting Supercells. Weather and Forecasting, **23**, 825-837.

Houze, R. (ed.) (1993). Cloud dynamics. San Diego, USA: Academic Press. ISBN: 0-12-356881-1.

Intermet (2014). Technical specifications for the BAT16G radiosonde instrument. Available at: http://www.diel.co.za/bat-16g.html last accessed: 15 February 2014.

Johns, R. & Doswell, C. A. III. (1992). Severe local storms forecasting. Weather and Forecasting, **7**, 588-561.

Klemp, J. (1987). Dynamics of tornadic thunderstorms. Annual Review of Fluid Mechanics, **19**, 369-402.

Klemp, J. & Wilhelmson, R. (1978a). The simulation of three-dimensional storm dynamics. Journal of Atmospheric Science, **35**, 1070-1096.

Knupp, K.R., Murphy, T.A., Coleman, T.A., Wade, R.A., Mullins, S.A., Schultz, C.J., Schultz, E.V., Carrey, L., Sherrer, A., McCaul, E.W. Jr., Carcione, B., Latimer, S., Kula, A., Laws, K., Marsh, P.T. & Klockow, K. (2014). Meteorological Overview of the Devastating 27 April 2011 Tornado Outbreak, Bulletin of the American Meteorological Society, **95(7)**, 1041-1062.

Kruger, A. C. (2004). Climate of South Africa, Climate Regions Report WS45. South African Weather Service, Pretoria, South Africa.

Kruger, A. C. (2007). Climate of South Africa, Precipitation Report WS47. South African Weather Service, Pretoria, South Africa.

Lang, T.J., Miller, L.J., Weisman, M., Rutledge, S.A., Barker III, L.J., Bringi, V.N., Chandrasekar, V., Detwiler, A., Doesken, N., Helsdon, J., Knight, C., Krehbiel, P., Lyons, W.A., MacGorman, D., Rasmussen, E., Rison, W., Rust, D. & Thomas, R.J. (2004). The Severe Thunderstorm Electrification and Precipitation Study. Bulletin of the American Meteorological Society, **85 (8)**, 1107-1125.

Lemon, L. & Doswell, C. A. III. (1979). Severe thunderstorm evolution and mesocyclone structure as related to tornadogenesis. Monthly Weather Review, **107**, 1184-1197.

Leontitsis, A. (2001). Boxcox: To calculate the Box-Cox normal transformation of a dataset 'x'. A MATLAB file. Available at: http://www.mathworks.com/matlabcentral/fileexchange/881-box-cox-transformation/content/boxcox.m last accessed: 19 October 2014.

Levitch, E. & Tsvetkov, E. (1984). Helical cyclogenesis. Physics Letters, **100A**, 53-56.

Lilliefors, H. (1967), On the Kolmogorov–Smirnov test for normality with mean and variance unknown. Journal of the American Statistical Association, **62**, 399–402.

Lilliefors, H. (1969), On the Kolmogorov–Smirnov test for the exponential distribution with mean unknown. Journal of the American Statistical Association, **64,** 387–389.

Lilly, D.K. (1985). The structure, energetics and propagation of rotating convective storms. Part II: Helicity and Storm Stabilization. Journal of the Atmospheric Sciences, **43(2)**, 126-140.

Lindsey, D. & Bunkers, M. (2005). Observations of a severe, left-moving supercell on 4 May 2003. Monthly Weather Review, **20**, 16-22.

Loots, K. (2009). Personal communication: Karl Loots, Forecaster, National Forecast Centre, SAWS, Pretoria, South Africa, e-mail and verbal conversation RE: Meyerton, South Gauteng supercell, 8 November 2009.

Louw, E. (2014). Personal communication: Elke Louw, Senior Meteorologist, New Zealand Metservice, Wellington, New Zealand, e-mail RE: Geraldine, South Island supercell, 16 January 2014.

Lynn, R. J. (2002). The WDSS-II Supercell Identification and Assessment Algorithm. 21st Conference on Severe Local Storms. San Antonio, Texas, USA.

MacGorman, D. R., Rust, D., van der Velde, O., Askelson, M., Krehbiel, P., Thomas, R., Rison, B., Hamlin, T. & Harlin, J. (2002). Lightning relative to precipitation and tornadoes in a supercell storm during MEaPRS. 21st Conference on Severe Local Storms, American Meteorological Society, San Antonio, Texas, USA, 423-426.

Maddox, R. (1976). An evaluation of tornado proximity wind and stability data. Monthly Weather Review, **104**, 133-142.

Mann, H. B. & Whitney, D. R. (1947). On a Test of Whether one of Two Random Variables is Stochastically Larger than the Other. Annals of Mathematical Statistics, **18 (1),** 50–60. doi:10.1214/aoms/1177730491.

Markowski, P. (2002). Hook Echoes and Rear-Flank Downdrafts: A Review. Monthly Weather Review, **130**, 852-876.

Markowski, P. & Richardson, Y. (2006). On the classification of vertical wind shear as directional shear versus speed shear. Weather and Forecasting: Notes and Correspondence, **21**, 242-247.

Markowski, P., Straka, J.M., Rasmussen, E.N. & Blanchard, D.O. (1998b). Variability of storm-relative helicity during VORTEX. Monthly Weather Review, **126**, 2959-2971.

Marwitz, J. (1972a). The structure and motion of severe hailstorms. Part 1: Supercell storms. Journal of Applied Meteorology, **11**, 166-179.

McCann, D.W. (1994). WINDEX -- A New Index for Forecasting Microburst Potential, Weather and Forecasting, **9**, 532-541.

McCaul, E., & Weisman, M. (2001). The sensitivity of simulated supercell structure and intensity to variations in the shapes of environmental buoyancy and shear profiles. Monthly Weather Review, **129**, 664-687.

McNulty, R. (1978). On Upper Tropospheric Kinematics and Severe weather Occurrences. Monthly Weather Review, **106**, 662-672.

McNulty, R. (1995). Severe and Convective weather: A Central Region forecasting Challenge. Weather and Forecasting, **10**, 187-202.

Moller, A., Doswell, C.A. III., Foster, M.P., & Woodall, G.R. (1994). The operational recognition of supercell thunderstorm environments and storm structures. Weather and Forecasting, **9**, 327-347.

Moncreiff, M., & Miller, M. (1976). The dynamics and simulation of tropical cumulonimbus and squall lines. Quarterly Journal of the Royal Meteorological Society, **120**, 373-394.

Monteverdi, J.P., Blier, W., Stumpf, G., Pi, W. & Anderson, K. (2001). First WSR-88D Documentation of an Anticyclonic Supercell with Anticyclonic tornadoes: The Sunnyvale - Los Altos, California, tornadoes of 4 May 1998. Monthly Weather Review, **129(11)**, 2805-2814.

Murphy, M.J. & Demetriades, N.W.S. (2005). An analysis of lightning holes in a DFW supercell storm using total lightning and RADAR information. Extended abstracts, Conference on Meteorological Applications of Lightning Data, San Diego, California, USA, American Meteorological Society, CD-ROM, 2.3.

NASA (2012). Lightning and Atmospheric Research at the GHCC. Available at: http://thunder.nsstc.nasa.gov/data/query/mission.png last accessed: 14 January 2014.

National Severe Storms Laboratory (2014). Available at: http://www.nssl.noaa.gov/ last accessed: 08 January 2014.

Newton, C.W. & Katz, S. (1958). Movement of large convective rainstorms in relation to winds aloft. Bulletin of the American Meteorological Society, **39**, 129-136.

Panneerselvam, C., Jeeva, K., Nair, K.U., Gurubaran, S., Rajaram, R., Dhar, A. & Rajaram, G. (2004). Observations of Atmospheric Maxwell Current at Indian Antarctic Station, Maitri. 19th Indian Expedition to Antarctica Department of Ocean Development, Technical Publication, **17**, 99-105.

Parker, M. D. (2014). Composite VORTEX2 Supercell Environments from Near-storm Soundings. Monthly Weather Review, **142**, 508-529.

Poolman, E.P. (1992). *Die voorspelling van haelkorrelgroei in Suid Afrika* (Forecasting of hail growth in South Africa). Unpublished MSc dissertation, Pretoria University, Pretoria, South Africa.

Potvin, C.K., Elmore, K.L. & Weiss S.J. (2010). Assessing the impacts of Proximity Sounding Criteria on the Climatology of Significant Tornado Environments. Weather and Forecasting, **25**, 921-930.

Powell, C. (2011a). Evaluating the IR 10.8-12.0 Satellite Difference Channel through Case Studies. Part II: A RADAR perspective. SAWS Nowcasting and Very Short Range Forecasting group. Pretoria, South Africa. Document reference: RES-PSN-NOW-001-2011-02-18.

Powell, C. (2011b). A Proposed Method for the Detection of Large/Damaging Hail in South Africa using S-Band Doppler Radar. SAWS Nowcasting and Very Short Range Forecasting group. Pretoria, South Africa. Document reference: RES-PSN-NOW-001-2011-07-22.

Powell, C. (2012). New Hail Mass Aloft product available in NFC. SAWS Nowcasting and Very Short Range Forecasting group. Pretoria, South Africa. Document reference: RES-PSN-NOW-001-2012-09-03.

Powell, C., Loots, K., Fernandes, L. & Todd. M. (2010). Severe Storm Outbreak Wreaks Havoc across South Africa, 24 October 2010. South African Weather Service, Pretoria, South Africa.

Pretoria News. (2012). Two killed as tornadoes hit Free State. Monday 25 June 2012.

Pyle, D. (2006). Severe Convective Storm Risk in the Eastern Cape Province of South Africa. Unpublished PhD thesis, Rhodes University, Grahamstown, Eastern Cape, South Africa.

Rae, K.J. (2000). Personal diary notes relating to severe storms. Calendar year 2000. Pretoria, Gauteng, South Africa.

Rae, K.J. (2001). Informal listing of hail events, 2000-2001, close to operational upper-air sites. South African Weather Service internal summary report, Pretoria, Gauteng, South Africa.

Rae, K.J. (2005). Gauteng Hail data 1984-1995, Postgraduate workshop, *Exploratorium*, 4 April 2005 Pretoria University, Gauteng, South Africa.

Rae, K.J. (2007a). Personal diary notes relating to severe storms. Calendar year 2007. Pretoria, Gauteng, South Africa.

Rae, K.J. (2007b). WMO Regional Area 1 Training Seminar: Severe Weather Forecasting. Presentation, 1 November 2007, SAWS Bolepi House, Pretoria, South Africa.

Rae, K.J. (2008). Personal diary notes relating to severe storms. Calendar year 2008. Pretoria, Gauteng, South Africa.

Ramsay, H. & Doswell, C. A. III (2005). A sensitivity study of hodograph-based methods for estimating supercell motion. Weather and Forecasting, **20**, 954-970.

Rasmussen, E.N. (2003). Refined supercell and tornado forecast parameters. Weather and Forecasting, **18**, 530-535.

Rasmussen, E.N. & Blanchard, D. O. (1998). A baseline climatology of sounding-derived supercell and tornado forecast parameters. Weather and Forecasting, **13(4)**, 1148-1164.

Rasmussen, E.N. & Wilhelmson, R.B. (1983). Relationship between storm characteristics and 1200 GMT hodographs, low-level shear and instability. Preprints, 13th Conference on Severe Local Storms, Tulsa, Oklahoma, USA, American Meteorological Society, J5-J8.

Reap, R.M. (1986). Evaluation of Cloud to Ground Lightning Data from the Western United States for the 1983-1984 Summer Seasons. Journal of Climate Applications and Meteorology, **25**, 785-799.

Rose, T., Kaser-Boyd, N., Maloney, M.P. & Maloney, M. (2001). Essentials of Rorschach assessment. John Wiley and Sons, New York, USA.

Rotunno, R. (1981). On the evolution of thunderstorm rotation. Monthly Weather Review, **109**, 171-180.

Rotunno, R. & Klemp, J. (1985). On the rotation and propagation of simulated supercell thunderstorms. Journal of Atmospheric Science, **42**, 271-292.

Rouault, M., Roy, S.S. & Balling, R.C. (2013). The diurnal cycle of rainfall in South Africa in the austral summer. International Journal of Climatology, **33**, 770-777.

Schaefer, J. T. (1986). The Dryline. In Mesoscale Meteorology and Forecasting, Ray, P.(ed.). Boston, U.S.A: American Meteorological Society. 547-572.

Schlesinger, R. (1980). A three-dimensional numerical model of an isolate thunderstorm. Part II: Dynamics of updraft splitting and mesovortex evolution. Journal of Atmospheric Science, **37**, 395-420.

Schmid, W., Schiesser, H-H., & Bauer-Messmer, H. (1997). Supercell storms in Switzerland: case studies and implications for nowcasting severe winds with Doppler RADAR. Meteorological Applications, **4**, 49-67.

Schulze, B. (1984). Climate of South Africa: Part 8 General Survey. 5th edition, WB28, 330 pp. Pretoria: South African Weather Bureau.

Schwartz, B.E. & Doswell, C.A. III (1991). North American Rawinsonde observations: Problems, concerns and a call to action. Bulletin of the American Meteorological Society, **72**, 1885-1896.

Shapiro, S.S. & Wilk, M.B. (1965). An analysis of variance test for normality (complete samples). Biometrika, **52 (3–4)**, 591–611. doi:10.1093/biomet/52.3-4.591.

Shewchuck, J. (2013). RAOB: The Complete Rawinsonde Observation Program, Version 6.3. Users Guide and Technical Manual. Environmental Research Services (ERS). Matamoras, Pennsylvania, USA.

Showalter, A. K. (1953). A stability index for thunderstorm forecasting. Bulletin of the American Meteorological Society, **34**, 250-252.

Sills, D., Wilson, J., Joe, P., Burgess, D., Webb, R. & Fox, N. (2004). The 3 November tornadic event during Sydney 2000: Storm evolution and the role of low-level boundaries. Weather and Forecasting, **19**, 22-41.

Singh, R. (1981). On the occurrence of tornadoes and their distribution in India. Mausam, **32**, 307-314.

Slonaker, R., Schwartz, B. & Emery, W. J. (1996). The occurrence of nonsurface superadiabatic lapse rates within RAOB data. Weather and Forecasting, **11**, 350-359.

South African Weather Service. (2013). Standard Work Instructions (SWI): Weather Related Alerts. Pretoria, South Africa. ISO9001 Document reference: FCAST-SWI-Weather Related Alerts-002.0

South African Weather Service. (2007). Diary of significant weather and nowcasts: 2007, National Forecast Centre (NFC). Pretoria, South Africa.

South African Weather Service. (2008). Diary of significant weather and nowcasts: 2008, National Forecast Centre (NFC). Pretoria, South Africa.

Steyn, P.C.L. & Hudak, D.R. (1982). *Die Heilbron Haelstorm*. South African Weather Bureau (SAWB). Monthly Newletter No 392. January 1982, Pretoria, South Africa.

Storm Prediction Center (2014). Available at: http://www.spc.noaa.gov/ Last accessed: 08 January 2014.

Stumpf, G. (2003). RADAR Detection of Severe Convective Storms, WWRP/WMO Latin American Nowcasting Workshop, 3 – 14 November 2003, Brazil, South America.

Terblanche, D.E. (1985). *Die Hailstorm van 1 November 1985*. South African Weather Bureau monthly newsletter. November 1985. 1-6.

The Citizen (2000). Golf ball size hail devastates the Vaal. Wednesday 6 December 2000.

Todd, M. (2007) Personal communication: Mark Todd, Forecaster, National Forecast Centre, SAWS, Pretoria, Gauteng, e-mail and verbal discussion RE: Fochville supercell, 19 and 20 October 2007.

Todd, M (2009). Severe Convection. Presentation 26 August 2009, Bloemfontein Forecast Office, Free State, South Africa.

Todd, M. (2011) Personal communication: Mark Todd, Forecaster, National Forecast Centre, SAWS, Pretoria, Gauteng, SMS and e-mail RE: Brits supercell, 2 and 3 October 2011.

Thompson, R., Edwards, R. & Hart, J. A. (2002). Evaluation and Interpretation of the Supercell Composite and Significant Tornado Parameters. Preprints: 21st Conference on Severe Local Storms San Antonio, Texas: American Meteorological Society.

Thompson, R., Edwards, R., Hart, J.A., Elmore, K.L. & Markowski, P. (2003). Close proximity soundings within supercell environments obtained from the Rapid Update Cycle. Weather and Forecasting, **18**, 1243-1261.

Thompson, R., Mead, C. & Edwards, R. (2004a). Effective bulk shear in supercell thunderstorm environments. Preprints: 22nd Conference on Severe Local Storms Hyannis, Massachusetts, USA. American Meteorological Society.

Thompson, R., Mead, C. & Edwards, R. (2004b). Effective storm-relative helicity in supercell thunderstorm environments. Preprints: 22nd Conference on Severe Local Storms Hyannis, Massachusetts, USA. American Meteorological Society.

Thompson, R., Mead, C. & Edwards, R. (2007). Effective storm-relative helicity and bulk shear in supercell thunderstorm environments. Weather and Forecasting, **22**, 102-115.

Trujillo-Ortiz, A. & Hernandez-Walls, R. (2003). DagosPtest: D'Agostino-Pearson's K2 test for assessing normality of data using skewness and kurtosis. A MATLAB file. Available at: http://www.mathworks.com/matlabcentral/fileexchange/loadFile.do?objectId=3954&objectType=FILE last accessed: 19 October 2014.

Tukey, J.W. (1977). Exploratory Data Analysis. Reading, Massachusetts, USA. Addison-Wesley.

Tyson, P. (1987). Climatic Change and Variability in Southern Africa. Cape Town, South Africa: Oxford University Press. ISBN: 0-19-570495-9.

University of Wyoming (2014). Upper air soundings page, Wyoming, USA. Available at: http://weather.uwyo.edu/upperair/sounding.html last accessed: 08 January 2014.

Vaisala (2014). Specification sheet for RS92-SGP radiosonde. Available at: http://www.vaisala.com/Vaisala%20Documents/Brochures%20and%20Datasheets/RS92SGP-Datasheet-B210358EN-F-LOW.pdf last accessed: 25 April 2014.

Van Tassel, L. (1955). The North Platte Valley tornado outbreak of June 27 1955. Monthly Weather Review, **117**, 1113-1140.

Visser, P.J. (2001). The Storm-Structure-Severity method for the identification of convective storm characteristics with conventional weather RADAR. Meteorological Applications, **8**, 1-10.

Visser, P. & van Heerden, J. (2000). Comparisons of hail kinetic energy derived from RADAR reflectivity with crop damage reports over the eastern Free State. Water SA, **26(1)**, 91-96.

Wang, C-C., Chen, G. T-J., Yang, S-C. & Chou, H-C. (2008). Wintertime supercell thunderstorms in a sub-tropical environment: A diagnostic study. Monthly Weather Review, **137**, 366-390.

Weisman, M.L., & Klemp, J. (1982). The dependence of numerically simulated convective storms on vertical wind shear and buoyancy. Monthly Weather Review, **110**, 504-520.

Weisman, M.L. & Klemp, J.B. (1984). The structure and classification of numerically simulated convective storms in directionally varying wind shears. Monthly Weather Review, **112**, 2479-2498.

Weisman, M.L. & Klemp, J.B. (1986). Characteristics of isolated convective storms. In Mesoscale Meteorology and Forecasting, Ray, P.(ed.). (331-358). Boston, USA, American Meteorological Society.

Wilks, D.S. (2011). Statistical Methods in the Atmospheric Sciences. Elsevier Academic Press, Oxford, United Kingdom.

WMO (1996). Guide to Meteorological Instruments and Methods of Observation. 6th edition. WMO Report 8, World Meteorological Organisation, Geneva, Switzerland.

ZAMG Austrian Institute of Meteorology (2013). Vienna, Austria. Available at: http://www.zamg.ac.at/cms/de/forschung/umwelt/publikationen last accessed: 28 September 2013.

Zeitler, J. & Bunkers, M. (2005). Operational forecasting of supercell motion: review and case-studies using multiple datasets. National Weather Digest, **29**, 81-97.

Zipser, E.J, Cecil, D.J., Liu, C., Nesbitt, S.W. & Yorty, D.P. (2006). Where are the most intense thunderstorms on earth? Bulletin of the American Meteorological Society, **87**, 1057-1071.

APPENDIX

The list below represents a chronology of historic southern African Highveld-based supercells from 1972 to present day, compiled by the author during the course of this study and numbering 29 such events. As such, this resource should not be considered to be an exhaustive list but rather a *capita selecta* of the overall population of Highveld supercells. Some storms occurred eyond the 200 km proximity range of the Irene RADAR, while in some cases, suitable upper air proximity sounding data was lacking. The 15 supercell cases utilised as the so-called SUP sample was a subset drawn from this listing.

No.	Date YYYYMMDD	Location	Province
1	19721129	Pretoria and Johannesburg	Gauteng
2	19820122	Steynsrus	Free State
3	19851101	Pretoria	Gauteng
4	19971229	Bethlehem	Free State
5	19991021	Heidelberg	Gauteng
6	20001205	Vereeniging	Gauteng
7	20041027	Potchefstroom	NorthWest
8	20071006	Westonaria	Gauteng
9	20071006	Schweizer-Reneke	North West
10	20071007	Groblersdal	Limpopo
11	20071008	Leandra (20km south of)	Mpumalanga
12	20071019	Fochville	NorthWest
13	20071106	Vaalwater	Limpopo
14	20071116	Ermelo	Mpumalanga
15	20071217	Bothaville	Free State
16	20081105	Parys	Free State
17	20091107	Meyerton	Gauteng
18	20101013	Soutpan	Free State
19	20101024	Marble Hall	Limpopo
20	20101024	Zastron	Free State
21	20101030	Pretoria	Gauteng
22	20101105	Ermelo (2 cells)	Mpumalanga
23	20111002	Brits	NorthWest
24	20111019	Krugersdorp	Gauteng
25	20120623	Multiple	Free state and Gauteng
26	20121020	Midrand	Gauteng
27	20131007	Villiers	Free State
28	20131019	Bapsfontein	Gauteng
29	20131128	Viljoenskroon/Midrand	Free State, North West and Gauteng